UNIVERSIDADE FEDERAL DO CEARÁ
CENTRO DE CIÊNCIAS
DEPARTAMENTO DE GEOLOGIA
PROGRAMA DE PÓS-GRADUAÇÃO EM GEOLOGIA

THAINARA FREIRES RODRIGUES

GEOLOGIA, PETROGRAFIA, GEOQUÍMICA E QUÍMICA DAS PIRITAS ASSOCIADAS ÀS OCORRÊNCIAS DE COBRE HIDROTERMAL DA PORÇÃO OESTE DA PROVÍNCIA BORBOREMA

FORTALEZA
2023

THAINARA FREIRES RODRIGUES

GEOLOGIA, PETROGRAFIA, GEOQUÍMICA E QUÍMICA DAS PIRITAS ASSOCIADAS ÀS OCORRÊNCIAS DE COBRE HIDROTERMAL NA PORÇÃO OESTE DA PROVÍNCIA BORBOREMA

Dissertação apresentada ao Programa de Pós-Graduação em Geologia da Universidade de Federal do Ceará, como requisito parcial para obtenção do título de Mestre em Geologia. Área de concentração: Geodinâmica e Recursos Minerais.
Orientador: Prof. Dr. Clóvis Vaz Parente

Coorientador: Prof. Dra. Lydia M. Lobato

FORTALEZA
2023

Dados Internacionais de Catalogação na Publicação
Universidade Federal do Ceará
Sistema de Bibliotecas
Gerada automaticamente pelo módulo Catalog, mediante os dados fornecidos pelo(a) autor(a)

F933g Freires Rodrigues, Thainara.
Geologia, petrografia, geoquímica e química das piritas associadas às ocorrências de cobre hidrotermal na porção oeste da Província Borborema / Thainara Freires Rodrigues. – 2023.
95 f. : il. color.

Dissertação (mestrado) – Universidade Federal do Ceará, Centro de Ciências, Programa de Pós-Graduação em Geologia, Fortaleza, 2023.
Orientação: Prof. Dr. Clóvis Vaz Parente. Coorientação: Profa. Dra. Lydia Maria Lobato.

1. Alterações Hidrotermais. 2. Ocorrências de Cobre. 3. Província Borborema. 4. Faixa Orós. I. Título.

CDD 551

THAINARA FREIRES RODRIGUES

GEOLOGIA, PETROGRAFIA, GEOQUÍMICA E QUÍMICA DAS PIRITAS ASSOCIADAS ÀS OCORRÊNCIAS DE COBRE HIDROTERMAL NA PORÇÃO OESTE DA PROVÍNCIA BORBOREMA

Dissertação apresentada ao Programa de Pós-Graduação em Geologia da Universidade de Federal do Ceará, como requisito parcial para obtenção do título de Mestre em Geologia. Área de concentração: Geodinâmica e Recursos Minerais.

Aprovada em 28/04/2023.

BANCA EXAMINADORA

Prof. Dr. Clóvis Vaz Parente

Universidade Federal do Ceará (UFC)

Prof. Dr. César Ulisses Veríssimo

Universidade Federal do Ceará (UFC)

Prof. Dr. Claudinei Gouveia de Oliveira

Universidade de Brasília (UNB)

AGRADECIMENTOS

Agradeço primeiro a Deus, por ter me dados forças para chegar até aqui, em seguida a minha família, especialmente a minha mãe, Maria e ao Eryck pelo apoio incondicional nos diversos momentos dificeis dessa trajetória, pelo incentivo constante, amor e carinho.

Aos meus irmão, Thiago e Vinicius, pela força, carinho e descontração de sempre, por sempre acreditarem em mim, em especial ao Thi que ainda me deu um empurrãozinho final me ajudando com a revisão.

Ao meu namorado, companheiro e amigo Eryck, pelo imenso apoio, incentivo, conselhos, dicas e mapas, rs. Por acreditar em mim mais que eu mesma. Obrigada por todos os momentos ao longo desses anos, por estar sempre ao meu lado.

Agradeço muito ao Prof. Clóvis, por ter tido muita paciência comigo, e não ter desistido de me ajudar, por ser sempre muito solícito e disposto a ensinar e aconselhar. A Profa. Lydia Lobato pelo fomento a pesquisa, ensinamento e conselhos ao longo de todo o desenvolvimento do trabalho. Ao Gabriel Berni, idealizador do trabalho. Ao Prof. Cristiano pela imensa ajuda no campo, indispensável para que eu concluísse a pesquisa. E aos demais professores que colaboraram com financiamento e intelectualmente para elaboração da pesquisa, Profa. Glaucia Queiroga, Prof. Adolf Fuck e Prof. Sérgio Bacelar.

Agradeço minha amiga Laryssa pelo imenso apoio intelectual e emocional, sem ela eu não teria chegado até aqui! Aos meus queridos amigos do clube de leitura que me acolheram no início do mestrado, Amanda, Rayssa, Cassiano e Linara. A minha amiga Claudia, com quem compartilho forças e experiencias na pesquisa desde a graduação. As minhas companheiras de casa e de vida em Goiás, Darli e Mari pelo incentivo e força nessa reta final.

RESUMO

Durante o eopaleozóico na Província de Borborema eventos transtensionais deram origem a diversas estruturas e rochas hospedeiras favoráveis à formação de depósitos minerais. Estudos anteriores descrevem as ocorrências de cobre associadas a óxidos de ferro na Província Borborema em bacia tipo rift, de forma isolada, com ênfase especial àqueles associados às brechas de quartzo-hematita nas bacias Carnaubinha/São Bento (Piauí) e Jaibaras/Cococi (Ceará). As semelhanças no estilo de mineralização, cenário tectônico e alteração hidrotermal sugerem que essas ocorrências fazem parte de um mesmo sistema mineral-hidrotermal de escala continental. Para confirmar essa hipótese, é necessário comparar os estilos de alteração hidrotermal e a geoquímica das diferentes áreas mineralizadas. Esta pesquisa visa fornecer a caracterização detalhada das ocorrências de cobre nas bacias eopaleozóicas de Carnaubinha e São Bento e do seu embasamento (região de Pio IX), porção sudoeste da Província de Borborema, definindo a relação das alterações hidrotermais associadas. Para a concretização desses propósitos, foram realizados estudos petrográficos, geoquímicos e de química mineral, visando estabelecer um modelo de sistema mineral para as principais ocorrências minerais de cobre dentro do arcabouço geodinâmico da Província de Borborema. Estudos petrográficos permitiram a identificação e caracterização da história hidrotermal da sequência metavulcano-sedimentar do Grupo Orós do Paleoproterozóico superior (~1,8Ga) e do seu embasamento, Complexo São Nicolau (~2,2Ga). As principais fases são representadas por alterações albita, k-feldspato, epídoto e clorita, silicificação e alteração sílico-hematitica, sendo as duas últimas fases associadas a ocorrências de cobre. Ocorrem como veios e *stockworks*, ou brechas pervasivas. Na Bacia de Carnaubinha, a alteração consiste em K-feldspato, Epidoto e Clorita, que ocorrem como veios estruturalmente controlados, enquanto as alterações de silicificação e sílica-hematita aparecem em veios, *stockworks* ou disseminadas pervasivamente junto aos conglomerados associadas a minerais de cobre. Na bacia de São Bento, a silicificação é o principal tipo de alteração e ocorre como veios e *stockworks;* a alteração hematítica ocorre como hematita dispersa na matriz e clastos do conglomerado, e associada à silicificação em conjuntos de veios; da mesma forma, a alteração clorítica ocorre na matriz e, veios tardios, sobrepondo a silicificação; a sulfetação é representada principalmente por pirita, com ocorrências subordinadas de calcopirita e bornita que ocorrem disseminadas. Alguns cristais de sulfetos são deformados e com fraturas preenchidas por silicificação. Estudos geoquímicos envolvendo análises de componentes principais das amostras do embasamento mostram que a alteração epidoto-clorita é caracterizada por maior CaO, Na_2O e MgO associados a La, Ce, Hf,

Zr, Y, Sr e Th, enquanto a alteração K-Felspatica possui aumento em K_2O, Al_2O_3, Na_2O_3 associados a Rb, Sn e Nb. As alterações sílico-hematitica, comuns junto às brechas, são enriquecidas em SiO_2 e Fe_2O_3 associadas a Pb, W, Sb, W, Sb, V, Ba, Mo e Co, e quando associadas às ocorrências de cobre mostram Cu, Bi, Ag Se e Te, como ganhos. As brechas silicificada associadas às ocorrências de cobre mostram Cr mais alta e ganhos como MnO, TiO_2, U e Hg. As brechas da bacia de Carnaubinha com alterações K-Felspatatica e Epidoto-Clorita têm o enriquecimento de CaO, Na_2O associado a Ga, La, Ce, Ti, Sr, Mn, Y, Li e Ta. Por sua vez, as brechas vulcanoclásticas de alteração sílica são enriquecidas em Al_2O_3, Na_2O e K_2O e Cs, Sc, Nb Th, Sn e Rb. O conglomerado silicificado rico em cobre tem ganhos de CaO, MgO, TiO_2 e MnO, além de Be, Cd, Zn, Li, Ni e P. Finalmente, as brechas sílico-hematíticas da bacia tem enriquecimento de Se, Ag, Cu, As, Te e Bi. Análises química da pirita mostram que os principais elementos de traços na brecha do embasamento são Co, Ni, Hg, Ag, As, Mn e Zn. A brecha sílico-hematítica da bacia Carnaubinha é caracterizada pelos elementos traços Co, Cu, Se, Hg Ni, Te, As e Mn, enquanto a brecha de silica-sulfetada apresenta enriquecimento semelhante em Co, seguido por Ni, Hg, As, Mn, Te, Zn, Ag e Cu. Os elementos traços principais nas piritas da bacia de São Bento são Hg, Cu, Co, Ag, Te, Zn, Mn e Se. As brechas de Carnaubinha e do embasamento têm altas razões Co/Ni, onde predominam valores > 10 enquanto para a bacia de Bento as proporções são predominantemente <2. As semelhanças nos estilos de alteração e na sequência paragenética que afetam a bacia de Carnaubinha e o embasamento, associados aos dados geoquímicos demonstram uma assinatura semelhante para essas alterações e ocorrências de cobre, indicando que elas fazem parte de um mesmo sistema hidrotermal. Na bacia de São Bento, as alterações são incipientes e o hidrotermalismo é menos evoluído. Da mesma forma, os resultados da química da pirita indicam uma fonte maior de fluidos magmático-hidrotermais junto às brechas da bacia Carnaubinha e do embasamento, enquanto a química das piritas de São Bento indicam fonte sedimentar com menor contribuição hidrotermal. Os resultados obtidos indicam que um mesmo sistema hidrotermal afetou em diferentes fases as rochas da Faixa Orós, seu embasamento e as bacias eopaleozóicas.

Palavras-chave: Mineralizações de Cobre; Faixa Orós; Análise de Componentes Principais; Química Mineral de Piritas.

ABSTRACT

The Eopaleozoic transtensional setting in Borborema Province displays many favorable structures and host rocks for the formation of mineral deposits. Previous studies describe the potential occurrence of copper deposits associated to iron oxides in different rift basins along Borborema Province, with special emphasis to those associated to quartz-hematite breccias in the basins of Carnaubinha/São Bento (Piauí State) and Jaibaras/Cococi (Ceará State). Similarities in mineralization style, tectonic setting and hydrothermal alteration suggest that these occurrences are part of a single continental scale mineral system. To confirm such hypothesis, it is necessary to compare the hydrothermal alteration styles and geochemistry of the different mineralized areas. This MSc research is intended to provide a detailed characterization of the copper occurrences in Carnaubinha and São Bento Eopaleozoic basins and related basement (Pio IX region), in the southwestern portion of Borborema Province, defining their associated hydrothermal alteration relationships. To address such purposes, petrological, geochemical and mineral chemistry analyses were performed, aiming the establishment of a mineral system model for the key localities within the geodynamic framework of the Borborema Province. Petrographic studies allowed the characterization of the hydrothermal alteration in the basement rocks of Orós Group and São Nicolau complex. They consist of Albite, K-feldspar, Epidote, Chlorite alterations, silicification and silica-hematite alteration, where the last two phases are associated to copper occurrences. They occur as veins and stockworks, or pervasively substituting the protolith. In Carnaubinha basin, the alteration consists of k-feldspar, epidote and chlorite, occurring predominantly as structurally controlled veins, while silicification and silica-hematite alteration occur as veins, stockworks and pervasively in the conglomerates, being also associated to the presence of copper minerals. In São Bento basin, silicification is the main alteration type and occur as veins and stockworks; hematite alteration occurs as dispersive hematite formation in the conglomerate matrix and clasts and associated to the silicification in veins sets; similarly, chlorite alteration occurs in the matrix, and as late veins overprinting the silicification; sulfide alteration is represented by abundant pyrite, while crystals are deformed and overprinted by silicification. Principal component analyses of the geochemistry results for the basement samples showed that epidote-chlorite alteration is characterized by higher CaO, Na_2O_3 and MgO associated to La, Ce, Hf, Zr, Y, Sr and Th, while k-feldspar have K_2O, Al_2O_3 and Na_2O_3 gains associated to Rb, Sn and Nb. While silica-hematite alteration breccias are SiO_2 and Fe_2O_3 enriched associated to Pb, W, Sb, W, Sb, V, Ba, Mo and Co. When associated to copper occurrences, they show Cu, Bi, Ag,

Se, Te and As gains. Silica-alteration breccias associated to copper occurrences show higher Cr and As gains. MnO, TiO_2, U and Hg occur in all copper breccias. Carnaubinha basin conglomerate breccias with k-feldspar and epidote-chlorite alterations have CaO, Na_2O_3 enrichment associated to Ga, La, Ce, Ti, Sr, Mn, Y, Li and Ta. Silica-alteration volcanoclastic breccias are enriched in Al_2O_3, Na_2O and K_2O, and Cs, Sc, Nb, Th, Sn and Rb. The silicified copper rich conglomerate is linked with CaO, MgO, TiO_2 and MnO, besides Be, Cd, Zn, Li, Ni and P. Finally, the basin silica-hematite breccias has Se, Ag, Cu, As, Te and Bi gains. Pyrite chemistry analyses showed the basement pyrites main trace elements are Co, Ni, Hg, Ag, As, Mn, Se and Zn. Carnaubinha basin silica-hematite breccia is characterized by Co, Cu, Se, Hg Ni, Te, As and Mn trace elements, while silica-sulfide breccia results show a similar enrichment in Co, followed by Ni, Hg, As, Se, Mn, Te, Zn, Ag and Cu. São Bento basin pyrite main trace elements are Hg, Cu, Co, Ag, Te, Zn, Mn and Se. Carnaubinha and basement breccias have high Co/Ni rations, majorly > 10 ppm, while for São Bento basin the ratios are predominantly < 2 ppm. Similarities in alteration styles and paragenetic sequence affecting Carnaubinha basin and basement rocks and geochemistry results demonstrate a similar signature for these alterations and copper occurrences indicate that these are part of a single hydrothermal alteration system. In São Bento basin, alterations are incipient, and the hydrothermal system is less evolved. Similarly, the pyrite chemistry results indicate that a higher magmatic-hydrothermal source of fluids for Carnaubinha basin and basement breccias, while São Bento pyrite indicate a sedimentary source with minor hydrothermal contribution. Compiled results indicate that the similar hydrothermal system affected in different stages the rocks of Orós mobile belt, its basement, and eopaleozoic basins.

Keywords: Copper Mineralizations; Orós Belt; Principal Component Analysis; Pyrite Chemistry.

SUMÁRIO

1 INTRODUÇÃO

Ao longo da Província Borborema, distribuem-se cerca de dez bacias eopaleozoicas do tipo rifte, controladas por zonas de cisalhamento transcorrentes, relacionadas ao colapso do Orógeno Brasiliano, e que apresentam diversas mineralizações de cobre e ferro associadas a brechas hidrotermais (PARENTE *et al*., 2004).

No setor sudoeste da Província, e a oeste do Sistema Orós-Jaguaribe, a região situada entre os municípios de São Julião, Fronteiras, Pio IX (PI), Campos Sales e Parambu (CE) possui um longo histórico de extrativismo mineral direcionado às indústrias de cal e cimento, rochas ornamentais e construção civil (MAAS, 2003). Os primeiros registros da ocorrência do cobre na região se deram a partir de estudos prospectivos para calcário em 1979, revelando a presença de malaquita dispersa em rochas da região do município de São Julião (PI), o que resultou na implementação do projeto Cobre Mandacaru pela Companhia de Desenvolvimento do Estado do Piauí (CONDEPI), a partir do qual foram descobertas novas concentrações de sulfetos e óxidos disseminados associados a granitos, rochas sedimentares e vulcanoclásticas (LOPES FILHO *et al*, 1982 *apud* MAAS, 2003; MACHADO, 2006). Na década de noventa, trabalhos de pesquisa realizados pela Western Mining Corporation (WMC) encontraram novas ocorrências de cobre associadas à zonas de alteração hidrotermal em rochas vulcânicas e graníticas (MAAS, 2003). Já nos anos 2000, trabalhos regionais de avaliação das ocorrências foram realizados pela Companhia Vale do Rio Doce (Atualmente Vale S.A.), o que atraiu outras empresas como a International Nickel Corporation (INCO), a Phelps Dodge e a Brasmim (MAAS, 2003). Posteriormente, empresas como a Teck-Cominco (Atualmente Teck-Resources Limited) e a Monster Copper Resources demonstraram interesse pela área, considerando suas similaridades a depósitos de classe mundial do tipo IOCG (iron oxide-copper-gold) (Machado, 2006). Atualmente, diferentes empresas possuem concessão de pesquisa para a cobre e ferro na região, tais como a Nexa Resources, Terrativa Minerais, a Laterra Mineração Ltda, a Front Copper Brasil Ltda., entre outras.

Desde a descoberta do depósito de Olympic Dam, na Austrália, depósitos IOCG (Iron-Oxide-Copper-Gold) têm adquirido grande importância na produção mundial de cobre, ouro, urânio, entre outros (HITZMAN *et al*; 1992; HITZMAN, 2000). Tais depósitos comumente localizam-se em associação com zonas de falhas relacionadas a ambiente de colapso orogênico, a mineralização ocorre na forma de brechas, *stockworks*, e tem-se intensa alteração hidrotermal da rocha hospedeira, que pode variar entre litotipos magmáticos, sedimentares e metamórficos (HITZMAN, 2000).

Diferentes trabalhos descrevem o potencial dessas mineralizações a oeste da Província Borborema associadas às bacias rifte, tais como Maas *et al*. (2003), Machado (2006), Parente *et al*. (2011), Saraiva e Rodrigues (2018) e Uvula e Didoné (2019), e também ao seu embasamento, como Silva e Carneiro (2018), Huhn *et al.* (2011) e Huhn *et al*. (2014). Nestes trabalhos, os autores descrevem as similaridades entre seus respectivos alvos e sistemas do tipo Iron Oxide-Copper-Gold (IOCG) e fornecem dados acerca das mineralizações de cobre associadas a brechas quartzo-hematíticas, merecendo destaque especial aquelas associadas às bacias Jaibaras e Cococi (Ceará), Carnaubinha e São Bento (Piauí), e o embasamento da Faixa Orós na região de Pio IX (Piauí).

As diversas similaridades no estilo da mineralização, ambiente tectônico e alterações hidrotermais sugerem que todas essas ocorrências fazem parte de um mesmo sistema mineral de escala regional. Para confirmar essa hipótese, e fornecer um novo critério de exploração para a região, é necessário comparar os estilos de alteração hidrotermal, a geoquímica e mineralogia do minério das diferentes áreas mineralizadas.

Este trabalho apresenta novos dados geológicos e geoquímicos acerca das mineralizações e alterações hidrotermais associadas às bacias de Carnaubinha e São Bento, bem como da região de Pio IX, embasamento da Faixa Orós. A contribuição discute sua possível origem e evolução, determinando a relação temporal entre as alterações e as ocorrências.

Estruturada em 6 capítulos, a dissertação traz em seu capítulo introdutório uma contextualização da área do trabalho e oferece um breve histórico da mesma, incluindo, também as justificativas e os objetivos gerais da pesquisa. O segundo capítulo busca apresentar de forma mais detalhada os objetivos do trabalho, no terceiro capítulo tem-se uma abordagem sobre o contexto geológico em que se insere a área de estudo desde as grandes unidades geotectônicas até o contexto regional, incluindo uma breve revisão bibliográfica a esse respeito.

O quarto capítulo contempla uma revisão bibliográfica sobre os depósitos do tipo IOCG, explicitando de forma breve sua origem, formação, evolução e características, com base na literatura. No capítulo cinco estão descritos os métodos utilizados na pesquisa e no tratamento dos dados utilizados, com sua fundamentação teórica. Por fim, o capítulo 6 e apêndice A contêm as considerações finais, onde os resultados da pequisa estão apresentados na forma de um artigo científico, submetido ao Brazilian Journal of Geology, que contempla as interpretações e discussões acerca dos dados obtidos.

2 OBJETIVOS

Este estudo tem como objetivo caracterizar as alterações hidrotermais e as mineralizações de cobre nas localidades de Carnaubinha, São Bento e Pio IX (Piauí), a fim de estabelecer um modelo de sistema mineral para estas, dentro do contexto geodinâmico da Província Borborema, a partir de:

(i) Caracterização petrográfica das rochas hospedeiras da mineralização;
(ii) Caracterização paragenética detalhada das alterações hidrotermais e mineralização, e seu zoneamento temporal e espacial;
(iii) Estudos geoquímicos de rocha total das alterações hidrotermais e brechas mineralizadas, a fim de determinar a assinatura geoquímica das alterações e sua relação com as ocorrências de cobre.
(iv) Caracterização da química mineral das piritas associadas às brechas das diferentes ocorrências, buscando estabelecer se as suas formações foram condicionadas por processos semelhantes, e se estes estão relacionados às ocorrências de cobre.

3 CONTEXTO GEOLÓGICO REGIONAL

3.1 Província Borborema

A Província Borborema é um importante cinturão orogênico de idade neoproterozoica situada na porção nordeste da plataforma Sul-Americana (ALMEIDA *et al*., 1981) (Figura 1). Consiste em um fragmento do extenso sistema orogênico neoproterozoico Brasiliano/Pan-Africano, resultante da colisão entre os crátons São Luís/Oeste Africano e São Francisco Congo em 600 Ma, incluindo o Bloco Parnaíba e rochas arqueano-paleoproterozoicas, que formavam seu embasamento, culminando na amalgamação final do continente Gondwana Oeste (ARTHAUD *et al*., 2008; KLEIN; MOURA, 2008; GANADE *et al*., 2014). Sua configuração é caracterizada por uma evolução através da aglutinação de blocos crustais arqueanos a complexos gnáissico-migmatíticos paleoproterozoico, que são sobrepostos por unidades supracrustais neoproterozoicas. Esses terrenos foram subsequentemente separados por zonas de cisalhamento regionais importantes e intrudidos por significante plutonismo de idade brasiliana (0.60 – 0.50 Ga) (BRITO NEVES; CORDANI, 1991; SANTOS *et al*., 1997; BRITO NEVES *et al*., 2000). Durante o Eopaleozóico, foi marcada por tectônica extensional que exibe diversas estruturas favoráveis à formação de depósitos minerais. A província é tida como parte de uma unidade muito maior, correlacionável à porção Pan-Africana do noroeste da África, por suas características litológicas e estruturais (BRITO NEVES *et al.*, 2001; MABESSONE, 2002; SANTOS *et al*., 2004; OLIVEIRA, 2008).

Caracterizada por uma longa, complexa e policíclica história geológica que resulta em uma variedade de compartimentações tectônicas, a Província Borborema, em seu embasamento, registra processos orogênicos e anorogênicos entre 3.5 e 0.51Ga. A orogenia neoproterozoica Brasiliana ocorreu de forma diacrônica pela província, mas com uma sequência de eventos similar, iniciando-se com um rifteamento continental e a formação de pequenos complexos vulcano-sedimentares e plutonicos (850 – 700 Ma); seguido por um extenso magmatismo cálcio-alcalino associado a subducção e formação de sequências metavulcanossedimentares pré e sin-colisionais (650 – 620 Ma); com plutonismo colisional entre 620 e 570 Ma; e, por fim, plutonismos pós-tectônicos e anorogênicos, soerguimentos e extrusões tectônicas (580 – 510 Ma) (BRITO NEVES *et al*. 2000; FETTER *et al*. 2000, 2003; KLEIN; MOURA, 2008).

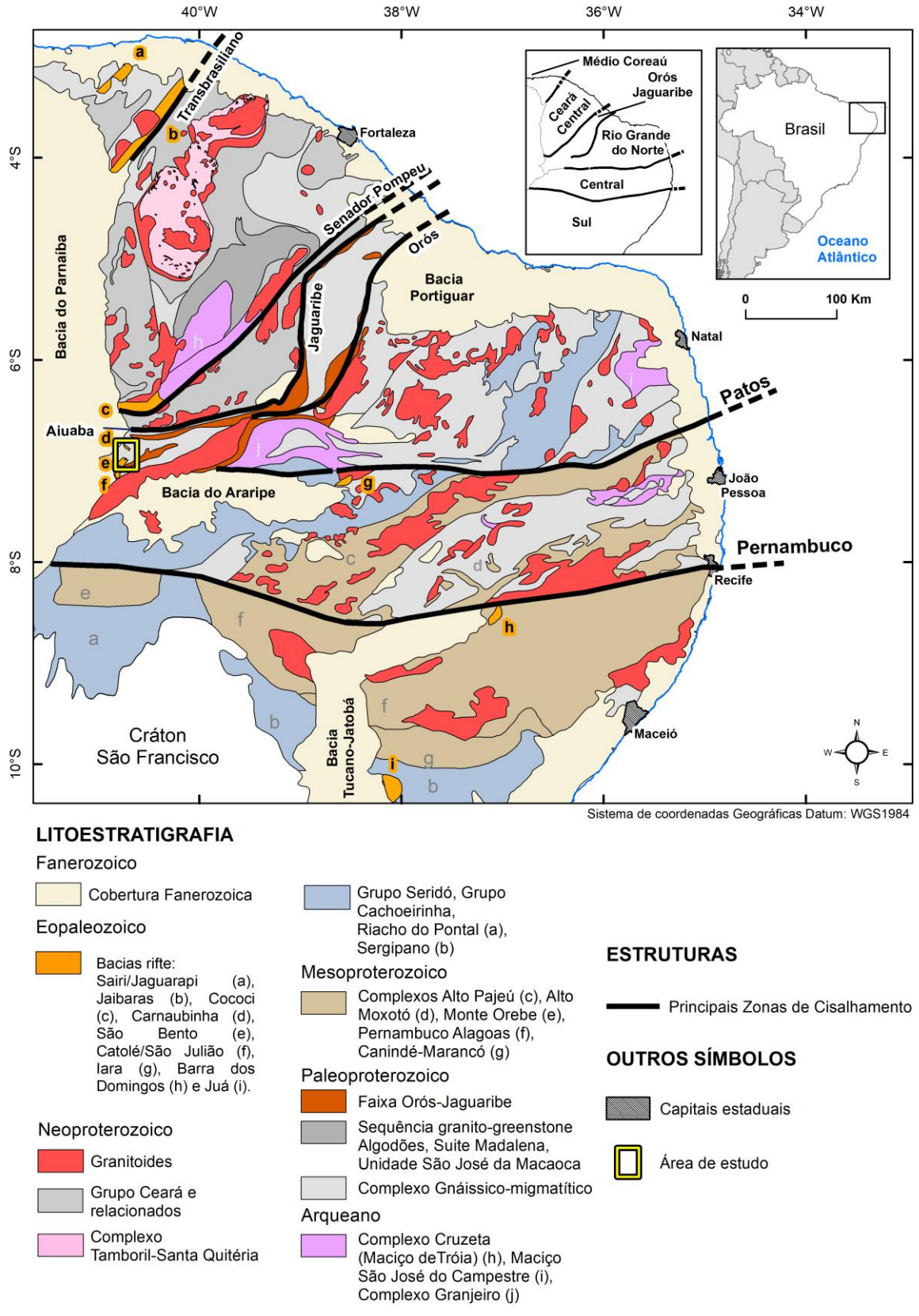

Figura 1. Configuração tectônica da Província Borborema (Fonte: Modificado de Parente *et al.*, 2014 e Medeiros, 2004).

Importantes zonas de cisalhamento delimitam a Província Borborema em três segmentos principais: Subprovíncias Setentrional, Zona Transversal (Central) e Sul (Externo) (DELGADO *et al*., 2003). Estas, por sua vez, são compartimentadas em domínios, terrenos e faixas de acordo com dados litoestratigráficos, estruturais e geocronológicos, além de assinaturas geofísicas. Brito Neves *et al*. (2000) propuseram a subdivisão da Província Borborema em cinco domínios tectônicos contínuos: i) Domínio Médio Coreaú (DMC); ii) Domínio Ceará Central (DCC); iii) Domínio Rio Grande do Norte (DRGN); iv) Domínio Zona Tranversal (DZT); e v) Domínio Sul ou Externo (DS).

O DMC está situado a norte da zona de cisalhamento Sobra-Pedro II (Lineamento Transbrasliano-Kandi) (Figura 1), e corresponde, provavelmente, a uma margem retrabalhada do Cráton São Luís/Oeste Africano. Consiste em um embasamento paleoproterozoico de rochas metamórficas de alto grau (Complexo Granja – ortognaisses TTG, granulitos e migmatitos) e seguimentos de sequências supracrustais neoproterozoicas (Faixa Martinópole-Ubajara – cinturões vulcano-sedimentares e sedimentos pelítico-carbonáticos), bem como granitoides pós orogênicos e a bacia rifte Jaibaras, que está situada ao longo do Lineamento Transbrasiliano (FETTER, 1999; BRITO NEVES *et al*., 2000; NOGUEIRA NETO, 2000; SANTOS *et al*., 2009).

O DCC é limitado pela zona de cisalhamento Sobral-Pedro II a noroeste, e pela zona de cisalhamento Senador Pompeu a sudeste, sendo coberto a sudoeste e oeste pelas rochas sedimentares da Bacia do Parnaíba (AMARAL, 2007) (Figura 1). Araújo *et al.* (2006) sugerem sua compartimentação em quatro unidades litotectonicas: um núcleo arqueano (Complexo Cruzeta – gnaisses TTG e greenstone belts); um embasamento paleoproterozoico (Grupo Novo Oriente – gnaisses tonalíticos a dioriticos); supracrustais paleoproterozoicas (Grupo Ceará – pelitos, wackes, quartzitos, mármores e calcissilicáticas) e um complexo granítico-migmatitico neoproterozoico a cambriano (Complexo Tamboril-Santa Quitéria – suíte de arco magmático continental) (FETTER, 1999; ARAÚJO, 2006). A bacia rifte Cococi se localiza ao longo da porção sudoeste da zona de cisalhamento Senador Pompeu.

O DRGN está localizado entre a zona de cisalhamento Jaguaribe-Tatajuba (OLIVEIRA; MEDEIROS, 2018) a oeste, e o Lineamento Patos, a sul. Os sedimentos costeiros da Bacia Potiguar e sedimentos cenozoicos cobrem seus limites a norte e a leste, respectivamente (Figura 1). Suas unidades correspondem aos terrenos Rio Piranhas, São José do Campestre e Granjeiro, e à Faixa Seridó (DELGADO et al., 2003). O terreno Rio Piranhas é formado por supracrustais e sequências metaplutônicas proterozoicas, enquanto os terrenos

Granjeiro e São José do Campestre consistem em núcleos arqueanos de metatonalitos-trondjemitos-granodioritos (TTG), rochas metamáficas com ortognaisses intercalados e plutonismo sienogranítico (DANTAS, 1997). A Faixa Seridó é uma sequência supracrustal de paragnaisses intercalados a mármores, xistos, quartzitos calcissilicáticas e metavulcânicas na base, seguidas por quartzitos e metaconglomerados com paragnaisses, xistos, wackes, mármores e metavulcanicas no topo (NASCIMENTO, 2000).

O Sistema Orós-Jaguaribe é uma faixa linear contínua de forma sigmoidal, limitada pela zona de cisalhamento Jaguaribe-Tatajuba a leste e a zona de cisalhamento Senador pompeu a oeste (OLIVEIRA; MEDEIROS, 2018). Seu embasamento é formado por dois blocos, Jaguaretama e São Nicolau, ambos formados por ortognaisses tonalíticos a trondhjemiticos e graníticos, geralmente bandados com porções migmatizadas. Este sistema é subdividido em duas sequências metavulcanossedimentares: Faixa Orós (xistos, quartzitos, mámores, calcissilicáticas, metabasaltos, metarriolitos, ortognaisses facoidais e porfiríticos) a oeste e a Faixa Jaguaribe (rochas ácidas piroclásticas, ortognaisses, diques dioríticos, xistos e quartzitos) a leste (PARENTE; ARTHAUD, 1995). Trabalhos mais recentes propõem a unificação da Faixa Orós-Jaguaribe e do Domínio Rio Grande do Norte em Domínio Seridó-Jaguaribe, argumentando a ausência de diferenças geológicas significativas entre os terrenos. Este então seria dividido em três estruturas maiores, denominados domínios São José do Campestre, a leste; Rio Piranhas-Seridó, na porção central, e Jaguaribeano, a oeste (HOLANDA *et al*., 2012; OLIVEIRA *et al.*, 2020). As áreas alvo deste estudo, representadas pelas bacias rifte Carnaubinha e São Bento, bem como seu embasamento ortognaissico, estão localizadas a oeste do Sistema Orós-Jaguaribe.

O Lineamento Patos, a norte, e o Lineamento Pernambuco, a sul, delimitam a Zona Transversal (DZT) (Figura 1). É representada por sequências turbidíticas (Grupo Cachoeirinha) com fácies proximais e distais; três terrenos (Alto Pajeú, Alto Moxotó e Rio Capibaribe) formados por sequências de rochas metavulcanossedimentares, metaplutônicas e graníticas (DELGADO *et al.,* 2003, VAN SCHMUS *et al*., 2011). A bacia rifte Iara está localizada em grabens delimitados pelo Lineamento Patos (PARENTE ; ARTHAUD, 2004; HUHN *et al*., 2011). O Domínio Sergipano (DS) está localizado a sul do Lineamento Patos e a norte do Cráton São Francisco, sendo composto por duas faixas de margem passiva (Riacho do Pontal e Sergipana) e três terrenos (Pernambuco-Alagoas, Paulistana-Monte Orebe e Canindé-Marancó) formados principalmente por sequências metavulcanossedimentares e, ocasionalmente, rochas metaplutônicas ultramáficas, além de suítes brasilianas de alto a médio potássio (DELGADO

et al., 2003).

3.2 Bacias Rifte da Província Borborema

As bacias rifte neste contexto foram formadas no chamado estágio transicional. De acordo com Teixeira *et al*. (2004), este pode ser definido de maneira simples como o fechamento final de uma bacia oceânica em consequência de colisão continental, completando o Ciclo de Wilson. Os mesmos autores também se referem a este como "molássico", embora o emprego deste termo seja inadequado. Inicialmente usado para designar sequências de bacias antearco alpinas, seu conceito se relaciona apenas com as características deposicionais da fácies sedimentar e não apresenta conotações tectônicas.

Parente *et al.* (2004) descrevem a existência de diversas bacias rifte eofanerozóicas ao longo da província Borborema (Figura 1), compostas por sequências clásticas imaturas, representadas por conglomerados, arenitos e folhelhos, apresentando mudanças gradacionais entre si, com possível associação a magmatismo bimodal. Os autores descrevem que essas bacias podem ser agrupadas de acordo com suas associações litológicas e ambientes tectonoestratigráficos em duas categorias diferentes, baseados na classificação de Brito Neves (1988): i) aquelas desenvolvidas ao longo de zonas de cisalhamento ou lineamentos tectônicos, como as de interesse para este estudo; e ii) bacias antearco e intra-arco.

Zonas de cisalhamento transcorrentes de direção NE-SW geralmente controlam a formação das bacias rifte na Província Borborema, por exemplo: i) Jaibaras – delimitadas pelos lineamentos Sobral-Pedro II a sul e Café-Ipueiras a oeste; ii) Cococi – delimitada pela zona de cisalhamento Senador Pompeu; e iii) Catolé/São Julião – delimitada pela zona de cisalhamento Tatajuba (PARENTE *et al.,* 2004). Parente *et al.* (2004) denominaram as associações sedimentares dessas bacias em Alfa Inferior e Alfa Superior, separadas por uma discordância erosiva. Elas são caracterizadas como produtos da progradação de leques deltaicos em corpos lacustres ou possivelmente mares rasos, onde podem estar associadas a material vulcânico e produtos de fluxo detrítico subaéreo.

As bacias Jaibaras, Cococi, Carnaubinha e São Bento apresentam similaridades importantes, como a presença de uma sequência clástica imatura, a ocorrência de sulfetos de cobre associados a rochas sedimentares e seu embasamento (MAAS *et al.,* 2003; MACHADO, 2006; PARENTE *et al*., 2011). Devido à sua importância para esta pesquisa, elas se encontram resumidamente descritas abaixo.

3.2.1 Bacia Jaibaras

A bacia é formada por rochas do Grupo Jaibaras, cujas sequências estão distribuídas em: i) Alfa Inferior – representada pelas formações Massapê, Pacujá e Parapuí; e ii) Alfa Superior – composta pelas formações Parapuí e Aprazível. Alterações hidrotermais afetam as rochas da bacia de forma penetrativa ou canalizada e comumente estão associadas a ocorrências de cobre e ferro.

A Formação Massapê compõe a base do Grupo Jaibaras e ocorre em uma porção restrita da bacia, geralmente associada à falha Café-Ipueiras (PEDROSA JUNIOR, 2015). É representada por conglomerados e brechas polimíticos, matriz suportada com clastos de tamanhos variando de seixo a calhau e composição variada indicando fontes proximais (GARCIA *et al*., 2018). A Formação Pacujá é formada por arenitos micáceos finos a médios intercalados a material pelítico e conglomerados. Representa a porção distal da Formação Massapê, ocorrendo principalmente na porção central do rifte (PARENTE *et al*., 2004; GARCIA *et al*., 2018). Essa assembleia sedimentar é interpretada como um ambiente fluvial em transição para um delta e, em sua porção distal, para um lago (OLIVEIRA, 2001).

A Formação Aprazível, similarmente a Formação Massapê, contém brechas e conglomerados polimíticos de matriz suportado, cujos clastos correspondem a fragmentos líticos das formações subjacentes e do embasamento cristalino. Isso assinala uma discordância erosiva com as unidades inferiores (GARCIA *et al*., 2018), associada a um possível pulso tectônico que impulsionou a subsidência da bacia (OLIVEIRA, 2001). As rochas magmáticas ocorrem adjacentes e no interior da bacia e são representadas pelas suítes graníticas Mucambo e Meruoca; pela Suíte Parapuí (fluxos de lava e rochas piroclásticos), e a Suíte Aroeira (subvulcânicas intermediárias a félsicas) (GARCIA et a., 2018).

Diferentes tipos de alteração hidrotermal estão associados à sequência vulcanossedimentar. Parente *et al*. (2011) descrevem alteração potássica, propilítica e hidrolítica nas bordas dos granitoides da bacia (Mucambo e Meruoca), epidotização, propilitização e hematitização nas rochas vulcânicas e nas brechas tectônicas. Óxidos de ferro e sulfetos de cobre associados às brechas tectônicas silicosas, originadas de riolitos, granitos, basaltos e arenitos caracterizam a mineralização (PARENTE et al., 2011).

3.2.2. Bacia Cococi

Localizada no Domínio Ceará Central (Figura 1), é representada pelo Grupo Rio

Jucá, que envolve as formações Angico Torto e Cococi. Representam a sequência Alfa Inferior. Repousando em discordância sobre essas formações, tem a Formação Melancia que corresponde parte da sequência Alfa Superior (PARENTE *et al*., 2004). Brechas hidrotermais, algumas mineralizadas em cobre, são comuns nesta bacia.

A unidade basal é representada pela Formação Angico Torto, formada por brechas e conglomerados arcosianos, de matriz suportado, cujos clastos correspondem a granitos, basaltos, gnaisses e milonitos. São encontrados predominantemente na borda da bacia, mas progradam lateralmente para arenitos e siltitos em direção ao centro da bacia, (GOMES; VASCONCELOS, 2000). Grande parte das brechas conglomeráticas exibe alterações hidrotermais do tipo quartzo-albita-carbonato, sericita-clorita-quartzo e hematitização associada a mineralização de sulfetos de cobre (MACHADO, 2006)

A Formação Cococi predomina ao longo da bacia, é formada por rochas pelíticas basais com estratificação plano-paralela e cores variando entre avermelhado e arroxeado, além de arenitos arcosianos no topo (GOMES; VASCONCELOS, 2000). A Formação Melancia consiste em brechas e conglomerados tipo clasto suportado, cujos clastos pertencem às unidades inferiores, semelhante à Formação Aprazível (Grupo Jaibaras). Ocorrem ainda arenitos finos, siltitos e pelitos na sua porção superior (GOMES; VASCONCELOS, 2000), sublinhando o final do ciclo de deposição erosivo. Santos Filho *et al*. (2015) enfatizam a ocorrência de rochas vulcânicas bimodais, básicas e ácidas, além de rochas vulcanoclásticas nos limites da bacia. Com base em sua extensão e em dados geofísicos, Santos Filho *et al* (2015) denominaram esta associação vulcânica de Formação Miranda.

3.2.3 Bacia Carnaubinha

Esta é uma pequena bacia disposta ao longo de um rifte de direção NW-SE sobre as rochas do Grupo Orós e Complexo São Nicolau, inserida no Domínio Rio Grande do Norte (Figura 1). Sua litoestratigrafia foi melhor definida apenas em estudos mais recentes por Saraiva e Rodrigues (2018) que descreveram duas unidades para as rochas da bacia: (1) Unidade Sedimentar composta por conglomerados polimiticos imaturos, variando entre grão e matriz suportado, e cores esverdeadas a arroxeadas, que podem ser intercalados por lentes de arenitos e siltitos ou folhelhos; e (2) Unidade Vulcânica caracterizada por diques vulcânicos ácidos que cortam a unidade sedimentar, e bastante hidrotermalizados.

A alteração hidrotermal é também intensa nas rochas da bacia e no embasamento adjacente, tem caráter multifásico, marcado por alterações potássica, calci-sódica e

silicificação, que é a mais pervasiva. Esta última comumente se associa à presença de mineralização de óxidos de ferro e sulfetos de cobre, que são hospedadas pelas rochas sedimentares da bacia e aos metarriolitos do embasamento (SARAIVA; RODRIGUES, 2018).

3.2.4 Bacia São Bento

A Bacia São Bento também está inserida no Domínio Rio Grande do Norte (Figura 1), localizando-se a sul da bacia Carnaubinha. Consiste em uma área pouco estudada, embora apareça cartografada nas folhas geológicas Fronteiras e Pio IX produzidas pela CPRM (Serviço Geológico do Brasil). Uvula e Didoné (2019) realizaram mapeamento geológico de semidetalhe na área da bacia e, segundo os autores, ela é formada por três calhas tectônicas paralelas entre si com direção preferencial SE-NW. Essas calhas são preenchidas por conglomerados polimíticos que exibem uma gradação entre clasto suportado com seixos variando de centimétricos a métricos na primeira calha, a oeste, até matriz suportada com seixos predominantemente centimétricos na última calha, a leste. Os clastos exibem composição variando entre granitos, riolitos, metasiltitos e arenitos, litotipos que compõem a Faixa Orós, embasamento da bacia (UVULA; DIDONÉ, 2019). Estes autores destacam ainda a presença de mineralizações de sulfetos de cobre e ferro disseminados nas bordas da bacia, associados à alteração silico-hematitica.

4 SÍNTESE BIBLIOGRÁFICA SOBRE OS DEPÓSITOS IRON OXIDE-COPPER-GOLD (IOCG).

A descoberta do depósito de Olympic Dam, no sul da Austrália em 1975, pela *Western Mining Corporation* despertou um interesse mundial em depósitos ricos em óxidos de ferro com sulfetos de cobre e ferro associados, em especial por apresentarem teores significativos de Cu e outros elementos como Au, Ag, U, ETRs, Co, Ni, Pd, Nb e P; e por não se encaixarem em nenhuma das classes de depósitos até então conhecidas (ROBERTS; HUDSON, 1983). A partir dos estudos de Hitzman *et al*. (1992) sobre depósitos de Olympic Dam e Redbank (Australia), Yukon e GreatBear (Canadá), Kiruna (Suécia) e Baya Obo (China), foi definida uma nova classe de depósitos hidrotermais chamada de Iron Oxide-Copper-Gold (IOCG) e sua subclasse tipo-Kiruna (Hitzman, 1992).

Desde então, diversos novos depósitos IOCG foram descobertos e alguns depósitos já conhecidos foram reclassificados, de modo que essa classe de depósitos representa algumas das mais importantes fontes mundiais de Cu-Au e outros elementos como U, Ag, Bi, Mo, ETRs

e Co (SKIRROW *et al*., 2019). As características chaves para classificação desses depósitos são, sucintamente: (i) Mineralização de cobre e, subordinadamente, ouro, com teores econômicos ou não; (ii) Mineralização hidrotermal com forte controle estrutural, associada a brechas, veios e/ou zonas de substituição; (iii) Abundância de óxidos de ferro (magnetita e hematita) com baixos teores de titânio; (iv) Enriquecimento em ETRs leves; (v) Ausência de relação espacial com intrusões ígneas, podendo haver relação temporal (HITZMAN *et al.*, 2000; WILLIAMS *et al*., 2005).

Com relação ao ambiente tectônico, Groves *et al*. (2010) destacam que a maior parte dos depósitos IOCG estão localizados em margens cratônicas arqueanas a paleo-mesoproterozoicas (Figura 2), e outros, como os depósitos de Candelaria e Manto Verde, de idades fanerozoicas, estão associados ao ambiente de arco magmático na cordilheira andina. Dessa forma, os depósitos pré-cambrianos seriam formados em ambientes extensionais, anorogênicos e limites de blocos litosféricos, enquanto os fanerozoicos ocorrem em limites convergentes, associados a zonas distais de colapso orogênico e bacias de retro-arco (GROVES *et al*., 2010). Os mesmos autores sugerem ainda uma subdivisão dos IOCG em cinco subgrupos (1) IOCG *sensu strictu*; (2) Depósitos de óxido de Fe rico em P; (3) Depósitos carbonatito-óxido de Fe e elementos litófilos; (4) Cu-Au pórfiro e Fe-skarn; (5) Substituição de alto grau de magnetita Au± Cu.

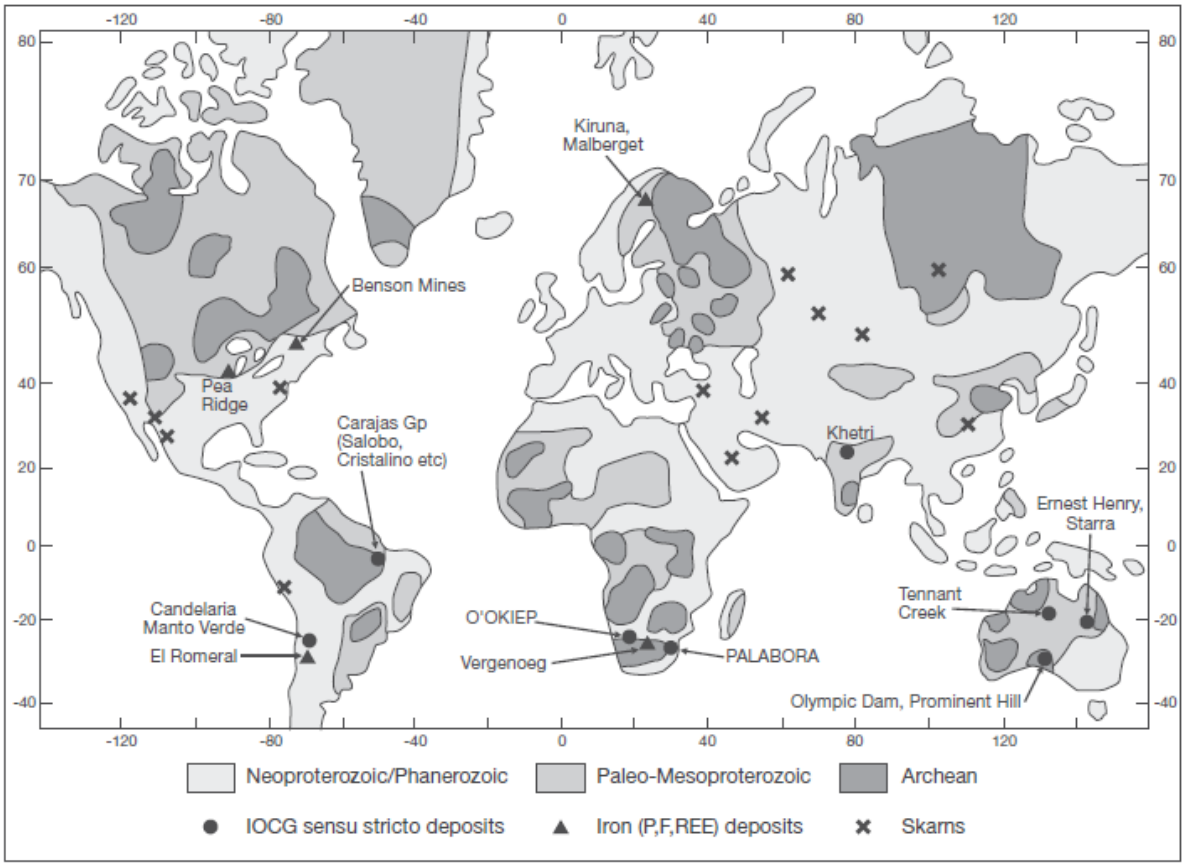

Figura 2 Distribuição geográfica dos depósitos com recursos maiores que 100t agrupados em IOCG sensu stricto, Óxido de ferro (P, F, ETR) e Skarn por Groves *et al.* (2010). A distribuição dos depósitos é apresentada em relação à posição dos Crátons Arqueanos e Paleo-Mesoproterozóicos apresentados por Artemieva e Mooney (2001). Fonte: Groves *et al*. 2010.

Esses depósitos ocorrem nas mais variadas associações geológicas e são hospedados tanto por rochas cristalinas como siliciclásticas. Em contrapartida, sempre ocorrem condicionados por controle estrutural, como grandes zonas de cisalhamento, zonas de falha ou contatos tectônicos (HITZMAN *et al*., 1992). Associado aos depósitos IOCG, tem-se a presença de zonas de alteração hidrotermal regionais, cuja intensidade e estilo são características chave na distinção entre estes depósitos e outros sistemas mineralizantes (BARTON, 2014). Segundo Barton (2014), todos os Sistemas IOCG exibem intensa variação nos teores de Na-Ca-K(-Fe) associada a perdas e ganhos de Fe, Si e elementos menores. A alteração hidrolítica (ácida) é comum em muitos deles e as maiores mudanças composicionais de caráter regional são nos elementos K e Na, que se manifestam principalmente na assembleia dos silicatos, onde K-feldspato e biotita desenvolvem zonas de alteração potássica e o plagioclásio sódico e a escapolita caracterizam a alteração sódio-cálcica. Ainda segundo este autor, em muitas dessas áreas os feldspatos têm coloração marrom a avermelhada característica, devido à inclusão de pequenos cristais de hematita, alteração “red rock”, como descrito por Wenner e Taylor (1987)

e Williams (1994) (BARTON, 2014). A alteração Na-Ca tende a se desenvolver, de forma extensiva, em regiões mais profundas e distais em relação à mineralização, enquanto a alteração potássica é mais tardia e ocorre em níveis intermediários a rasos. A alteração ácida ocorre nos níveis mais superficiais (HITZMAN *et al.*, 2000; WILLIAMS *et al*., 2005).

Embora exista amplo conhecimento acerca das características que compõem depósitos IOCG, não existe ainda consenso acerca dos mecanismos responsáveis por sua origem e formação. Diferentes modelos genéticos foram propostos, sendo a fonte dos fluidos mineralizantes a principal controvérsia entre os pesquisadores. Williams *et al*. (2005) classificam esses modelos em dois grupos, sendo que o primeiro envolve fontes magmáticas e, no segundo, os fluidos são não-magmáticos. Segundo Williams *et al*. (2005), os modelos magmáticos envolvem a formação de fluidos metalíferos, oxidados, pobres em enxofre e coevos ao magmatismo e a sua fonte pode estar relacionada a magmas cálcio-alcalinos primitivos de ambientes intracratônicos ou arco magmático. Os modelos não magmáticos relacionam os fluidos à superfície terrestre, ou bacias rasas, ou fluidos evoluídos de ambientes metamórficos rasos a intermediários. As intrusões magmáticas seriam só agentes indutores do mecanismo de circulação dos fluidos (WILLIAMS *et al.*, 2005).

Pollard (2000) observou que muitos depósitos IOCG são resultado de mistura entre fluidos hidrotermais de origem magmática e fluidos superficiais meteóricos (Olympic Dam e TennantCreek) e bacinais de origem evaporítica (Candelaria). Segundo Pollard (2000), a incorporação de componentes da rocha hospedeira ou fluidos não-magmáticos é comum nesses depósitos, proporcionado pelos níveis profundos de geração dos fluidos. Estudos isotópicos e de inclusões fluidas corroboram para uma natureza híbrida desses fluidos mineralizantes (BARTON; JOHNSON, 2000; CHIARADIA *et al*., 2006; MONTEIRO *et al.*, 2008; XAVIER *et al*., 2008). Segundo Barton e Johnson (2004), os modelos genéticos para sistemas IOCG requerem fluidos relativamente oxidados, pobres em enxofre e salinos, e apesar das muitas variações possíveis, eles podem ser definidos em três categorias de acordo com a Figura 3, que resultam em diferentes configurações das zonas de alteração, mineralização e paragênese.

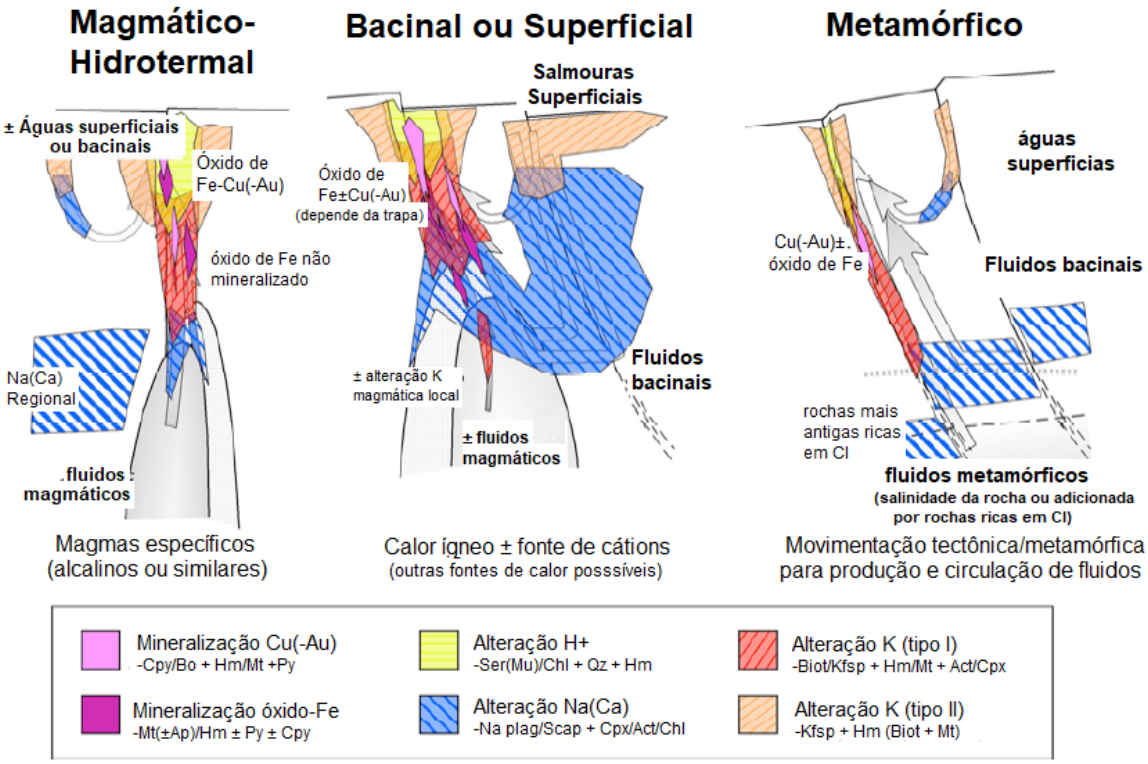

Figura 3 Ilustração esquemática da circulação dos fluidos e características hidrotermais dos modelos de formação para os depósitos IOCG (Modificado de Barton e Johnson, 2004).

No Brasil, a Província Mineral de Carajás apresenta a maior concentração de depósitos IOCG de classe mundial conhecidos, cujas idades vão desde o Neoarqueano (2.75 e 2.57 Ga; XAVIER *et al.*, 2012) ao Paleoproterozoico (2.0 e 1.88 Ga; MORETO *et al.*, 2015). Outros sistemas IOCG no país ocorrem na Província Borborema, região nordeste, como o prospecto Aurora (HUHN *et al*. 2011) e o depósito Riacho do Pontal (HUHN *et al*. 2014, 2018). Ambos têm a sua formação associada à Orogênese Brasiliana, idade neoproterozoica, apesar da ausência de dados geocronológicos. Observam-se, ainda, no oeste da Província Borborema, diversas ocorrências de cobre associadas às zonas de alteração e brechas hidrotermais em bacias rifte eopaleozoicas, relacionadas com possíveis sistemas IOCG por diferentes autores (MAAS *et al.*, 2003; MACHADO, 2006; PARENTE *et al.*,2011; SARAIVA; RODRIGUES, 2018; UVULA; DIDONÉ, 2019). A mineralização pós-data a sedimentação dessas bacias, cujo período de formação tem sido atribuído ao Cambro-Ordoviciano, ainda carece de dados geocronológicos específicos, sobretudo, quanto à idade da mineralização.

5 MÉTODOS

5.1 Revisão bibliográfica

Realizada em todas as etapas de desenvolvimento do presente trabalho, a pesquisa bibliográfica teve como foco os depósitos e sistemas minerais associados a IOCGs no mundo

todo. Além disso, houve enfoque na literatura acerca das alterações hidrotermais associadas, assembleia mineral características e assinaturas geoquímicas, além da mobilidade de elementos e a sua relação com os processos formadores da mineralização. Por fim, a pequisa bibliográfica também incluiu trabalhos acerca da química mineral de sulfetos, com enfoque em piritas associadas a depósitos minerais de cobre e ferro.

5.2 Petrografia

Foi realizado o estudo petrográfico de 24 lâminas delgadas confeccionadas a partir de amostras coletadas em campo, com o objetivo de se determinar a assembleia mineral característica das diferentes ocorrências minerais e alterações hidrotermais que afetam as rochas da região das bacias de Carnaubinha, São Bento e embasamento da região de Pio IX.

5.3 Análise geoquímica de rocha total

Foram analisadas 12 amostras coletadas em campo, preparadas e analisadas pelo laboratório ALS Brasil Ltda. Os processos de preparação envolveram britagem, moagem, pulverização e quarteamento e as análises performadas foram (i) fusão com borato de lítio e determinação por FRX (fluorescencia de raios x), (ii) calcinação para determinação de perda ao fogo *(LOI – lost on ignition*), e (iii) digestão com água régia e determinação por ICP-MS (Espectrometria de Massa por Plasma Acoplado Indutivamente).

5.4 Tratamento dos dados geoquímicos

Além das 12 análises químicas realizadas para essa pesquisa, foram utilizados os dados geoquímicos de 9 amostras do relatório da Folha Pio IX (PARENTE *et al*., 2014) que integram, em parte, dados referentes a área de interesse, totalizando 21 amostras. Esses dados foram compilados, tratados e processados no software *ioGAS*^{TM} para interpretação e análise de mobilidade dos elementos nas alterações hidrotermais através de diagramas *biplots*.

Ao se trabalhar com dados geoquímicos como os aqui utilizados, têm-se o *closure effect*, um fenômeno inerente a dados dessa natureza e ocorre porque os dados composicionais expressam apenas dados relativos que não representam um todo, sendo limitados por uma constante (e.g. 100%) (AITCHISON, 1986). Esse tipo de dado pode produzir fatores irreais e tendenciosos, forçando a correlação entre variáveis. O método de análise de dados composicionais logratio (AITCHINSON, 1986) permite que esses dados sejam expressos como números reais (e.g. Euclidianos). Na transformação *centred logratio (clr*) (Equação 1), a transformação dos dados fechados em dados abertos e isométricos se dá através da média

geométrica de todas as partes (i.e., componentes composicionais) como divisor das variáveis, seguida pela transformação logarítmica das razões (AITCHINSON, 1986), por meio da seguinte equação:

$clr(x) = zi = \log xi/g(XD) \quad (i = 1; \ldots ; D)$ (equação 1)

D é o número de componentes para um vetor composicional x.

A referida equação foi aplicada aos dados geoquímicos aqui utilizados, resultando em coordenadas isométricas úteis para análise de diagramas bivariantes e cálculo de Componentes Principais (Principal Component Analysis – PCA).

Razões molares de elementos (MERs) foram também adotadas para representar os efeitos de transferência de massa associados a alterações hidrotermais (PEARCE 1968; STANLEY; MADIESKY 1994; STANLEY, 2017). O uso de MER permite uma investigação das rochas em termos de seus minerais constituintes e elimina *o closure effect* (PEARCE 1968; STANLEY; MADIESKY 1994; STANLEY, 2019).

O método PCA (Principal Component Analysis – PCA) é um método de análise de dados multivariada que tem como objetivo reduzir o número de variáveis necessárias para descrever a variação observada num conjunto de dados, por meio de combinações lineares das variáveis (componentes), que descrevem a distribuição dos dados (GRUNSKY, 2001). Para o presente estudo, utilizou-se o modo RQ para PCA (ZHOU *et al*., 1983), aplicados através do software ioGAS^{TM,} cuja vantagem consiste em apresentar os *loadings e scores* (coordenadas) das componentes principais e das variáveis (elementos) e objetos (amostras) na mesma escala, permitindo assim observar amostras correlacionadas e afinidade geoquímicas entre as variáveis (GRUNSKY, 2010). Dessa forma, os dados podem ser apresentados em *biplots*, onde a proximidade das amostras com um ou mais elementos reflete seu enriquecimento no(s) tal(is) em relação as amostras mais distantes, permitindo comparar a assinatura geoquímica de diferentes alterações hidrotermais.

5.5 Química mineral

As microsanálises foram realizadas em piritas de 4 lâminas delgadas polidas no Laboratório de Microscopia e Microanálises – LMic do Departamento de Engenharia Geológica (DEGEO), Escola de Minas (UFOP). A Microssonda eletrônica - JXA8230 (Jeol) operou com tensão de 20kV, corrente de feixe de 40nA e spots de 5nm. Imagens de elétrons retro-espalhados (BSE) foram obtidas em todos os grãos analisados. Foram analisados os elementos Fe, S, Au,

As, Se, Zn, Te, Sb, Ag, Bi, Cu, Ni, Sn, Co, Mn, Mo e Hg. Os resultados são apresentados na forma de boxplots.

6 CONSIDERAÇÕES FINAIS

Os resultados deste trabalho são apresentados na forma de um artigo preliminar (Apêndice A), que foi submetido para publicação no periódico científico Brazilian Journal of Geology.

REFERÊNCIAS

AITCHINSON, J. **The Statistical Analysis of Compositional Data**. London: Chapman & Hall Ltd, 1986.

ALMEIDA, F.F.M. *et al*. Brazilian structural provinces: an introduction. **Earth-science Reviews**, Amsterdam, v. 17, n. 1-2, p.1-29, 1981.

ARAÚJO, C. E. G. **Mapeamento Lito-estrutural de Uma Porção a NW do Arco Magmático de Santa Quitéria, região de Caracará-CE, auxiliado por Técnicas de Sensoriamento Remoto.** Monografia de Graduação em Geologia – Universidade Estadual de Campinas, Campinas, 2006.

ARTHAUD, M. *et al.* Geology of Northern Borborema Province, NE Brazil and its correlation with Nigeria, NW Africa. **Geological Society**, v. 294, p. 49-67, 2008.

BARTON, M. D. **Iron Oxide(–Cu–Au–REE–P–Ag–U–Co) Systems**. Tucson: University of Arizona, Elsevier Ltd., 2014.

BRITO NEVES, B. B.; SCHMUS, W. R. V.; FETTER, A. H. Noroeste da África – Nordeste do Brasil (Província Borborema) Ensaio comparativo e problemas de correlação. **Revista do Instituto de Geociências – USP**, v. 1, p. 59-78, 2001.

BRITO NEVES, B. B. *et al*. Tectonic history of the Borborema Province, northeastern Brazil. *In*: **Tectonic Evolution of South America**, v. 1, p. 151-182, 2000.

BRITO NEVES, B. B. The Cambro-Ordovician of the Borborema Province. **Boletim IG - Série Científica**, v. 29, p. 175-193, 1998.

BRITO NEVES, B.B.; CORDANI, U.G. Tectonic Evolution of South America during the Late Proterozoic. **Precambrian Research**, v. 53, p. 23-40, 1991.

CHIARADIA, M. *et al*. Origin of fluids in iron oxide–copper–gold deposits: constraints from δ37Cl, 87S/86Sr and Cl/Br. **Mineralium Deposita**, v. 41, p. 565–573, 2006.

DANTAS, E. L. *et al*. Archean accretion in the Caldas Brandão Massif, Borborema Province, Northeast Brazil. **Revista Brasileira de Geociências**, v. 28, n. 2, p. 221-228, 1997.

DELGADO, I. M. *et al*. Geotectônica do Escudo Atlântico. *In*: BIZZI, L. A. *et al*. **Geologia, Tectônica e Recursos Minerais do Brasil: Textos, Mapas & SIG**. Brasília: CPRM, 2003, p. 227-334.

FETTER, A. *et al.* Evidence for Neoproterozoic continental arc magmatism in the Santa Quitéria Batholith of Ceará State, NW Borborema Province, NE Brazil: Implications for the assembly of West Gondwana. **Gondwana Research**, v. 6, n. 2, p. 265-273, 2003.

FETTER, A. H. *et al.* U-Pb and Sm-Nd Geochronological constraints on the crustal evolution and basement architecture of Ceará State, NW Borborema Province, NE, Brazil: Implications for the existence of the paleoproterozoic supercontinent "Atlantica". **Revista Brasileira de Geociências**, v. 30, n. 1, p. 102-106, 2000.

FETTER, A. H. **U/Pb and Sm/Nd geochronological constraints on the crustal framework and geologic history of Ceará state, NW Borborema province, NE Brazil:** implications for the Assembly of Gondwana. 164 p. il. Tese de Doutorado - Departamento de Geologia, Universidade de Kansas, Kansas, 1999.

GANADE DE ARAÚJO, C. E.; WEINBERG, R. F.; CORDANI, U. G. Extruding the Borborema Province (NE-Brazil): A two-stage Neoproterozoic collision process. **Terra Nova**, v. 26, n. 2, p. 157-168, 2014.

GOMES, J. R. C.; VASCONCELOS, A. M. **Jaguaribe SW: folha SB.24-Y:** estados do Ceará, Pernambuco e do Piauí. Programa Levantamentos Geológicos Básicos do Brasil – PLGB. Rio de Janeiro: CPRM – Serviço Geológico do Brasil, 2000.

GRANT, J. A. The isocon diagram; a simple solution to Gresens' equation for metasomatic alteration. **Economic Geology**, v. 81, p. 1976-1982, 1986.

GRESENS, R. L. Composition-volume relationship of metasomatism. **Chemical Geology**, v. 2, p. 47-65, 1967.

GROVES, D. I.; BIERLEIN, F. P.; MEINERT, L. D.; HITZMAN, M. W. Iron Oxide Copper-Gold (IOCG) deposits through Earth history: Implications for origin, lithospheric setting, and distinction from other epigenetic iron oxide deposits. **Economic Geology**, v. 105, n. 3, p. 641-654, 2010.

GRUNSKY, E. C. The interpretation of geochemical survey data. **Geochemistry: Exploration, Environment, Analysis**, v. 10, n. 1, p. 27-74, 2010.

GRUNSKY, E. C.; SMEE, B. W. The differentiation of soil types and mineralization from multi-element geochemistry using multivariate methods and digital topography: **Journal of Geochemical Exploration**, v. 67, p. 287–299, 1999.

HITZMAN, M. W. Iron Oxide-Cu-Au deposits: What, where, when, and why. *In*: **Hydrothermal iron oxide copper-gold and related deposits: A global perspective**, v. 1, p. 9-25, 2000.

HITZMAN, M. W.; ORESKES, N.; EINAUDI, M. T. Geological characteristics and tectonic setting of Proterozoic iron oxide (Cu-U-Au-LREE) deposits. **Precambrian Research**, v. 58, p. 241–287, 1992.

HOLLANDA, M. H. B. M. **Geocronologia de eventos magmáticos e mineralizações associadas no Precambriano da Faixa Seridó, Província Borborema**. São Paulo: Instituto de Geociências e Astronomia, Universidade de São Paulo, 2012. 94 p. Tese de Livre Docência.

HUHN, S. R. B. *et al.* Caracterização geológica do prospecto de Óxido de Ferro-Cobre-Ouro (IOCG), Aurora, Ceará, Brasil. **Revista Brasileira de Geociências**, v. 41, n. 3, p. 523-538, 2011.

HUHN, S. R. B. *et al*. Geology of the Riacho do Pontal iron oxide copper-gold (IOCG) prospect, Bahia, Brazil: hydrothermal alteration approached via hierarchical cluster analysis. **Brazilian Journal of Geology**, v. 44, n. 2, p. 309-324, 2014.

HÜHN, S. R. B.; SILVA, A. M. Favorability potential for IOCG type deposits in the Riacho do Pontal Belt: new insights for identifying prospects of IOCG-type deposits in NE Brazil. **Brazilian Journal of Geology**, v. 48, n. 4, 2018.

JANOUŠEK, V.; FARROW, C. M.; ERBAN, V. Interpretation of whole-rock geochemical data in igneous geochemistry: introducing Geochemical Data Toolkit (GCDkit). **Journal of Petrology**, v. 47, p. 1255-1259, 2006.

JOHNSON, D. A.; BARTON, M. D. Time-Space Development of an External Brine-

Dominated, Igneous-Driven Hydrothermal System: Humboldt Mafic Complex, Western Nevada, Part I. *In*: DILLES, J. H.; BARTON, M. D.; JOHNSON, D. A.; PROFFETT, J. M.; EINAUDI, M. T. (Eds.). **Contrasting Styles of Intrusion-Associated Hydrothermal Systems: Guidebook Series**, Vol. 32. Society of Economic Geologists, p. 127-144, 2000.

KLEIN, E. L.; MOURA, C. A. V. São Luís craton and Gurupi belt (Brazil): possible links with the West-African craton and surrounding Pan-African belts. *In*: PANKHURST, R. J.; TROUW, R. A. J.; BRITO NEVES, B. B.; DE WIT, M. J. (Eds.). **West Gondwana: pre-Cenozoic correlations across the South Atlantic region**. Geological Society London, Special Publications 294, p. 137-151, 2008.

LARGE, R. R.; GEMMELL, J. B.; PAULICK, H.; HUSTON, D. L. The alteration box plot: A simple approach to understanding the relationship between alteration mineralogy and lithogeochemistry associated with volcanic-hosted massive sulfide deposits. **Economic Geology**, v. 96, n. 5, p. 957-971, 2001.

MAAS, M. V. R. **Integração de dados de geofísica aérea e geologia aplicada a exploração mineral no setor sudoeste do cinturão cuprífero Orós-Jaguaribe – Província Borborema**. Dissertação (Mestrado) - Instituto de Geociências, Universidade de Brasília, Brasília, 2003.

MABESSONE, J. M. História Geológica da Província Borborema (NE Brasil). **Revista de Geologia da UFC**, v. 15, p. 119-129, 2002.

MACHADO, M. A. **Caracterização descritiva e genética de ocorrências cupro-hematíticas no setor sudoeste do Sistema Orós-Jaguaribe Província Borborema**. Dissertação (Mestrado) - Instituto de Geociências, Universidade de Brasília, Brasília, 2006.

GARCIA, M. G. M.; PARENTE, C. V.; SILVA FILHO, W. F.; ALMEIDA, A. R. Age of magmatic events in the Eopaleozoic Jaibaras Basin, NE Brazil: Constraints from U-Pb zircon geochronology. **Journal of South American Earth Sciences**, Volume 84, 2018.

MEDEIROS, V. C. **Evolução Geodinâmica e Condicionamento Estrutural dos Terrenos Piancó-Alto Brígida e Alto Pajeú, Domínio da Zona Transversal, NE do Brasil**. Tese de Doutorado, Centro de Ciências Exatas e da Terra, Universidade Federal do Rio Grande do Norte, Natal, 2004.

MONTEIRO, L. V.; XAVIER, R. P.; DE CARVALHO, E. R.; HITZMAN, M. W.; JOHNSON, C. A.; DE SOUZA FILHO, C. R.; TORRESI, I. Spatial and temporal zoning of hydrothermal alteration and mineralization in the Sossego iron oxide-copper-gold deposit, Carajás Mineral Province, Brazil: paragenesis and stable isotope constraints. **Mineralium Deposita**, v. 42, p. 129-159, 2008.

MORETO, C. P. N.; MONTEIRO, L. V. S.; XAVIER, R. P.; CREASER, R. A.; DUFRANE, S. A.; TASSINARI, C. C. G.; SATO, K.; KEMP, A. I. S.; AMARAL, W. S. Neoarchean and Paleoproterozoic iron oxide-copper-gold events at the Sossego Deposit, Carajás Province, Brazil: Re-Os and U-Pb geochronological evidence. **Economic Geology**, v. 110, p. 809-835, 2015.

NASCIMENTO, M. A. L. **Petrologia do magmatismo Tardi-Brasiliano no Maciço São José de Campestre (RN/PB), com ênfase no Plúton Alcalino Caxexa**. Centro de Ciências Exatas e da Terra, Universidade Federal do Rio Grande do Norte, Natal, 2000.

NOGUEIRA NETO, J. A. **Evolução Geodinâmica das faixas granulíticas de Granja e Cariré, extremo noroeste da Província Borborema**. PhD Thesis, Instituto de Geociências e Ciências Exatas, Universidade Estadual Paulista, 2000.

OLIVEIRA, R. R.; VILALVA, F. C. J.; ALVES, A.; MEDEIROS, V. C.; DALAN, C. A. The Catolé do Rocha Batholith (RN-PB): A reduced A2-type granitic magmatism in the Rio Piranhas-Seridó Domain, Borborema Province, Northeastern Brazil. **Geologia USP Série científica**, v. 20, p. 166-190, 2020.

OLIVEIRA, R.; MEDEIROS, W. Deep crustal framework of the Borborema Province, NE Brazil, derived from gravity and magnetic data. **Precambrian Research**, v. 315, p. 45-65, 2018.

OLIVEIRA, R. G. de. **Arcabouço geofísico, isostasia e causas do magmatismo cenozóico da Província Borborema e de sua margem continental (Nordeste do Brasil)**. Tese (Doutorado) - Centro de Ciências Exatas e da Terra, Universidade Federal do Rio Grande do Norte, Natal, 2008.

OLIVEIRA, D. C.; MARTINS, G.; BRANCO, R. M. G. C. Um modelo alternativo para a formação da bacia do Jaibaras: implicações para a evolução final da cadeia brasiliana/pan-africana no noroeste da província Borborema. **Revista de Geologia da UFC**, Fortaleza, v. 14, n. 1, 2001.

PARENTE, C. V. *et al*. Contexto geológico, tipológico e geoquímico isotópico das brechas hidrotermalizadas de ferro e cobre tipo IOCG associadas à bacia Eopaleozóica Jaibaras, da Província Borborema, Brasil. *In:* FRANTS, J. C.; MARQUES, J. C.; HARDY, J. (Eds.). **Contribuições da Metalogenia do Brasil**. Vol. 1, p. 175-197, 2011.

PARENTE, C. V.; ARTHAUD, M. H. O. Geologia e tipologia do minério da ocorrência de Cu-Fe associada à Sequência Metavulcano-Sedimentar Cachoeirinha, região de Aurora-CE. **Revista de Geologia da UFC**, v. 17, n. 2, p. 157-172, 2004a.

PARENTE, C. V.; SILVA FILHO, W. F.; ALMEIDA, A. R. Bacias do estágio de transição do domínio setentrional da Província Borborema. *In*: MANTESSO NETO, V. *et al.* (Eds.). **Geologia do Continente Sul-Americano**: Evolução da obra de Fernando Flávio Marques de Almeida. São Paulo: Editora Beca, 2004. p. 525-536.

PARENTE, C. V.; ARTHAUD, M. H. O. Sistema Orós-Jaguaribe no Ceará, NE do Brasil. **Revista Brasileira de Geociências**, v. 25, n. 4, p. 297-306, 1995.

PEARCE, T. H. A contribution to the theory of variation diagrams. **Contributions to Mineralogy and Petrology**, v. 19, p. 142–157, 1968.

PEDROSA JUNIOR, N. **Interpretação e Modelagem de Dados Geofísicos no Estudo da Evolução Geotectônica do Rifte de Jaibaras – NE do Brasil**. Tese (Doutorado) – Instituto de Geociências, Universidade de Brasília, Brasília, 2015.

POLLARD, P. J. An intrusion-related origin for Cu-Au mineralization in iron oxide-copper-gold (IOCG) provinces. **Mineralium Deposita**, v. 41, p. 179-187, 2006.

POLLARD, P. J. Evidence of a magmatic fluid source for iron oxide-Cu-Au mineralisation. *In*: PORTER, T. M. (ed.). **Hydrothermal Iron Oxide Copper-Gold and Related Deposits**: A Global Perspective. Adelaide: PGC Publishing, 2000. p. 27–41.

ROBERTS, D. E.; HUDSON, G. R. T. The Olympic Dam copper-uranium-gold-silver deposit, Roxby Downs, South Australia. **Economic Geology**, v. 78, p. 799-822, 1983.

SKIRROW, R. G.; MURR, J.; SCHOFIELD, A.; HUSTON, D. L.; VAN DER WIELEN, S.; CZARNOTA, K.; COGHLAN, R.; HIGHET, L. M.; CONNOLLY, D.; DOUBLIER, M.; DUAN, J. Mapping iron oxide Cu-Au (IOCG) mineral potential in Australia using a

knowledge-driven mineral systems-based approach. **Ore Geology Reviews**, v. 113, 2019.

SANTOS FILHO, F. F. B.; MAGINI, C.; CASTELO BRANCO, R. M. G. Interpretação das Assinaturas Geofísicas Relacionadas a Estrutura da Bacia de Cococi e Mineralizações de Barita – SW do CE. **Revista de Geologia da UFC**, v. 28, n. 2, p. 79-100, 2015.

SANTOS, E. J. Ensaio preliminar sobre terrenos e tectônica acrescionária na Província Borborema. *In*: **CONGRESSO BRASILEIRO DE GEOLOGIA**, 39., Salvador. Anais. Salvador: SBG, 1996. v. 6, p. 47-50.

SANTOS, T. J. S.; GARCIA, M. G. M.; AMARAL, W. S.; CABY, R.; WERNICK, E.; ARTHAUD, M. H.; DANTAS, E. L.; SANTOSH, M. Relics of eclogite facies assemblages in the Ceará Central Domain, NW Borborema Province, NE Brazil: Implications for the assembly of West Gondwana. **Gondwana Research**, v. 15, p. 3-4, 2009.

SANTOS, T. J. S. *et al*. Structural and geochronological studies of the Médio Coreaú Domain, NE Brazil: Contraints on Brasiliano/Pan-African tectonic evolution in the NW part of the Borborema Province. **Journal of the Virtual Explorer**, v. 17, n. 9, p. 9, 2004.

SARAIVA, C. E. R.; RODRIGUES, T. F. R. **Mapeamento geológico e petrografia das ocorrências de cobre da Bacia de Carnaubinha, Pio IX - Piauí**. Monografia de Graduação em Geologia – Universidade Federal do Ceará, Fortaleza, 2018.

SILVA, J. G. F. da S.; CARNEIRO, L. de S. **Mapeamento geológico e das alterações hidrotermais associadas às ocorrências de ferro na região de Pio IX – PI**. Monografia de Graduação em Geologia – Universidade Federal do Ceará, Fortaleza, 2018.

STANLEY, C. R. Molar element ratio analysis of lithogeochemical data: a toolbox for use in mineral exploration and mining. **Geochemistry: Exploration, Environment**, Analysis, v. 20, p. 233–256, 2019.

STANLEY, C. R.; MADEISKY, H. E. Lithogeochemical exploration for hydrothermal ore deposits using Pearce element ratio analysis. *In*: **Geological Association of Canada. Short Course Notes 11**. Waterloo, 1994. p. 193–212.

UVULA, E. E.; DIDONÉ, M. E. Z. **Mapeamento Geológico E Petrografia Das Ocorrências De Cobre Na Bacia De São Bento, Extremo Leste Do Piauí-Pi.** Monografia de Graduação em Geologia – Universidade Federal do Ceará, Fortaleza, 2019.

VAN SCHMUS, W. R.; KOZUCH, M.; BRITO NEVES, B. B. Precambrian history of the Zona Transversal of the Borborema Province, NE Brazil: Insights from Sm–Nd and U–Pb geochronology. **Journal of South American Earth Sciences**, v. 31, p. 2–3, 2011.

VERÍSSIMO, C. U. V. *et al*. The Itataia phosphate-uranium deposit (Ceará, Brazil) new petrographic, geochemistry and isotope studies. **Journal of South American Earth Sciences**, v. 70, p. 115–144.

PARENTE, C. U. V. *et al*. **Carta geológica da folha Pio IX:** SB. 24-YA-VI. 2014.

WILLIAMS, P. J. *et al.* Iron oxide copper-gold deposits: Geology, space-time distribution, and possible modes of origin. **Economic Geology**, p. 371-405, 2005.

XAVIER, R. P.; WIEDENBECK, M.; TRUMBULL, R. B.; DREHER, A. M.; MONTEIRO, L. V. S.; RHEDE, D.; ARAÚJO, C. E. G.; TORRESI, I. Tourmaline B-isotopes fingerprint marine evaporites as the source of high-salinity ore fluids in iron oxide copper-gold deposits, Carajás Mineral Province (Brazil). **Geology**, v. 36, p. 743-746, 2008.

XAVIER, R. P.; MONTEIRO, L. V. S.; MORETO, C. P. N.; PESTILHO, A. L. S.; MELO, G. H. C.; SILVA, M. A. D.; AIRES, B.; RIBEIRO, C.; SILVA, F. H. F.; SILVA, L. V. *et al*. The iron oxide copper-gold systems of the Carajás mineral province, Brazil. **Society of Economic Geologists**, v. 16, p. 433-453, 2012.

ZHOU, D.; CHANG, T.; DAVIS, J. C. Dual extraction of R-mode and Q-mode factor solutions. **Journal of the International Association for Mathematical Geology**, v. 15, n. 5, p. 581-606, 1983.

APÊNDICE A: ARTIGO – Geology, petrography, geochemistry and pyrite chemistry of the hydrothermal copper occurrences from the Western Borborema Province.

Abstract

The Eopaleozoic extensional setting in Borborema Province displays many favorable structures and host rocks for the formation of mineral deposits. Previous studies describe the potential occurrence of copper deposits associated to iron oxides in different rift basins along Borborema Province, with special emphasis to those associated to quartz-hematite breccias in the basins of Carnaubinha/São Bento (Piauí State) and Jaibaras/Cococi (Ceará State). This research provides a characterization of the copper occurrences in Carnaubinha and São Bento Eopaleozoic basins and related basement, in the southwestern portion of Borborema Province, through petrological, geochemical and mineral chemistry data, aiming the establishment of a mineral system model for the key localities within the geodynamic framework of the Borborema. Hydrothermal alteration in the basement rocks of are Albite, K-feldspar, Epidote, Chlorite alterations, silicification and silica-hematite alteration, where the last two phases are associated to copper occurrences. In Carnaubinha basin, the alteration consists of k-feldspar, epidote and chlorite, silicification and silica-hematite are also associated to the presence of copper minerals. In São Bento basin, silicification is the main alteration; hematite alteration occurs; similarly, chlorite alteration; sulfide alteration is represented by pyrite, overprinted by silicification. Geochemistry data show that Cu-rich, silica-hematite breccias also contain high Cr, Mo, Ag, Ba, La and U, while high Cu-silica-sulfide breccias have high Co, Ni, Cd and Bi. The K/Al vs Na/Al diagram demonstrate a sodic affinity for the feldspar, epidote and silica-sulfide samples. The signature can be divided in: Co, Se, Ag, As, Bi and Sb for the silica-hematite alteration samples, and Ni, Cr, As and Cd (Be, Zn) for the silica-sulfide alteration. Pyrite chemistry for Carnaubinha and basement breccias have high Co/Ni ratios, majorly > 10 ppm, while for São Bento basin the ratios are predominantly < 2 ppm. Similarities in alteration styles and paragenetic sequence affecting Carnaubinha basin and basement rocks and geochemistry results demonstrate a similar signature for these alterations and copper occurrences indicate that these are part of a similar hydrothermal alteration system. In São Bento basin, alterations are incipient and the hydrothermal system is less evolved. Similarly, the pyrite chemistry results indicate that a higher magmatic-hydrothermal source of fluids for Carnaubinha basin and basement breccias, while São Bento pyrite indicate a sedimentary source with minor hydrothermal contribution. Compiled results indicate that the similar hydrothermal system affected in different stages the rocks of Orós mobile belt, its basement, and eopaleozoic basins.

1 Introduction

The Borborema Province (BP) has distributed in its territory about ten Eopaleozoic rift basins, controlled by transcurrent shear zones, related to the collapse of the Brasiliano Orogeny (600 Ma), and these have many copper and iron mineralization associated to hydrothermal breccias (Parente *et al*., 2004).

In the southeast portion of the BP, the region west to the Orós-Jaguaribe System has a long history of mineral exploration, as well as prospection for copper minerals. The interest in some of these occurences has increased due to their similarities with the world-class IOCG (iron-oxide-copper-gold) deposits (Machado, 2006). Since the discovery of Olympic Dam in Australia, such deposits have gained importance for the world production of copper, gold, uranium and other metals (Hitzman *et al*; 1992; Hitzman, 2000). They occur at fault zones related to orogenic collapse environments, mineralization takes place as breccias and stockworks, with intense hydrothermal alteration of the host rock that may have a magmatic, sedimentary or metamorphic origin (Hitzman, 2000).

Various authours discuss the potential of these occurrences to the west of the BP associated to rift basins, such as Maas *et al*. (2003), Machado (2006), Parente *et al*. (2011), Saraiva e Rodrigues (2018) and Uvula and Didoné (2019), and their basement - Silva e Carneiro (2018), Huhn *et al*. (2011) and Huhn *et al*. (2014). These authors describe the similarities of the targets and systems like IOCG, providing data on copper mineralization associated to quartz-hematite breccias, with focus on those associated to Jaibaras and Cococi (Ceará State), Carnaubinha and São Bento (Piauí state) basins, and the basement from the Orós Mobile Belt (OMB) in the region of Pio IX (Piauí state).

The several similarities in mineralization style, tectonic environment and hydrothermal alteration suggest that these occurrences may be part of the same regional scale mineral system. To confirm such hypothesis and provide a new exploration criterion to the region, it is necessary to compare hydrothermal alterations styles, geochemistry and mineralogy of the ore in the different mineralized areas.

This research provides new geological and geochemical data about the occurrences and hydrothermal alteration associated to the Carnaubinha and São Bento basins, as well as the Pio IX region OMB basement. This contribution discusses their possible origin and evolution, determining a temporal relation between their hydrothermal alteration and copper occurrences.

2 Geological Setting

The Borborema Province (PB) is an important Neoproterozoic orogenic belt, situated at the northeast portion of the South-American platform (Almeida *et al*., 1981). It consists in a fragment of extensive Brasiliano/Pan-African orogenic system. It includes the Parnaíba block and an Archean-Paleoproterozoic basement, culminating in the final amalgamation of the West Gondwana continent (Arthaud *et al*., 2008; Klein and Moura, 2008; Ganade *et al*., 2014). The BP configuration is characterized by an evolution through the agglutination of Archean crustal blocks to Paleoproterozoic gneissic-migmatitic complexes, superimposed by Neoproterozoic supracrustal sequences, subsequently separated by regional shear zones and intruded by Brasiliano-age plutonism (0.60 – 0.50 Ga) (Brito Neves; Cordani, 1991; Santos *et al*., 1997; Brito Neves *et al*., 2000). During the Eopaleozoic, the BP was marked by extensional tectonics, exhibiting many structures favorable to the formation of mineral deposits.

A long, complex and polycyclic history characterizes the BP, resulting in a varied tectonic compartmentation. Its basement registers anorogenic and orogenic processes that dates from 3.5 to 0.51 Ga. The Brasiliano Neoproterozoic orogeny occurred diachronically in the province, with a similar sequence of events, starting with continental rifting and the formation of small volcano-sedimentary and plutonic complexes (850 – 700 Ma); followed by an extensive calc-alkaline magmatism associated to subduction and the formation of metavolcanosedimentary, pre-collisional sequences (650 – 620 Ma); collisional plutonism between 620 to 570 Ma; and, finally post-tectonic and anorogenic plutonism, uplifts and tectonic extrusions (580 – 510 Ma) (Brito Neves *et al*. 2000; Fetter *et al.* 2000, 2003; Klein and Moura, 2008).

Important shear zones divide the BP in domains, terranes or belts. Brito Neves *et al.* (2000) proposed its subdivision into five continuum tectonic domains: i) Médio Coreaú Domain (DMC), ii) Ceará Central Domain (CCD), iii) Rio Grande do Norte Domain (RGND), iv) Zona Tranversal Domain (ZTD), and v) South Domain (SD) (Figure 1). Studies propose the unification of the Orós-Jaguaribe Belt to the Rio Grande do Norte Domain, arguing the absence of significant geological and geophysical differences between these terranes. Therefore, the RGND can thus be divided into three larger structures: São José do Campestre domains, to the east; Piranhas-Seridó River, in the central portion, and Jaguaribeano, to the west (Holanda *et al*., 2012; Oliveira and Medeiros, 2018; Oliveira *et al*., 2020).

The Orós-Jaguaribe belts (OJB) (Parente and Arthaud, 1995, Medeiros et al., 2008) are inserted in the RGND, comprising a sigmoidal structure, limited to the east by the Jaguaribe-Tatajuba and Senador Pompeu transcurrent shear zone to the west (Oliveira; Medeiros, 2018). It consists of two mobile belts, divided by two blocks of Paleoproterozoic tonalitic to trondhjemitic, banded orthogneisses with migmatized portions (Parente and Arthaud, 1995). To the west, the Orós Mobile Belt (OMB) is formed by schists, quartzites, marbles, calc-silicate rocks, metabasalts, matarhyolites and porphyritic orthogneisses. To the west, the Jaguaribe Mobile Belt is composed of acidic, pyroclastic rocks, orthogneisses, diorite dikes, schists and quartzites (Parente and Arthaud, 1995).

The studied area is located in the southwestern portion of the Orós Jaguaribe system. The Paleoproterozoic geological units (Figure 1) correspond to the São Nicolau and Jaguaretama basement complexes. The former predominates in the northern portion of the map, and consists of locally migmatized orthogneisses, with tonalitic to granodioritic compositions. It also encompasses the Orós Group, where the metasedimentary sequence corresponds to feldspathic schists with intercalated calc-silicatic rocks and calcitic to dolomitic marbles; the metavolcanic sequence is characterized by felsic (rhyolitic to dacitic) to mafic (basalt to andesites) rocks. Minor units correspond to Paleoproterozoic intrusive suites and Neoproterozoic migmatites (leucocratic granites and metagabbros). The Cambro-ordovician rocks are represented by the Rio Jucá Group that corresponds to the sedimentary sequences of the Carnaubinha and São Bento basins. The main lithological units consist of polymictic conglomerates, with intercalated sandstones and mudstones in the Carnaubinha basin; in the eastern portion an arkose sandstones unit with minor conglomerates predominate; and in the São Bento basin, a bimodal volcanic unit is mapped in the western portion. In the northwestern portion of the area, the Paleozoic Serra Grande Group outcrops, corresponding to the basal unit from the Parnaíba basin; it is composed of conglomeratic sandstones.

A polycyclic deformation of dominantly transcurrent nature affects the Orós System rocks in the area between the NE-SW-trending Aiuaba and Senador Pompeu shear zones (e.g., Parente et al. (2014). Kinematic indicators and low angle Sn near the contact between the São Nicolau Complex (west) and Orós Group (east) suggest the formation of a S shape transpressional zone, indicating a dextral movement. Such deformation is preserved in the orthoderived rocks of the region as a mylonitic to ultramylonitic texture (Parente and Arthaud, 1995). In the late phases of the Brasiliano orogeny, episodes of tectonic reactivation of the main structures are evidenced by the presence of pseudotachylyte in the big drag fold in

the Pio IX region and the formation of the Rift Basins, such as Carnaubinha and São Bento (Parente et al. 2014). Extensive hydrothermal alteration zoning associated with iron oxides and copper occurrences affect the rocks of São Nicolau Group (Silva and Carneiro, 2018), near NW-SE and NNE-SSW fault zones south of Pio IX city (Figure 1).

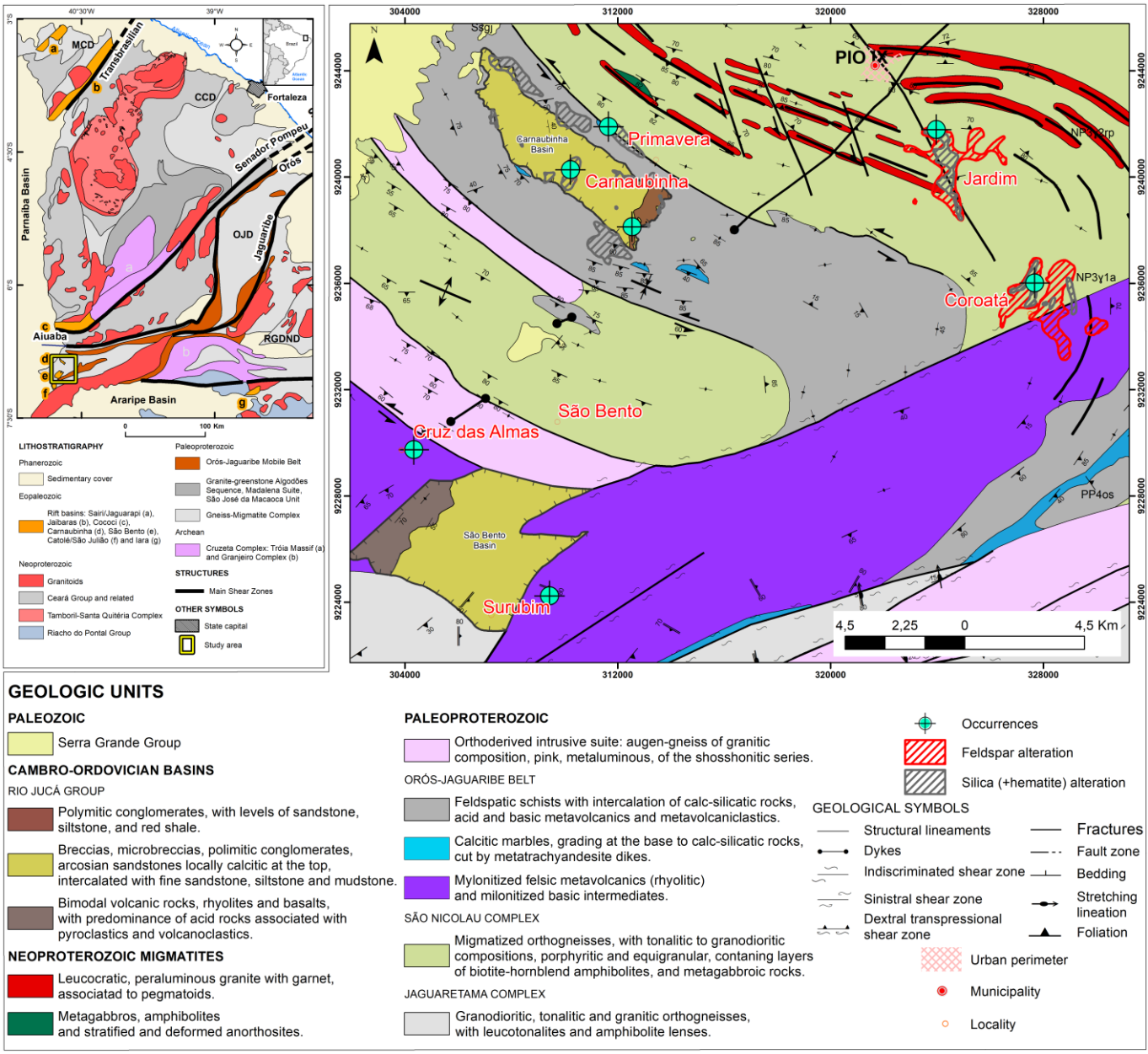

Figure 1. Simplified geological map of the Borborema Province highlighting the region under study, indicating the Orós Mobile Belt, the rift basins and the study area geological setting (source: modified from Veríssimo et al., 2016; Medeiros, 2004; Parente et al., 2014; Silva and Carneiro, 2018; Saraiva and Rodrigues, 2018).

3 Rift basins in the BP and their IOCG-type mineralization

According to Teixeira et al. (2004) "transitional stage" can be defined simply as the

closing of an oceanic basin in consequence of a continental collision, completing the Wilson Cycle, it corresponds to the stage where the formation of the Borborema Province rift basins took place. Parente et al. (2004) describe the existence of several EoPhanerozoic rift basins along the Borborema Province, which are composed simply of immature clastic sequences, represented by conglomerates, sandstones and shale, presenting gradational changes between each other, with possible association to bimodal magmatism. According to lithological association and tectonostratigraphic environment, Brito Neves (1998) indicates that these basins can be grouped into two different categories: i) along shear zones or tectonic lineaments, such as those of interest for this study, and ii) foreland and intra-arc basins. The rift basins in the Borborema Province (Figure 1) are generally controlled by NE-SW- or E-W-directed transcurrent shear zones, as for example: i) Jaibaras - delimited by the Sobral-Pedro II (east) and Café-Ipueiras (west) lineaments; ii) Cococi/Rio Jucá - delimited by the Senador Pompeu shear zone; and iii) Catolé/São Julião, located along the Tatajuba shear zone. The basins of greater extension occur in the west of the province, overlapped by sediments of Parnaíba Basin (Parente et al; 2004) (Figure 1). In the Northern Subprovince rift basins, the sedimentary associations were denominated by Parente et al. (2004) as Alfa Inferior and Alfa Superior, being separated by an erosional unconformity. They are characterized as products of progradating deltaic fans in lacustrine bodies (or possible shallow seas), which might be associated to volcanic material and products of subaerial detritic flow.

The Jaibaras, Cococi, Carnaubinha and São Bento basins show important similarities, such as the presence of a mature clastic sequence, copper sulfides occurrences associated to the sedimentary and volcanic sequences, besides its basement (Maas et al., 2003; Machado, 2006; Parente et al., 2011). Parente et al. (2011) describe the presence of potassic, propylitic and hydrolytic alterations associated to the granitoids of the Jaibaras basin borders, as well as epidote, propylitic and hematite alteration in its volcanic rocks and tectonic breccias. Iron-oxides and copper sulfides associated to silica-rich breccias in the rhyolites, granites and basalts characterize these occurrences (Parente et al., 2011). Machado (2006) also characterizes the presence of hydrothermal alteration in the conglomeratic breccias from the Cococi basin, where copper sulfides occur associated to quartz-albite-carbonate, sericite-chlorite-quartz and hematite alteration. In the Carnaubinha basin, Saraiva and Rodrigues (2018) describe intense hydrothermal alteration affecting the basin and associated basement rocks, with the presence of potassic, calcic-sodic alteration and intense multistage silicification, commonly associated to iron-oxides and copper sulfides. Similarly, for the São Bento basin, hydrothermal alteration

zones with silicification in the sediments and more intensely in the basement rocks were mapped by Uvula and Didoné (2019).

4 Analytical procedures and data analysis

For this study, whole rock geochemistry of 12 samples representing the main hydrothermal alteration affecting the basement and Carnaubinha basin rocks, as well as the main copper occurrences, were obtained through XRF (X-Ray Fluorescence) and ICP MS (Inductively Coupled Plasma Mass Spectrometry) at the ALS Brasil Ltda. Lab. Twenty four polished thin sections were studied using a transmitted and reflected light microscope, aiming to characterize the occurrences and hydrothermal alteration types. Geochemical data of 9 samples from the Folha Pio IX (Parente et al., 2014) report were compiled with the other analyzed samples, totalizing 21 samples. These data were treated and processed using the ioGAS^{TM} software for interpretation and analysis of elements mobility during hydrothermal alteration using biplot diagrams. The mineral chemistry analyses were performed on pyrite of 4 different polished thin sections in the Microscopy and Microanalyses Lab (LMic) of the department of Geologic Engineering (DEGEO), from Escola de Minas (UFOP). The Electronic Microprobe - JXA8230 (Jeol) operated in the tension of 20 kV, beam current of 40 nA with five wavelength dispersive spectrometers (WDS) coupled with one EDS Oxford detector and analyzed spots of 5 nm. Back-scattered electrons images were obtained for the analyzed grains. The following elements were analyzed and are represented here in boxplots Fe, S, Au, As, Se, Zn, Te, Sb, Ag, Bi, Cu, Ni, Sn, Co, Mn, Mo and Hg.

The closure effect is a characteristic of the compositional data. It occurs as a consequence of the “closed data”, that is, the representation of a whole or a sum to a constant value (e. g. weight percent, concentration in ppm or ppb) (Aitchison, 1986). These data can produce unreal tendencies, forcing the correlation between variables. Therefore, the use of specific data treatment is necessary when using compositional data, to avoid the closure effect. The compositional data analysis method of logration (Aitchinson, 1986) allows these data to be expressed as real Euclidian numbers. In the centered log ratio (clr) (equation 1) transformation, the changing of closed data into open isometric is done through the geometric mean of all parts (e.g., compositional components) as the divisor of the variables, followed by the logarithmic transformation of the ratios (Aitchison, 1986), as indicated in the following equation

$$clr(x) = zi = \log xi/g(XD)$$

($i = 1; \ldots; D$) (equation 1)

where D is the number of components to a compositional vector x.

The clr transformation was applied to the data, resulting in isometric coordination, used in bivariate diagrams and in the Principal Components Analysis (PCA).

Hydrothermal alteration is common in different types of mineral deposits. Where intense, it may obliterate the precursor rock's original features, as well as their chemical composition (Monteiro et al. 2008; Montreuil et al. 2013). In the absence of previous knowledge of the geochemistry of the host rocks, conventional mass balance methods such as those described by Gresens (1967) and Grant (1986) can be used, and the Molar Element Rations (MERs) are a good alternative to represent the effects of mass transfer associated to hydrothermal alteration (Pearce, 1968; Stanley and Madiesky, 1994; Stanley, 2017). Molar Element Ratios use allows an investigation of the rocks in terms of constituent minerals, and also eliminates the closure effect (Pearce, 1968; Stanley and Madiesky, 1994; Stanley, 2019).

Principal Component Analysis (PCA) is a multivariate data analysis method that aims to reduce the number of variables necessary to describe the variation observed in a dataset, using linear combinations of the variables (components) that describe the distribution of the data (Grunsky, 2001). In the present paper, the RQ method for Principal Component Analysis (PCA) (Zhou et al., 1983) was applied using the ioGAS^{TM,} software. Its advantage consists in presenting loadings and scores (coordinates) of the principal components, variables (elements) and objects (samples) in the same scale, allowing the observation of the correlated samples, and geochemical affinities through the variables (Grunsky, 2010). Therefore, the data can be presented in biplots, where the proximity of the samples with one or more element reflects its enrichment in such elements, contrasting to the distant samples, allowing, in that way, the comparison of the geochemical signature of the different types of hydrothermal alteration.

5 Local Geologic Context

5.1 Characteristics of Hydrothermal Alteration and Copper Occurrences in the Orós Mobile Belt related basement.

Different types of hydrothermal alteration (albite, K-feldspar, hematite, silica, sulfide alteration) affect rocks of the Orós Mobile belt and related basement. In some localities such as Jardim and Coroatá (east of the area) (Figure 1), hydrothermal zoning is evident, and the chronological order of hydrothermal events can be established. In general, hydrothermal alteration is spread regionally, throughout the orthogneisses from the São Nicolau Complex and

the metarhyolites from the Orós Group, following an overall similar pattern. Near areas of brittle-ductile deformation, such as faults and shear zones, alteration is more intense and commonly pervasive, commonly causing complete obliteration of the protolith. When incipient is present mainly as vein sets. Locally, silicification zones can be related to copper enrichment. Features of each hydrothermal alteration types are described below in this section and summarized in supplementary data Table 1.

Albite alteration is widely distributed in the São Nicolau Group orthogneisses and less commonly in the Orós Group metarhyolites. Occurs regionally as veins and stockworks, where close to faults it may affect rocks pervasively (Figure 2A). Albite is pinkish in the breccias; hydrothermal albite is distinguished from early plagioclase of the orthogneisses because the latter exhibits deformed albite twinning (Figure 2B). Albite alteration precedes K-feldspar alteration since this mineral is partially replacing some of the neoformed albite.

K-feldspar alteration is abundant in both orthogneiss and metarhyolites (Figure 2C) and, locally, in metasedimentary rocks of the Orós Group. The pervasive style is more common, imprinting a pinkish to reddish color similar to albite alteration. In thin section, the alteration is marked by the replacement of plagioclase by red K-feldspar (Figure 2D). The darker color of K-feldspar results from very fine hematite staining, a common feature in rocks of the OMB.

Epidote alteration in contrast with albite and K-feldspar alteration, is conditioned only by veins and stockwork-style structure, commonly superimposing the alteration types above (Figures 2E). Where intensive, veins form epidositic breccias. In thin section, epidote appears as both fine aggregates and as fine-grained prismatic crystals (Figure 2F).

Chlorite alteration is restricted to the São Nicolau orthogneisses, characterized by the substitution of the mafic minerals biotite and amphibole (hornblende) commonly preserving their original lamellar habit (Figure 2G). Chlorite alteration is commonly associated to epidote alteration in veins cutting K-feldspar altered rocks. Chloritic breccias (Figure 2H) may occur where all mafic minerals have been replaced.

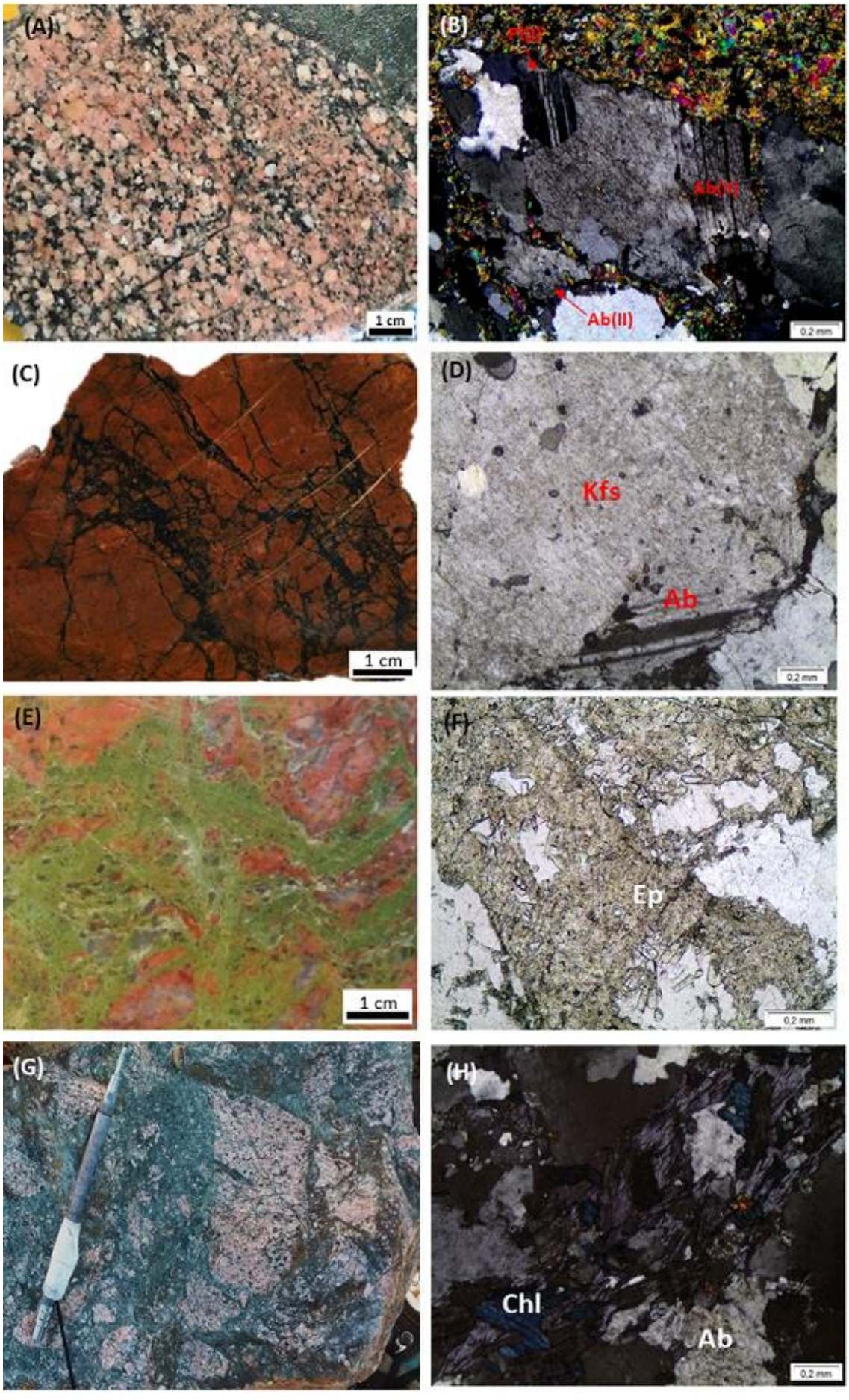
(A)
1 cm
(B)
Pl(I)
Ab(I)
Ab(II)
0.2 mm
(C)
1 cm
(D)
Kfs
Ab
0.2 mm
(E)
1 cm
(F)
Ep
0.2 mm
(G)
(H)
Chl
Ab
0.2 mm

Figure 2. Basement types of hydrothermal alterations: (A) Orthogneiss altered by hydrothermal pink albite, mafic minerals altered to chlorite (B), (D), (F) & (H) Photomicrographs under transmitted light, in crossed nicols (B) & (H). (B) Replacement of early orthogneiss plagioclase (Pl) by hydrothermal albite (Ab). (C) Orós Group metarhyolite north of the Carnaubinha locality with K-feldspar pervasive alteration overprinted by late quartz-hematite veins. (D) K-feldspar altered orthogneiss, where late K-feldspar (Kfs) replaces hydrothermal albite (Ab). Epidote stockwork-style veins superimposing albite in altered São Nicolau orthogneiss. (E) Epidote veins cutting the Orós Group metarhyolite affected by early K-feldspar alteration, south of the Carnaubinha basin. (F) Epidote (Ep) veins showing fine aggregates and prismatic crystals. (G) Chloritic breccia outcropping in Jardim. (H) Chlorite alteration in the São Nicolau orthogneiss; chlorite (Chl) replacing amphibole and biotite in albite (Ab) alteration orthogneiss.

Silicification is one of the most abundant hydrothermal alteration types in rocks of the OMB. It is regionally widespread in varied lithologies such as the orthogneisses, metavolcanic and metasedimentary rocks. This is the most significant alteration because it is commonly accompanied by the precipitation of copper minerals. Multiple phases and styles of silicification can be identified in the five main occurrences studied (Jardim and Coroatá, east of the area, Surubim and Cruz das Almas, south of the area, and Primavera, west of the area) associated to the Orós system rocks (Figure 1). Their features are summarized in supplementary data Table 2.

In general, silicification is characterized by quartz enrichment commonly associated to hematite, which superimposes feldspars, epidote and chlorite alteration. Further away from the main fault (Pio IX) and shear zones (Figure 1), these form isolated veins of quartz and/or hematite in fractures. When intense, may form stockwork breccias (Figures 3A, C, D).

Alteration is also pervasive (Figure 3C, D, E), where the protolith is replaced by microcrystalline silica associated to fine hematite and/or Fe hydroxides; in this case, sericitization of the protolith feldspars is common (Figures 3C, E). Pervasive alteration also occurs as fine-grained quartz associated to specular hematite (Figures 3D, E). Late, coarser-grained quartz veins that cut pervasive quartz alteration may exhibit comb-textured crystals and fine hematite (Figures 3E, F).

In Primavera, the occurrence of iron metasomatism is related to the precipitation of iron oxides and/or hydroxides in cavities associated to chalcedony (Figure 3A). This silicification zone is associated to an occurrence of hematite and massive magnetite along the

basement corresponding to the São Nicolau Complex orthogneiss. The relation between silicified blocks with hematite and massive magnetite blocks is not clear, even though they outcrop in the same area. In thin section, they are composed mainly by magnetite (60%) and ilmenite (30%) (Figure 3B), where the former exhibits oxy-exsolution ilmenite lamellae and martitized borders; these grains interstices contain accessories such as spinel (5%) and/or clinopyroxene (5%). The oxides may contain very fine-grained sulfide inclusions (<1%).

Infill-breccia quartz and very fine-grained quartz enrichment dominate at Cruz das Almas (e.g., Taylor, 2009) are observed. The former leads to brecciation of the protolith, subsequently affected by later veining (Figure 3C) of fine- to medium-grained quartz associated to some copper minerals. Hematite is less abundant when compared to the other occurrences.

Pyrite formation is commonly associated to the pervasive silica-hematite (Figure 3D) alteration in breccias in Surubim and Coroatá where copper sulfides are less common. In the latter, they are disseminated, usually microfractured, or in association to silica-hematite veins (Figure 3D), forming cubic hexagonal crystals. In Primavera and Jardim, copper enrichment is essentially related to pervasive silica-hematite alteration (Figures 3D,E), but it is also present in the late quartz veins with some hematite, while in Cruz das Almas copper minerals are restricted to late veins. They consist of chalcopyrite, commonly altered to chalcocite and covellite (Figure 3E), and other secondary minerals such as malachite and goethite (Figure 3F).

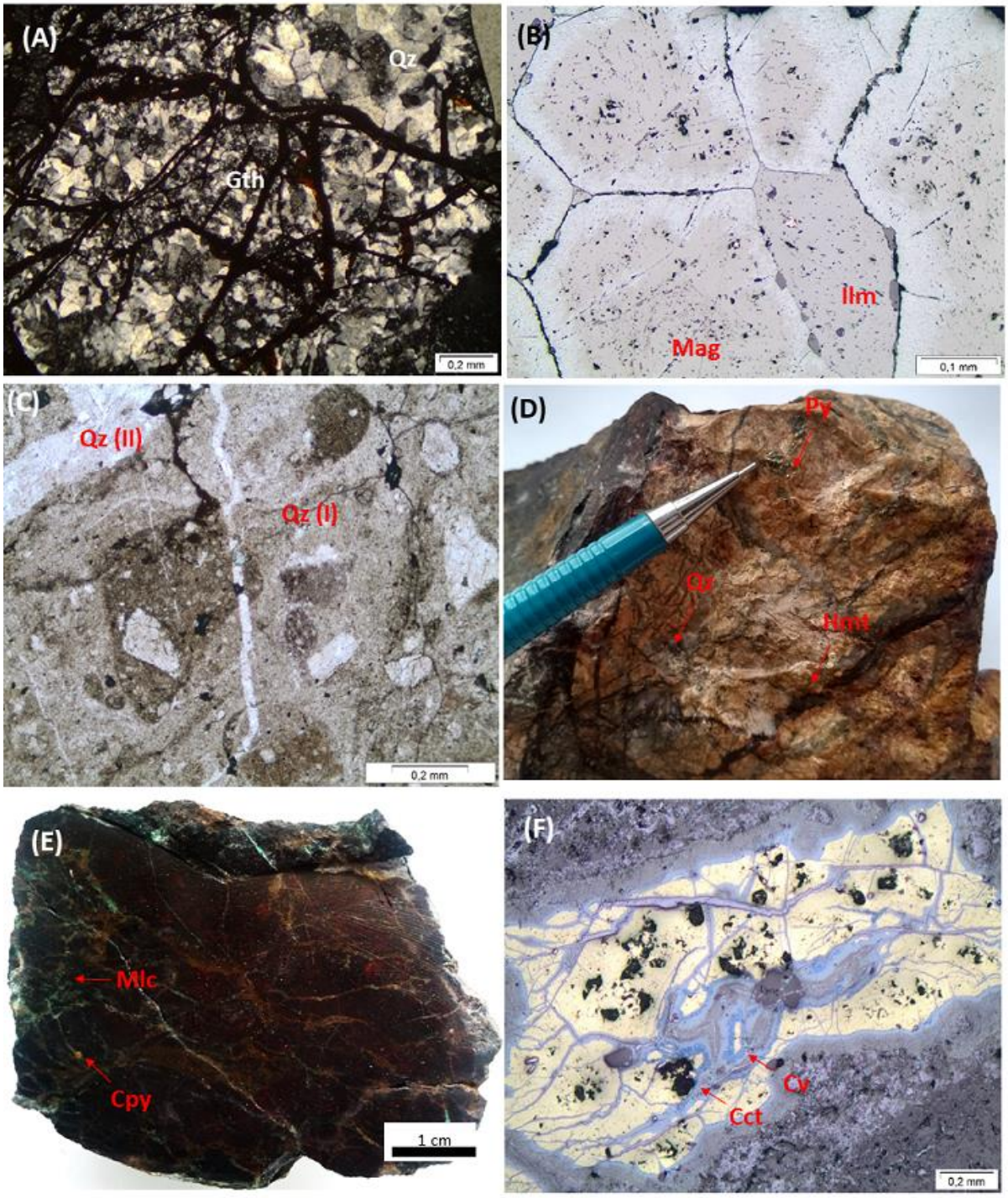

Figure 3. Silica-hematite breccias from the Primavera occurrence (A) Photomicrograph of goethite (Gth) precipitating along cavities associated to calcedony (Qz) in the silica-hematite breccias. (B), (C) & (F) Photomicrographs under transmitted light, crossed nicols (F). (B) Magnetite (Mag) and ilmenite (Ilm) in a magnetite block. (C) Photomicrographs under reflected light in parallel nicols of silicified breccia from Cruz das Almas, showing very fine pervasive silicification (Qz i) cut by later veins of quartz (Qz ii). (D) Coroatá silica-hematite breccias showing abundant, disseminated pyrite (Py), associated to silica-hematite (Qz) (Hmt) veins. Primavera silica-hematite breccias (E) Abundant malachite (Mlc)

veins and preserved copper sulfides (Cpy). (F) Preserved chalcopyrite core, with borders altered to chalcocite (Cct) and covelitte (Cv).

2 Characteristics of Hydrothermal Alteration and Copper Occurrences in the Eopaleozoic South Rift Basins.

In the Carnaubinha basin, hydrothermal alteration affects mainly the conglomerates and volcanoclastic breccias. Where intense, alteration can result in the formation of tectonic-hydrothermal breccias. In chronological order, alteration includes formation of hydrothermal K-feldspar, quartz (silicification), hematite, epidote and chlorite, with silicification being associated to the copper enrichment phase. In the São Bento basin conglomerates, hydrothermal alteration is more incipient. The alteration types are limited to silicification, hematite, chlorite and sulfide. Nevertheless, they follow a similar pattern to those of the Carnaubinha alteration types.

K-feldspar alteration in Carnaubinha is characterized by the precipitation of adularia in veins, being restricted to conglomerates (Figure 4A, B) in association with quartz and calcite. Calcite crystals fill cavities between feldspar and quartz (Figure 4B).

Silicification is represented by quartz enrichment, in Carnaubinha it occurs in two styles i) pervasively throughout the rocks, or as ii) veins and stockwork vein sets. Silicification zones are usually associated to formation of breccias and it is the most expressive hydrothermal alteration type in the basin.

i) It is an early phase that commonly obliterates the protolith features of conglomerates (Figure 4C). It initially replaces the sedimentary matrix and evolves to the complete substitution of the clasts.

ii) The channeled style has multiple phases of veins (stockwork texture) (Figure 4C), from which two can be differentiated: a microcrystalline quartz stage that may contain fine calcite and hematite, and a late phase of medium- to coarse-grained milky quartz, commonly associated to coarse-grained calcite, fine iron and/or copper sulfides (pyrite and chalcopyrite) and hematite (Figure 4G). Veins of milky quartz rarely affect the sandstones.

In São Bento basin silicification is commonly associated to chlorite (Figure 4D); pyrite and hematite may occur. Later veins of coarse-grained quartz exhibit comb texture and basal sections; they exhibit fracturing associated to iron oxides and chlorite. Veins may form stockwork vein sets (Figure 4E).

Carbonate alteration occurs in the conglomerates of both basins as individual crystals in the matrix. Carbonate also cuts the rocks as structurally controlled veins (Figure 4F), it is commonly related to epidote alteration and silicification, and typically fills cavities in K-feldspar and quartz veins (Figures 4B). Sandstone may also contain thin calcite veins.

Hematite forms concurrently with silicification in Carnaubinha. It is concentrated in the central-southern and southeastern regions in the basin associated to silicification zones. In the former, hematite alteration is related to channeled silicification only as veins and stockwork-style breccias.

In the southeastern region, hematite alteration is more intense, while hematite is associated to both pervasive and channeled silicification, resulting in breccias with three stages of alteration (Figure 4G). In the first stage, sparse hematite and/or goethite is associated to dark microcrystalline silica that pervasively replaces the protolith. The second stage is composed by more abundant hematite/goethite, in the form of fine aggregates associated to fine quartz also with a pervasive character. In the third phase, hematite and/or goethite and limonite occur as veins of fine aggregates associated to medium- to coarse-grained tabular quartz.

In São Bento conglomerates hematite alteration is characterized by anhedral hematite mainly associated to the rock matrix involving the clasts; it may also occur inside the clasts. In the late hydrothermal quartz veins, hematite occurs as coarse-grained crystals (Figure 4H).

Sulfide alteration and copper enrichment are mapped in the SE region of the Carnaubinha basin, in association to the silica-hematite, pyrite-rich, and silica-rich breccias with no associated copper minerals (Figure 4I). Pyrite forms coarse-grained rhombic crystals, some of which precipitated along silicification associated to fine quartz veins. However, some are disseminated in the matrix of breccias, exhibiting intense fracturing and are cut by quartz veins.

Where present, copper sulfides are represented by chalcopyrite, bornite, covellite, chalcocite (Figure 4J) in association with hydrothermal quartz-calcite or quartz veins (late-stage silicification) (Figures 4F). Secondary minerals such as malachite, azurite and goethite may also be present. Chalcopyrite is the most abundant copper sulfide, while bornite is rarer. They are commonly altered to chalcocite and covellite along its borders, and locally oxidized to

goethite / hematite. Malachite and less common azurite fill fractures.

In São Bento is sulfide alteration is represented only by abundant pyrite in the conglomerates; they are usually deformed (Figure 4K) and may exhibit oxidized borders. Coarser pyrite crystals are usually very fractured filled by late silicification. The late quartz crystals can exhibit growth perpendicular to pyrite crystals (Figure 4L); pyrite may also be obliterated resulting in the formation of boxwork cavities.

Chlorite alteration is the second-most expressive hydrothermal alteration type in both basins. It is very abundant as a matrix mineral in the conglomerates imprinting a grayish color, in which very fine lamellae contour the clasts. The matrix substitution can evolve to clasts where chlorite forms crystals along fractures and grain borders giving the clasts a “speckled” aspect, forming chloritic breccias, occurring in Carnaubinha basin. These have a matrix and some of the clasts substituted to chlorite that may be associated to fine-grained epidote. Lamellar chlorite aggregates can also overprint quartz-calcite veins (Figure 4M). In São Bento conglomerates chlorite also invades the clasts through zones of weaknesses such as fractures along quartz veins that crosscut the conglomerates and overprint the pervasive silicification as fine lamellar aggregates.

Epidote alteration occurs in Carnaubinha basin occurs mainly in structurally controlled veins and veinlets and is only associated to conglomerates; it crosscuts quartz (Figure 4N) and/or K-feldspar veins. Fine-grained aggregates of epidote form veins and medium-grained crystals that may precipitate in quartz veins (Figure 4H). Epidote also appears as fine-grained aggregates associated to calcite, chlorite and fine- to medium-grained quartz (Figure 4G).

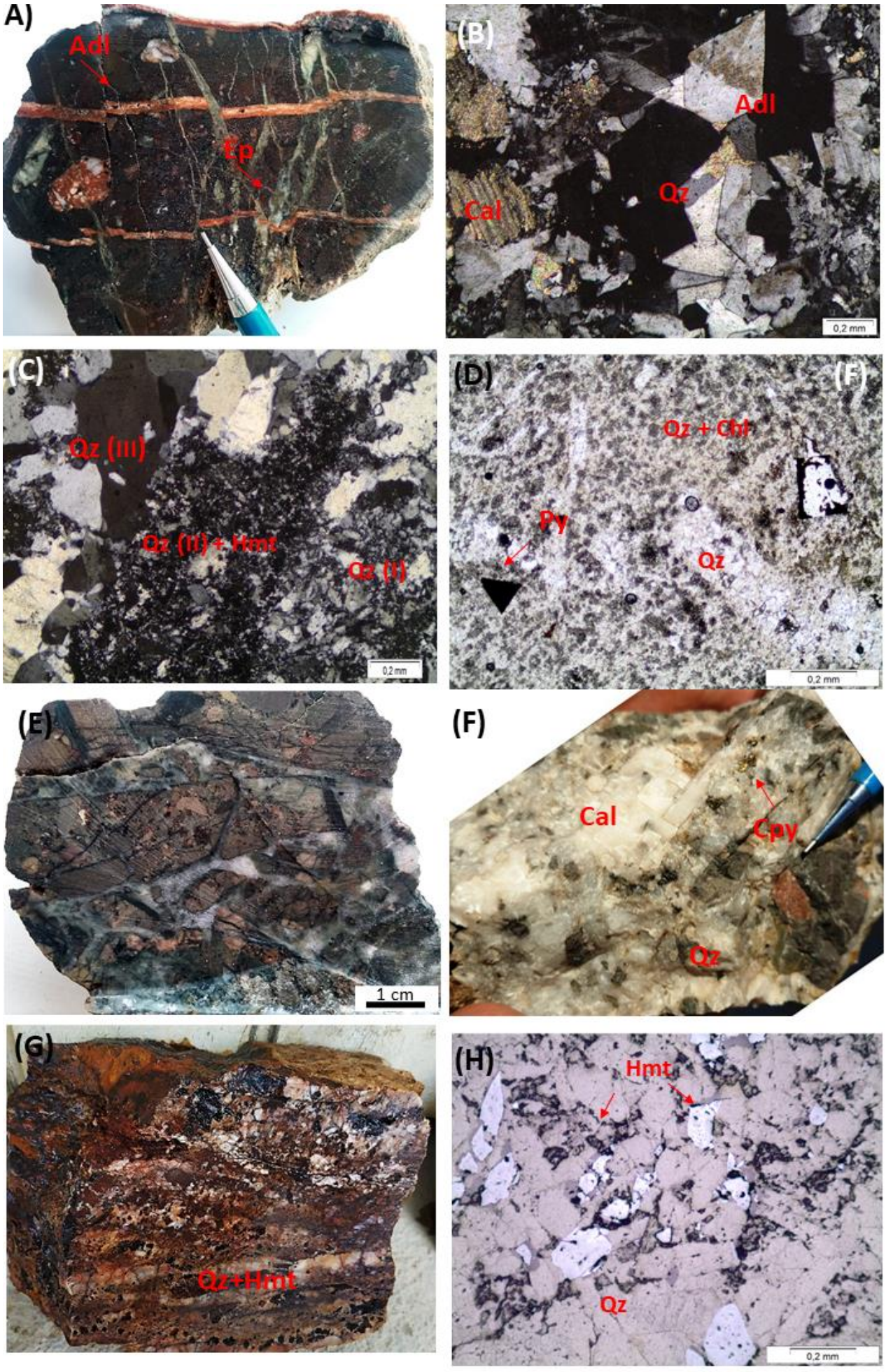
A)
Adl
Ep
(B)
Adl
Qz
Cal
0,2 mm
(C)
Qz (III)
Qz (II) + Hmt
Qz (I)
0,2 mm
(D)
(F)
Qz + Chl
Py
Qz
0,2 mm
(E)
1 cm
(F)
Cal
Cpy
Qz
(G)
Qz+Hmt
(H)
Hmt
Qz
0,2 mm

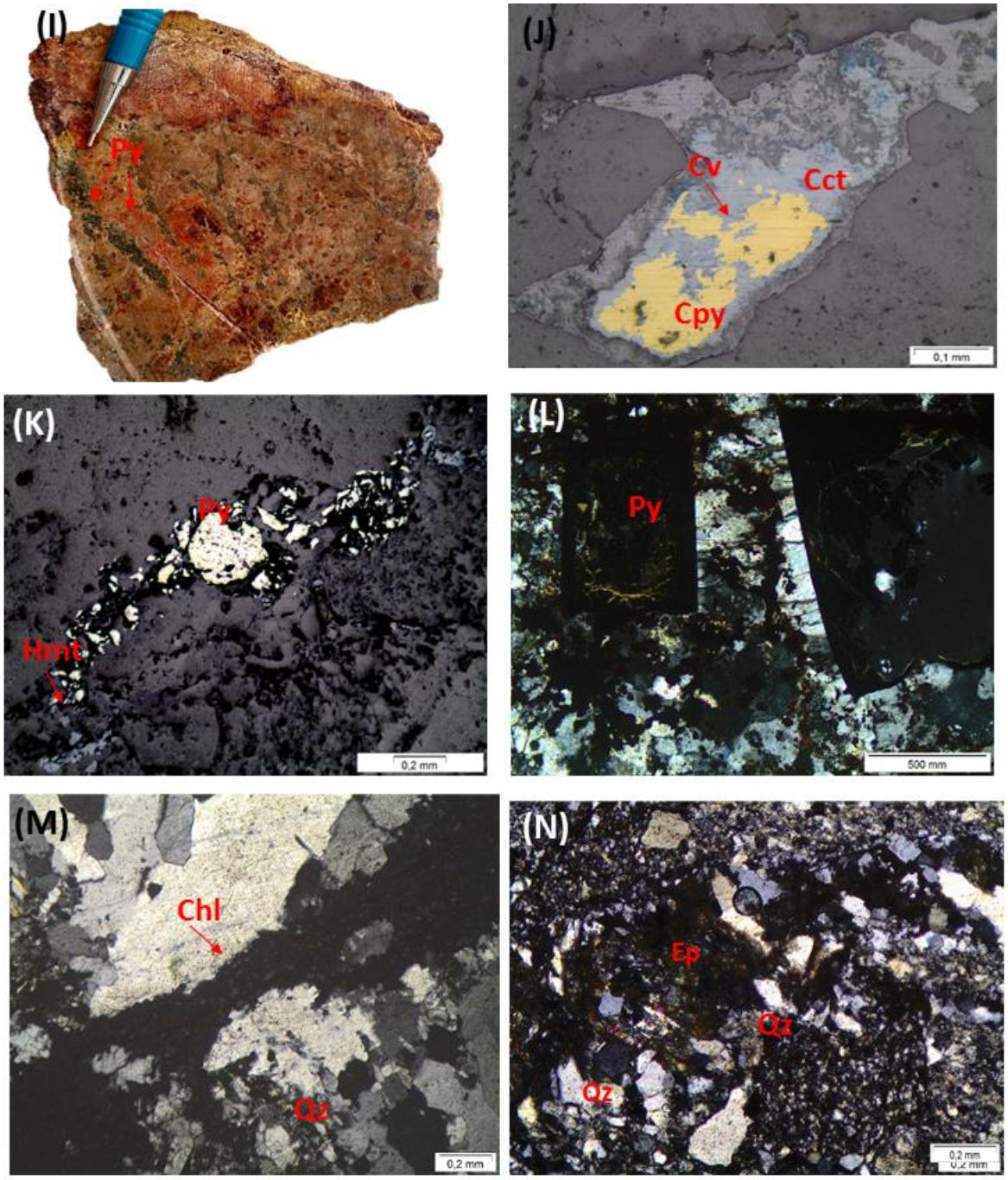

Figure 4. (A) Carnaubinha basin conglomerate cut by K-feldspar (Adl) and epidote (Ep) veins. (B) (C) (L) (M) & (N) Photomicrographs under polarized light, crossed nicols. (B) K-feldspar vein showing rhombic adularia (Adl) with diffuse twinnig associated to quartz (Qz) basal sections and calcite (Cal) filling cavities (C) Silicified conglomerate with an early phase of pervasive silicification: quartz (Qz) (I) cut by late veins of medium-grained quartz (Qz) (II) and hematite (Hmt), and coarse-grained quartz (Qz) (III). (D) Photomicrographs under polarized light, parallel nicols showing coarse-grained, late quartz (Qz) vein with fine chlorite (Chl) filling fractures. (E) Conglomerate cut by late quartz veins. (F) Carnaubinha conglomerate cut by veins of quartz (Qz) and coarse-grained calcite (Cal) with chalcopyrite (Cpy). (G) Southeastern region conglomerate affected by silica-hematite (Qz) (Hmt) alteration with fine

chalcopyrite. Photomicrographs under reflcted light (H) (J) (K). (H) Hematite (Hmt) alteration in the São Bento conglomerate. (I) Carnaubinha silicified volcaniclastic breccias with abundant pyrite (Py). (J) Chalcopyrite (Cpy) altering to calchocite (cct) and covellite (Cv) associated to the silicification in Carnaubinha conglomerates. (K) Deformed pyrite (Py) in the contact between clasts with borders altered to hematite (Hmt). (L) Quartz (Qz) growing perpendicular to pyrite (Py). (M) Chlorite (Chl) micro veins cutting silicification (Qz). (N) Fine aggregate of epidote (Ep) associated to chlorite overprinting silicified (Qz) conglomerate.

6 Geochemistry

The results for samples representing the different types of alteration affecting the basement and the Carnaubinha basin rocks, and the main associated copper occurrences, are compiled in the supplementary data (Table 3). For the basement rocks, it is important to highlight that the petrographic analyses showed that K-feldspar and albite alterations are commonly present in the rocks affected by subsequent hydrothermal alteration. Therefore, most rocks used to represent the other alteration types were most likely also affected by the early-stage feldspar alteration.

In the basement rocks, SiO_2 shows the greatest variations (48.07 to 90.11%). Higher values are associated to silicification and lower values are in samples of epidote-chlorite and silica-hematite alteration where hematite alteration is more intense. The feldspar and alteration breccias show higher concentrations of K_2O (1 – 4%) and Na_2O (2-3%). Where superimposed by the epidote-chlorite alteration, the contents for CaO (2 – 13%) and Fe_2O_3 (2 – 18%) are increased, associated to gains of MnO (0.02 – 0.06%), MgO (0.02 – 0.08%) and P_2O_5 (0.02 – 0.05%) in minor proportions, while the alkali contents decrease. Rubidium, Ba and Sr are the main trace elements in these two alteration types, while Zn, Zr, V, Ga and Th also occur as relevant concentrations (10 ~ 100 ppm). Similar elements behavior occurs in the silica-hematite alteration overprinting the feldspar breccias. High Fe_2O_3 concentrations are associated to lower alkalis contents and the main trace elements are W, Zr, Sr, Ce, Nb, La, Mo, Rb and Sn. In the silica-hematite breccias, SiO_2, Al_2O_3 and Fe_2O_3 are the main oxides, higher SiO_2 and Al_2O_3 concentrations occur together, while Fe_2O_3 shows inverse behavior. These breccias can have associated copper occurrences; other common trace elements are Cr, Mn, P, V, Ni, Co, Ce, Sr, Zn, and Mo, W and U in a smaller scale. In the silica-sufide alteration breccia, SiO_2, Al_2O_3 and Na_2O_3 are the main oxides; it can also contain high copper concentrations and important trace elements are Ba, Ce, La and Y.

Carnaubinha basin K-feldspar alteration in the conglomerate is restricted to veins

and show no significant geochemical enrichment for the alkalis and CaO. However, Fe_2O_3 and MgO contents are more expressive; similar pattern occurs in the chlorite-epidote conglomerate breccia, despite the extensive replacement of the protolith. As for trace elements concentrations, Mn, Sr, Ba, Cr, Zn, P and La are common to the conglomerates, with different alteration types. The silicified conglomerate shows high SiO_2, associated to CaO and Cu, while an expressive decrease of other major elements is observed. The other silica alteration volcanoclastic breccias show moderate values for SiO_2, higher alkalis and Al_2O_3 contents, with some variance for the Fe_2O_3 that decreases to MnO, MgO with an increase of CaO. Barium, Mn, Zn, P, and minor Cu, Ni, Cr, Co are the main trace elements. Finally, the silica-hematite alteration volcanoclastic breccia shows the major Fe_2O_3 and lower SiO_2 values; P_2O_5 is slightly higher when compared to the other alteration types. Copper has high contents, and P, Mn, Ba, Se, Cr, Bi, Fe, Zn, Co and V also show good concentrations.

When compared to the major elements (supplementary data Figure 1), the concentrations of Cu increase with SiO_2; in contrast, CaO and MnO contents decrease. In the rich Cu silica-hematite breccias from the basement, MgO and Fe_2O_3 are low and slightly increase in the silica alteration Cu rich breccias from the basement and Carnaubinha basin. In the silica-hematite breccias and silica alteration breccias Cu enrichment is also associated to Cr, Mo, Ag, Ba, La and U; however, Co, Ni, Cd and Bi only increase with Cu in the silica alteration sample, while Ba decreases in concentration. Thorium and Pb decrease with Cu gains in all alteration types. The silica-hematite and silica alteration breccias from the basement and basin show the highest contents in U, Bi, Ag and Ba, and intermediate values for V around (20 to 100 ppm); silica-hematite breccias are richer in such elements. While the altered orthogneisses have intermediate Zn, Ag and Bi concentrations, they present higher values for U, Ba and V. Finally, the basin conglomerates show the highest Zn concentrations and low Bi and Ag; the contents for U, Ba and V are intermediate.

6.1 Alteration index diagram

Two alteration indices have been used to evaluate the behavior of the chemical elements, according to different types of alteration: the molar diagram K/Al vs Na/Al, used to discriminate rocks with potassium and sodium alteration from the least altered rocks, which are around 0.4 Na/Al and low K/Al (e.g., Benavides et al., 2008; Van der Wielen et al., 2013). Albitization increases with the increase of the Na/Al ratio in relation to the less altered rocks, and the zones with chlorite, sericite and K-feldspar vary in function of the K/Al ratio (e.g., chlorite in zone of low K/Al ratio, sericite - moderate and K-feldspar-high). As illustrated in

the diagram of Figure 5, the Carnaubinha conglomerate, K-feldspar and epidote-chlorite alteration breccias show Na/Al ratios from 0.5 to 0.63 with K/Al ratios lower than 0.20, evidencing a stronger sodic alteration. The silicified conglomerate with copper sulfides plots close to the low alteration samples. Volcanoclastic breccias with silica-hematite alteration have Na/Al ratios varying from 0.5 to 0.73. The higher values might indicate the presence of sodic enrichment in the clasts; the silica-hematite alteration breccia plot in the lowest ratio values for both elements.

In the basement rocks, the feldspar alteration samples divide clearly in sodic and potassic alteration extremes. Silica-hematite alteration samples vary from very low ratio values, for both elements, to 0.60 for Na/Al and 0.25 for K/Al. The highest ratios coincide with copper-richer breccias; the silica-alteration breccia with copper sulfides have 0.73 for Na/Al ratio and K/Al ratio under 0.05.

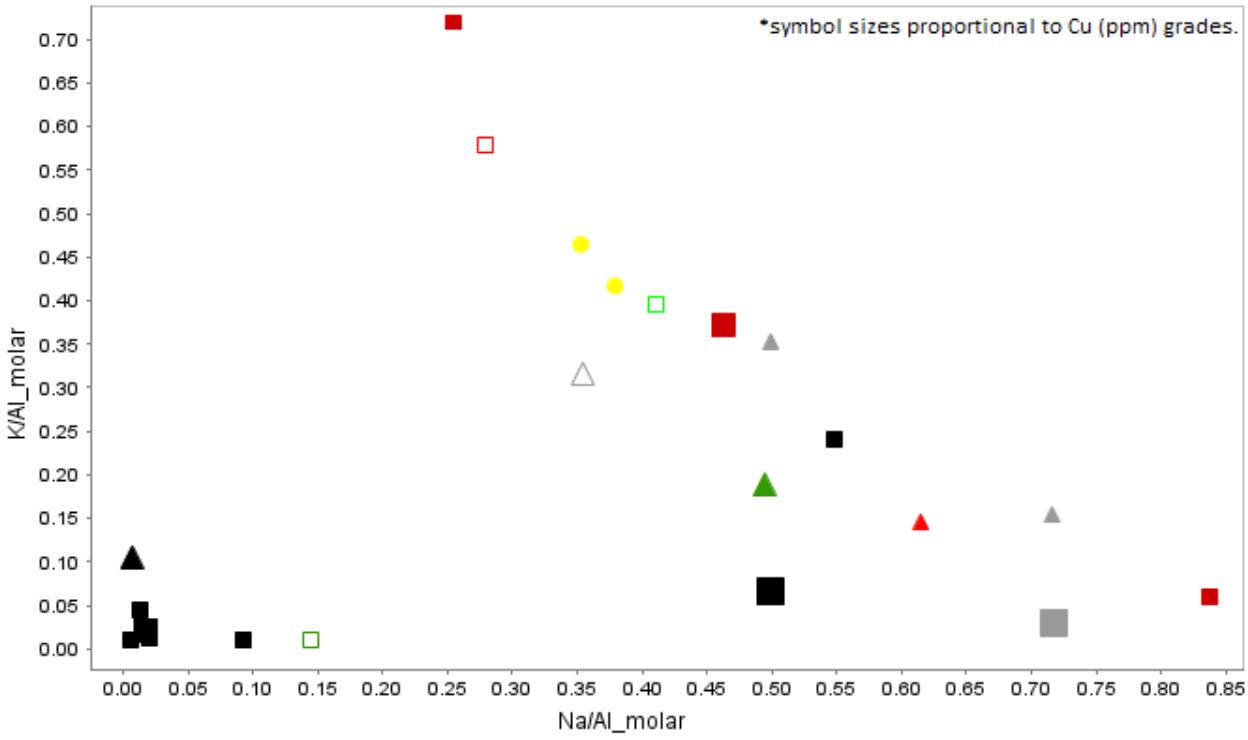

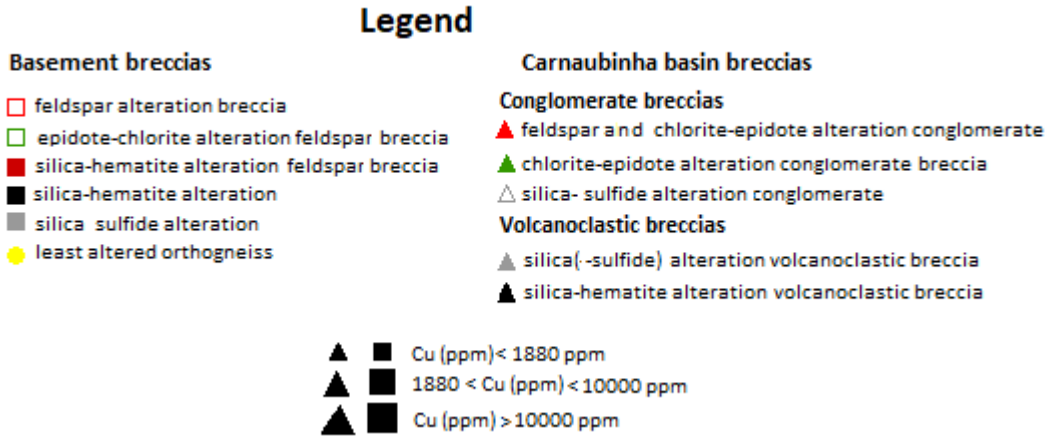

Figure 5. Molar element ratio diagram for K and Na normalized by Al.

6.2 Principal Component Element Patterns (PCA)

The relationship between elements and samples and the dimensional reduction of the data can be evaluated using the Principal Component (PCA) multivariate analysis (Grunsky, 2010). The total rock geochemistry PCA analysis was performed after centered log-ratio transformation, aiming to highlight the chemical variations in the different types of alteration affecting the studied rocks. Samples with many zero values and elements that did not show results for most samples were excluded from this analysis, since this null data precluded the log-ratio transformation. In total, 11 samples were plotted using PC biplots (Figure 6), where the samples position relatively to the analyzed 9 major oxides and 45 trace elements lines indicates the degree of depletion or enrichment of those elements for each sample. Supplementary data Table 4 summarizes the results for the principal component analysis for the hydrothermally altered rocks; the PC1 versus PC2 biplot represents 49.80 % of the total variation within the data.

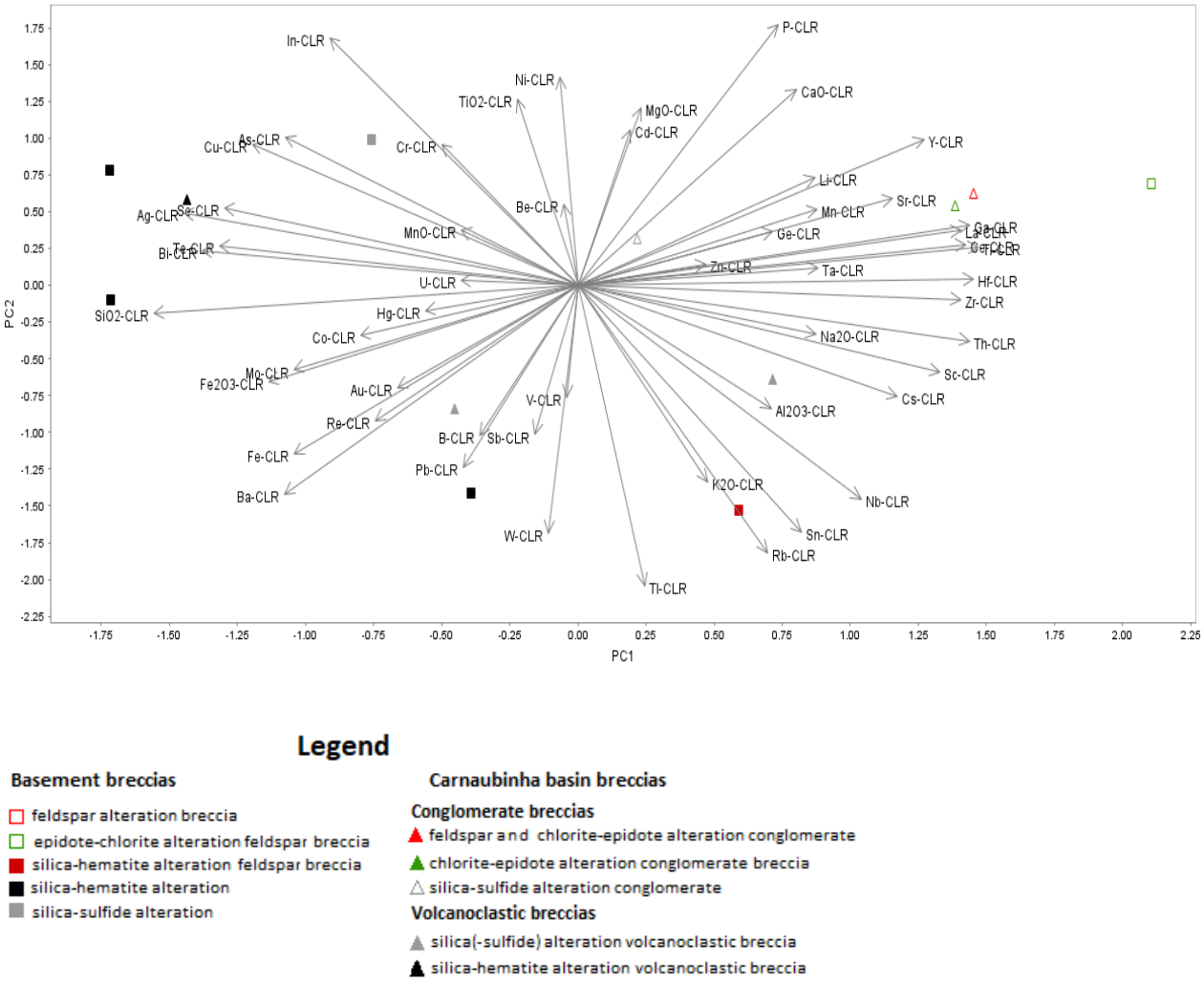

Figure 6. Projected principal component analysis results PC1 vs. PC2 of the crl-transformed whole-rock geochemistry from the west Borborema hydrothermal alteration breccias.

The basement breccias, associated to K-feldspar, albite and epidote-chlorite alteration, plot along the positive PC1 and vary in the PC2 axis, for the epidote-chlorite alteration; CaO, Na_2O_3 and MgO are the major elements gains, and as for trace elements highlights are La, Ce, Ga, Hf, Zr, Y, Sr and Th. For the K-feldspar alteration breccia K_2O, Al_2O_3 and Na_2O gains stand out, associated to Rb, Sn and Nb. The silica-hematite breccias show opposite behavior plotting on the negative PC1 and PC2 axes, with SiO_2 and Fe_2O_3 gains, and Pb, W, Sb, W, Sb, V, Ba, Mo and Co for trace elements. As for the copper-rich, silica-hematite breccias, SiO_2 gains are more expressive, associated to Cu, Bi, Ag, Se, Te and As. The silica alteration breccia associated to copper occurrence shows different trace elements trend, with Cr, As and Cu. MnO, TiO_2, U and Hg occuing similarly in the different types of copper-rich breccias.

In the Carnaubinha basin rocks, the conglomerate breccia with low K-feldspar and

epidote-chlorite alteration plots close to the chlorite-epidote alteration conglomerate. These plot in the positive PC1 and PC2 axes, and show gains in CaO, Na_2O, lower MgO and Al_2O_3, associated with the trace elements, Ga, La, Ce, Ti, Sr, Mn, Y, Li and Ta. The silica alteration breccia plots in the negative PC2, close to Al_2O_3, Na_2O and K_2O, and Cs, Sc, Nb, Th, Sn and Rb. The silicified conglomerate with copper enrichment plots still in the positive PC 1, but distant to the other basin samples, close to the major elements CaO, MgO, TiO_2 and MnO, besides Be, Cd, Zn, Li, Ni and P. Two samples plot in the negative PC 1, the silica-sulfide and the silica-hematite breccias; the first one is in the negative PC2, close to elements Pb, Re, Au, Fe, Ba, Pb, V and W. The latter is in the positive PC2, associated to Se, Ag, Cu, As, Te and Bi gains.

7 Pyrite Mineral Chemistry

Pyrite has been widely used in ore deposits genesis studies due to its abundance and resistance under varied environmental conditions (Keith et al., 2018; Deditius et al., 2014; Hou et al., 2016; Tan et al., 2022). Pyrite is ubiquitous to the breccias in the western Borborema region, as it occurs in the different types of alteration breccias. For this study, micropobe analyses of pyrite were performed in breccias for the different occurrences, which consist of a silica-hematite breccia and a silica-sulfide-breccia from the Carnaubinha basin, a feldspar breccia with silica-hematite alteration from the basement region of Coroata and a silicified conglomerate from São Bento basin. The results are summarized in the supplementary material Table 5; images from the analyzed grains are in supplementary data Figure S2.

Pyrite of breccias from the Carnaubinha basin consist mostly of euhedral and homogeneous crystals; some crystals are affected by brittle deformation. In the silica-hematite breccias, pyrite is in the matrix and in volcanic clasts as coarser grained. The chemistry results show that clastic pyrite contains Zn and Au (up to 0.015 and 0.04 ppm), absent in the alteration matrix pyrites. Cobalt reaches high concentrations in pyrite clasts, up to 3.77%, it is the most abundant trace element. In general, the Carnaubinha basin silica-hematite breccia pyrites main trace elements are Co (up to 3.7 %), Cu (up to 0.17 %), Se, Hg (up to 0.05 %) Ni (up to 0.11 %), Te, As (up to 0.05 %), Mn; Ag and Zn can also occur and Au, Sn and Sb are rarer (Figure 8A to J). The silica-sulfide breccia results show a similar enrichment in Co (up to 2.6 ppm), followed by Ni (up to 0.13 %), Hg (up to 0.06 %), As (up to 0.06 %), Se, Mn, Te, Zn, Ag (up to 0.02 %) and Cu (up to 0.017 %). Gold, Sn and Bi are rarer (Figure 7). Similarly, as in the silica-hematite breccia.

The São Bento basin conglomerates pyrites are anhedral, commonly affected by brittle-ductile deformation, which is probably associated to brecciation and hydrothermal alteration processes, occurring in the sedimentary matrix and clasts borders (Fig. S4C). The chemical analysis show that Hg (up to 0.07%), Cu (up to 0.02%), Co (0.06%), Ag (up to 0.03%), Te, Zn, Mn and Se are the main trace elements, while Au, As and Sn can also be present (Figure 8). São Bento basin pyrite is the richest in gold contents of all the analyzed occurrences, reaching 0.13% in concentration (Figure 8E), which occurs mainly in crystal borders. They show low Co (up to 0.05 %) contents when compared to the other samples (Figure 7B).

The Coroatá pyrite is hosted by hydrothermal feldspathic breccia, associated to altered orthogneiss; it is subhedral and exhibits brittle deformation features (Supplementary data Figure S4C). Their presence is associated to overprinting features marked by a set of stockworks-style veins, composed of pyrite, quartz and hematite that overlap and record different stages of development. Pyrite shows varied textural features and overprinting veins. Some crystals are euhedral, others fractured, reflecting a prolonged hydrothermal process associated to brittle deformation. Mineral chemistry results show that the main trace elements are Co, Ni, Hg, Ag, As, Mn, Se and Zn; Te, Cu and Au can occur (Figure 7).

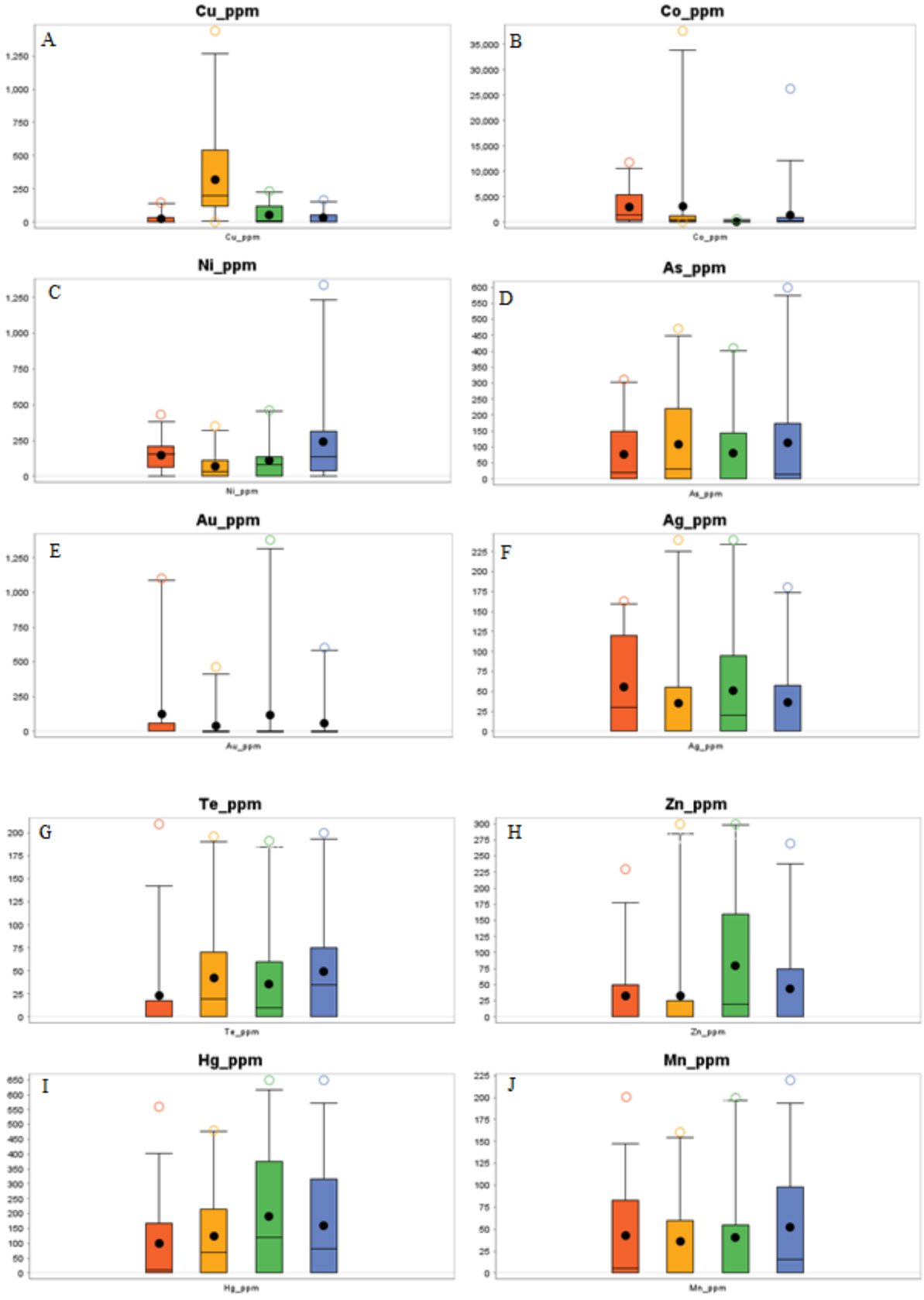
Cu_ppm
A
Co_ppm
B
Ni_ppm
C
As_ppm
D
Au_ppm
E
Ag_ppm
F
Te_ppm
G
Zn_ppm
H
Hg_ppm
I
Mn_ppm
J

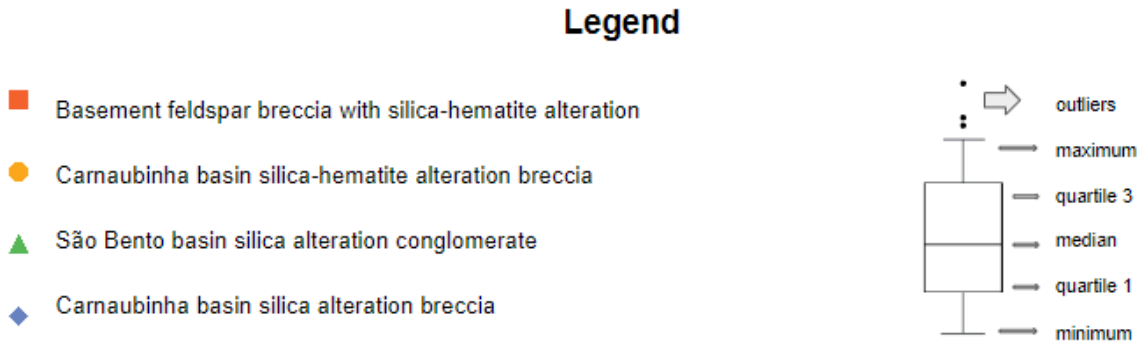

Figure 7. Individual boxplots showing the content for Cu, Co, Ni, As, Au, Ag, Te, Zn, Hg and Mn in the pyrites of analyzed samples.

7.1 Cobalt Nickel ratio

Pyrite incorporates different trace elements such as Co, Ni, As, Au, Ag, Se, Te and other metals; they occur as solid solutions within this sulfide or as micro to nano mineral inclusions (Large et al., 2009; Keith et al., 2018; Deditius et al., 2011). Cobalt and nickel ratios in pyrite have long been used to discriminate prospects and mineralization origins, due to its sensibility to environmental changes and physicochemical conditions (Loftus-Hills and Solomon., 1967; Bajwah et al., 1987). Sedimentary-derived pyrite is characterized by Co/Ni < 2 (Bralia et al., 1979, Bajwah et al., 1987; Large et al., 2014; Reich et al., 2016); hydrothermal (vein) pyrite has Co/Ni > 1, while volcanogenic ore pyrite Co/Ni ratios vary from 10 to 50 (Bajwah et al., 1987; Bralia et al., 1979; Hou et al., 2016). The Co/Ni ratios for the studied pyrite show great variations for the same sample. The Carnaubinha silica-hematite alteration volcanoclastic breccia pyrite ratios (Figure 8) vary from 0.33 to 1257, where 93% of the ratio values are > 2, while silica alteration in the volcanoclastic breccia varies from 0.39 to 187, 70.37% of the ratios are > 2, both breccia plot predominantly in the hydrothermal origin. The basement breccia pyrites Co/Ni ratio varies between 0.2 to 441, 82 % of the ratio values are > 2 and 57 % of them are > 10. Finally, São Bento basin conglomerate pyrites Co/Ni ratios range from 0.12 to 10.66, 75% of the spots' ratios are under 1.

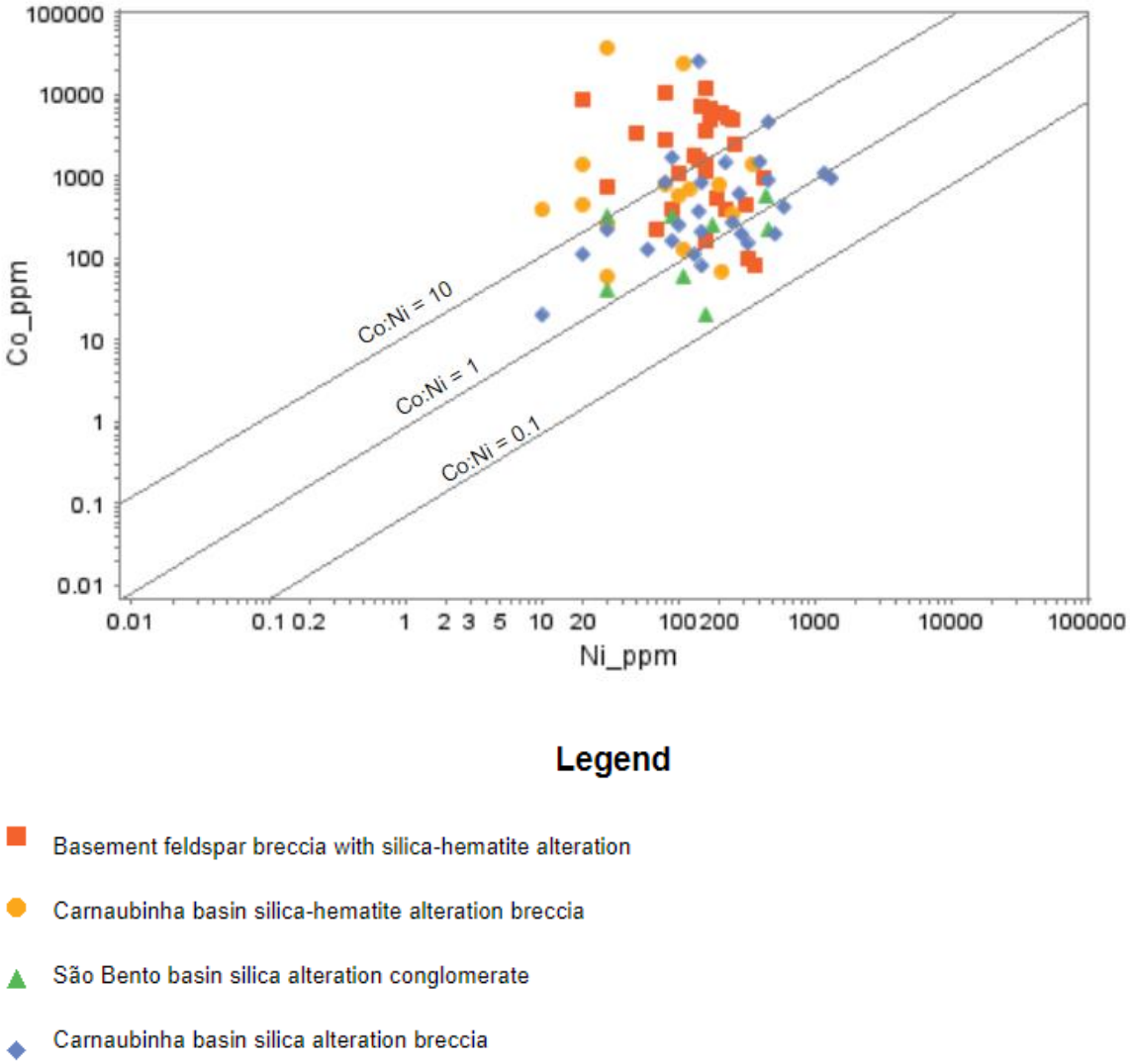

Figure 8. Co:Ni ratio diagram, showing the distribution of the analyzed pyrite samples. Basement n=28, Carnaubinha silica-hematite alteration n=15, Carnaubinha silica alteration n= 27, São Bento basin n=8.

8 Discussion

8.1 The paragenetic sequence of hydrothermal alterations in studied areas

Hydrothermal alteration evolution produced similar features in the different studied areas, despite varying from incipient veins to complete obliteration of the protholith.

In rocks from the OMB and basement, pre-copper enrichment alterations include albite, K-feldspar, epidote and chlorite alteration zones, in this order. Multi-stage hematite and quartz developed concurrently to the precipitation of copper and iron sulfides that were ultimately superimposed by supergene alteration. Hydrothermal evolution is summarized in

Figure 9. Similar patterns occur for different protoliths, such as the acid metavolcanics and the orthogneisses, alteration exhibits a zoning is similar to the one described for IOCG deposits (Haynes, 2000; Barton, 2014).

In the Carnaubinha basin, the distal, sodic alteration is not present, while other pre copper precipitation phases correspond to K-feldspar, epidote and chlorite alteration. These are more incipient in the sedimentary rocks, predominating as veins, except for chlorite alteration, widely spread in the basin, also forming breccias. In the basin, a silicification phase with no iron oxides occurs, associated to calcite, copper minerals and other sulfides. The silica-hematite alteration, also associated to copper minerals precipitation, is very similar to the one affecting basement rocks. They occur in multi-stages with more than one input of silica and/or hematite, varying from incipient veins to stockwork-style and pervasive breccias, although the occurrence of copper is mainly as only one phases. All these alteration types are also superimposed by supergene process and summarized in Figure 9.

In the São Bento basin, alteration is incipient. There are no copper occurrences associated to these sediments; however, hydrothermal alteration is similar to other areas, consisting of hematite, chlorite and sulfide alteration, as well as silicification. Alteration in the São Bento basin does not show similar features to other areas, except for silicification. Hematite and chlorite occur in clasts and matrix, deformed, and might have a sedimentary origin, but also overprint quartz veins forming larger crystals. Sulfide alteration is characterized only by pyrite formation; petrographic relation indicates that they predecease silicification, while crystals show deformation and fractures filled by quartz, indicating pre-hydrothermal origin, possibly synsedimentary. The hydrothermal evolution at the São Bento basin is represented in Figure 9.

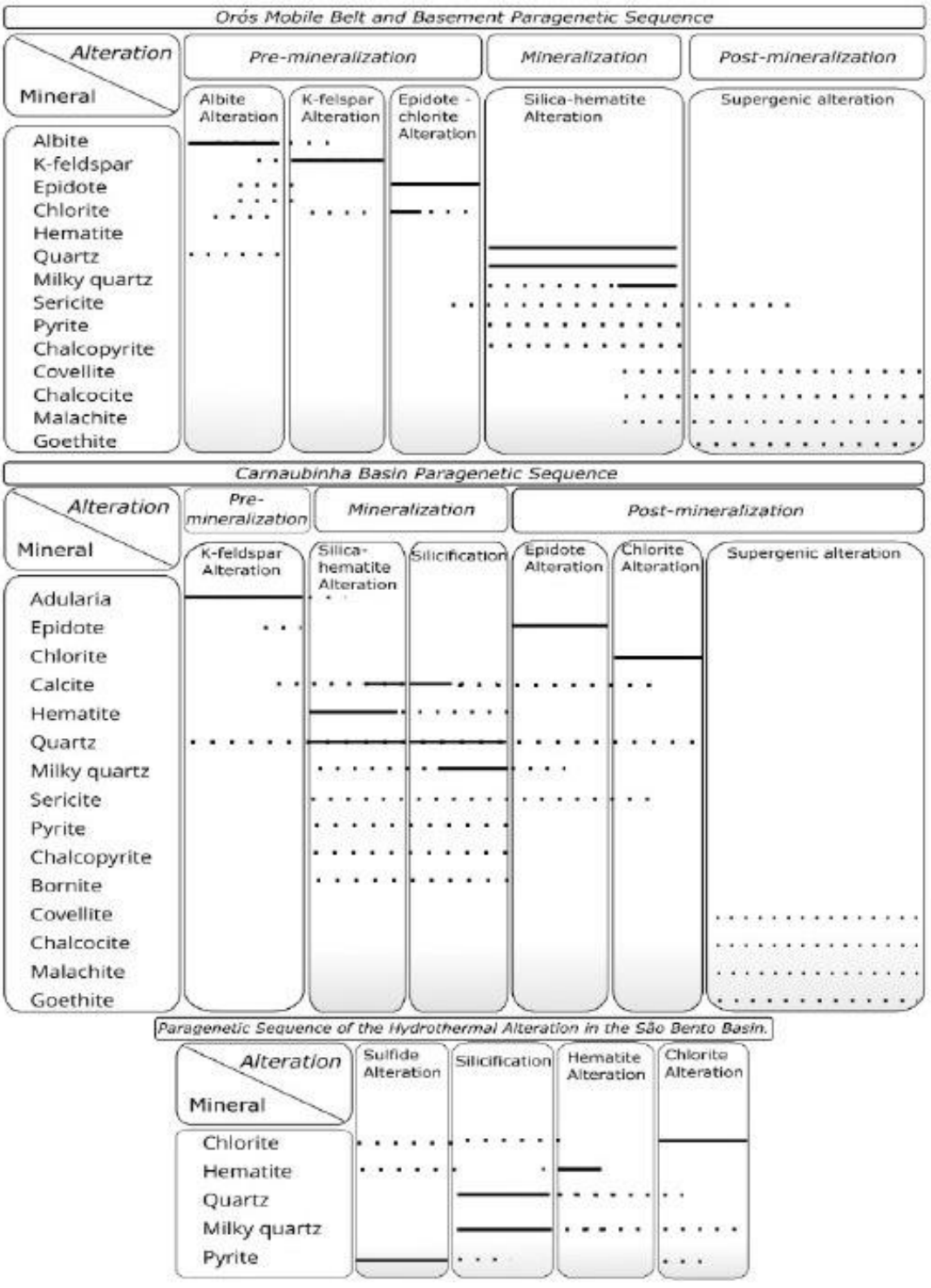

Figure 9. Paragenetic sequence associated to the hydrothermal alteration in the different studied regions.

8.2 The origin and correlation of copper occurrences in the OMB, basement and Carnaubinha basin

The copper occurrences can be divided in two groups: silica-hematite and silica-

sulfide alteration. The occurrences associated to silica-hematite alteration have very similar features, despite different protoliths (orthogneiss, acid metavolcanic or conglomerate), where copper enrichment takes place during pervasive silica-hematite alteration and-or to late veins and stockworks, through the precipitation of copper sulfides, predominantly chalcopyrite. This suggests that hematite formation is mainly conditioned by the hydrothermal fluid, which origin does not reflect the host rock composition. Most likely, a common source originated a fluid that spread regionally and precipitated iron oxides and copper sulfides in different regions.

8.3 Hydrothermal alteration: Geochemical signature and elements mobility

In general, copper occurrences can be divided geochemically into two hydrothermal associations, according to the PCA analyses: i) silica-hematite alteration, affiliated with stronger inputs of Co, Se, Ag, As, Bi and Sb, whose association is observed in orthogneiss breccias from the Jardim region, in the Primavera locality in the borders of theCarnaubinha basin and inside the basin at its southeastern portion, where the protolith is highly altered, but most likely consists in volcanic rocks; ii) silica-sulfide alteration, associated to Ni, Cr, As and Cd, with lower iron and other metal inputs, occurring in the orthogneiss from the Cruz das Almas occurrence and inside the Carnaubinha basin, associated to the conglomerates; this last one showing important gains of Be and Zn.

8.4 The origin of pyrite associated to the hydrothermal alteration types

According to Co/Ni ratios, the Carnaubinha basin volcanoclastic breccias pyrite is interpreted as having a magmatic-hydrothermal origin, characterized by high concentrations of Co. The silica-hematite alteration breccia shows a greater Co enrichment when compared to the silica-alteration breccia, and that can be explained by a higher magmatic contribution in the alteration fluid (e.g., Tan et al., 2022). Similarly, the basement feldspar breccia with silica-hematite alteration pyrites shows the highest Co/Ni ratios, reflecting the predominance of a magmatic source of fluid associated to a minor hydrothermal input origin. Otherwise, the São Bento basin silicified conglomerate pyrite has the lowest ratios, evidencing a synsedimentary origin for this sulfide, while the local higher ratios can result from the hydrothermal interaction with the alteration fluids causing the conglomerate silicification.

8.5 The hydrothermal copper occurrences from the western Borborema Province and IOCG type deposits.

Many are the similarities between the studied occurrences and the IOCG type

deposits. The hydrothermal alteration types are regionally distributed in the area. Analogues to IOCG alteration styles are described by Barton (2014): regional sodic alteration is represented here by albite alteration, followed by potassic alteration that corresponds to K-feldspar replacement of the silicates assemblage, mainly by other feldspars; calcic alteration is represented by epidote and chlorite and, finally, the acidic alteration corresponds to the silicification phase. In the basement and the OMB rocks, all the alteration types above precede copper enrichment, except for silicification, that would represent the final stage of hydrothermal alteration associated to the formation of iron-oxides (hematitization) and copper sulfides, in the main IOCG deposits copper mineralization is commonly associated to the Na-Ca-K alterations, but also occurs in the late stages iron rich alterations. In Carnaubinha basins, there is no early sodic alteration; potassic alteration is very incipient, but similarly silicification bears the copper occurrences, although not strictly associated to iron oxides, while the calcic phases, epidote and chlorite alteration are late to the copper enrichment. The regional structural setting is marked by an early, ductile and later, brittle deformation episode, where the latter appears to have conditioned the hydrothermal alteration zones and formation of copper occurrences.

Hydrothermal alteration and the expressive presence of iron oxides, associated to structurally controlled veins, stockworks and pervasive breccias, in an orogenic collapse environment with no spatial association with intrusive igneous rocks in the studied area, are similar characteristics to the IOCG systems as described by Williams et al. (2005).

The Carnaubinha basin occurrences can thus be interpreted as formed at shallow crustal levels, due to the abundance of silica and vein textures, the presence of adularia-type K-feldspar, epidote, and chlorite alteration. According to Haynes (2000), these alteration types can characterize marginal and shallow zones of IOCG systems, and the OMB and basement can be associated to intermediate zones, where alkaline alterations are more abundant (Haynes, 2000).

The geochemical data also show that the silica-hematite breccias have a Co-Ag-Se-As-Bi-Sb signature, similar to that described by Barton (2014) for distal IOCG deposits (e.g., Great Bear, Mumin et al., 2007).

8.6 The origin of the copper occurrences in the western Borborema Province.

The characteristics of the different occurrences here described allow a better understanding of the similarities and differences of the copper occurrences in the western BP. The transtensional setting in the end of the Brasiliano orogeny provided the formation of

pathways and derived the circulation of fluids in the region; the fluids probably have different origins, but as evidenced by the pyrite chemistry, a magmatic input played an important role. These events may have started with the opening of the rift basins and the formation of important fault zones, such as the Pio IX and Coroatá faults (Figure 1). These allowed the uprising of deep fluids that may have mixed with shallower-derived fluids, resulting in the formation of hydrothermal zones associated to copper occurrences. They lasted longer than the Brasiliano orogeny, since they overprinted the Cambro-Ordovician sediments. These events happened repeatedly through some period, as evidenced by the multiple stages of alteration identified in the studied rocks, and these probably did not affect simultaneously all the region, which is reflected in differences observed in the hydrothermal alteration assemblages and chronology. Mixing of different of fluids of different origins may have resulted in the differences between the studied occurrences, while the occurrences of similar assemblage and compositions may reflect a same event of greater influence.

9 Conclusions

The Orós Mobile Belt and its associated basement rocks were affected by a hydrothermal alteration zoning consisting in albite, K-feldspar, epidote and chlorite alteration, followed by silicification and hematitization associated to the formation of copper minerals. Silica-hematite alteration took place in multiple stages. Similarly, rocks from the Carnaubinha basin are hydrothermally altered by K-feldspar, followed by silicification and silica-hematite alteration. These last two phases affect the rocks pervasively in multiple stages and copper sulfides may be present. These alterations are subsequently overprinted by epidote and chlorite alterations. In the São Bento basin, hydrothermal alteration is mainly represented by silicification, also overprinted by late chlorite alteration, and pyrite in conglomerates precedes hydrothermal alteration.

Geochemistry data show that Cu-rich, silica-hematite breccias also contain high Cr, Mo, Ag, Ba, La and U, while high Cu-silica-sulfide breccias have high Co, Ni, Cd and Bi. The K/Al vs Na/Al diagram (Figure 6) demonstrate that even though weak, a sodic affinity is found in the studied rocks, especially for the feldspar, epidote and silica-sulfide samples. The geochemistry signature can be divided in two streams: Co, Se, Ag, As, Bi and Sb for the silica-hematite alteration samples, and Ni, Cr, As and Cd (Be, Zn) for the silica-sulfide alteration. This suggests that different fluid compositions led to the formation of the copper occurrences.

Pyrite chemistry allowed the interpretation of the fluid source associated to the

formation of the breccias. In this sense, the Carnaubinha and the Coroatá basin breccias, northwest of the studied area, show high Co/Ni ratios, indicating a magmatic hydrothermal source, while the São Bento basin pyrite has low Co/Ni ratios indicating a sedimentary origin.

All these hydrothermal alteration zones and copper occurrences may have had a similar origin, although multiple stages of alteration took place, and more than one source for the fluids may have occurred. To better constrain these origins and properly establish the relationship between these occurrences, it is necessary to generate more detailed data such as the age of the occurrences. We would suggest Re-Os dating of the pyrite and fluid inclusions analyses in the quartz veins and associated calcite for the basin breccias as a means to identify the fluid composition, formation conditions and source.

ACKNOWLEDGMENTS

The authors thank Professor Adolf Fuck and the Microscopy and Microanalises Lab (LMIc) of Universidade Federal de Ouro Preto (UFOP) for financing the geochemistry and micropobe analysis. TFR is greatefull to the Brazilian National Research Council (CNPq) for the Msc scholarship grant

REFERENCES

Aitchinson, J. 1986. The Statistical Analysis of Compositional Data. London, Chapman & Hall Ltd, 416 p.

Almeida, F.F.M. de *et al.* 1981.Brazilian structural provinces: an introduction. Earth-science Reviews, Amsterdam, 17(1-2):1-29.

Araújo, C. E. G. 2006. Mapeamento Lito-estrutural de Uma Porção a NW do Arco Magmático de Santa Quitéria, região de Caracará-CE, auxiliado por Técnicas de Sensoriamento Remoto. Geology Graduation Monograph – Universidade Estadual de Campinas, Campinas, 91 p.

Arthaud, M., Caby, R., Fuck, R., Dantas, E., Parente, C. 2008. Geology of Northern Borborema Province, NE Brazil and its correlation with Nigeria, NW Africa. Geological Society, 294:49-67.

Bajwah, Z., Seccombe, P., Offler, R. 1987. Trace element distribution, Co: Ni ratios and genesis of the big cadia iron-copper deposit, new south wales, australia. Mineralium Deposita. 22:292-300.

Barton, M. D. 2014. Iron Oxide(–Cu–Au–REE–P–Ag–U–Co) Systems. University of Arizona,

Tucson, USA. Elsevier Ltd, 27 p.

Benavides, J., Clark, A., Stanley, C., Oates, C. 2008. Exploration guidelines for copper-rich iron oxide-copper-gold deposits in the Mantoverde area, northern Chile: The integration of host-rock molar element ratios and oxygen isotope compositions. Geochemistry-Exploration Environment Analysis. 8:343-367.

Bralia, A., Sabatini, G., Troja, F. 1979. A revaluation of the Co/Ni ratio in pyrite as geochemical tool in ore genesis problems. Mineral. Deposita 14:353–374.

Brito Neves, B. B. *et al*. 2000. Tectonic history of the Borborema Province, northeastern Brazil. Tectonic Evolution of South America, 1:151-182.

Brito Neves, B. B. 1998. The Cambro-Ordovician of the Borborema Province. Boletim IG - Série Científica, 29:175-193.

Brito Neves, B. B., Schmus, W. R. V., Fetter, A. H. 2001. Noroeste da África – Nordeste do Brasil (Província Borborema) Ensaio comparativo e problemas de correlação. Revista do Instituto de Geociências – USP, 1:59-78.

Brito Neves, B.B.; Cordani, U.G. Tectonic Evolution of South America during the Late Proterozoic. Precambrian Research, v. 53, p. 23-40. 1991.

Chiaradia M., Banks D., Cliff R., Marschik R., de Haller A. 2006. Origin of fluids in iron oxide–copper–gold deposits: constraints from $\delta^{37}Cl$, $^{87}S/^{86}Sr$ and Cl/Br. Mineralium Deposita, 41:565–573.

Dantas, E. L.; Hackspacher, P. C.; Vanschmus, W. R.; Neves, B. B. B. 1997. Archean accretion in the Caldas Brandão Massif, Borborema Province, Northeast Brazil. Revista Brasileira de Geociências, 28(2):221-228.

Deditius A.P., Utsunomiya S., Kesler S.E., Reich M. And Ewing R.C. 2011. Trace Elements Nanoparticles In Pyrite. Ore Geology Reviews, 42:32-46.

Deditius, A., Reich, M., Kesler, S., Utsunomiya, S., Satoshi, U., Chryssoulis, S., Walshe, J., Ewing, R. 2014. The Coupled Geochemistry Of Au And As In Pyrite From Hydrothermal Ore Deposits. Geochimica Et Cosmochimica Acta. 140:644–670.

Delgado, I. M. *Et al*. Geotectônica Do Escudo Atlântico. In: Bizzi, L. A. Et al. 2003. Geologia, Tectônica E Recursos Minerais Do Brasil: Textos, Mapas & Sig. Brasília: Cprm, 227-334 P.

Fetter, A. *Et al*. Evidence For Neoproterozoic Continental Arc Magmatism In The Santa Quitéria Batholith Of Ceará State, Nw Borborema Province, Ne Brazil: Implications For The Assembly Of West Gondwana. 2003. Gondwana Research, 6(2):265-273.

Fetter, A. H. *Et al*. U-Pb And Sm-Nd Geochronological Constraints On The Crustal Evolution And Basement Architecture Of Ceará State, Nw Borborema Province, Ne, Brazil: Implications For The Existence Of The Paleproterozoic Supercontinent "Atlantica". 2000. Revista Brasileira De Geociências, 30(1):102-106.

Fetter, A. H. U/Pb And Sm/Nd Geochronological Constraints On The Crustal Framework And Geologic History Of Ceará State, Nw Borborema Province, Ne Brazil: Implications For The Assembly Of Gondwana. 1999. Ph.D. Thesis. University of Kansas, Kansas. 164 p.

Ganade De Araújo C.E., Weinberg R.F., Cordani U.G. 2014. Extruding The Borborema Province (Ne-Brazil): A Two-Stage Neoproterozoic Collision Process. Terra Nova, 26(2):157-168.

Garcia, M. G. M.; Parente, C. V.; Silva Filho, W. F.; Almeida. A. R. Age Of Magmatic Events In The Eopaleozoic Jaibaras Basin, Ne Brazil: Constraints From U-Pb Zircon Geochronology. 2018. Journal Of South American Earth Sciences, 84.

Gloyn-Jones, J.; Kisters, A. Regional folding, low-angle thrusting and permeability networks: Structural controls of gold mineralization in the Hope reef at Fairview Mine, Barberton Greenstone Belt, South Africa, Ore Geology Reviews, 102: 585-603, 2018.

Gomes, J. R. C.; Vasconcelos, A. M. Jaguaribe Sw: Folha Sb.24-Y: Estados Do Ceará, Pernambuco E Do Piauí. 2000. Programa Levantamentos Geológicos Básicos Do Brasil – Plgb. Rio De Janeiro, Cprm – Serviço Geológico Do Brasil.

Grant, J. A. The Isocon Diagram; A Simple Solution to Gresens' Equation for Metasomatic Alteration. 1986. Economic Geology, 81:1976-1982.

Gresens R.L. Composition-Volume Relationship of Metassomatism. 1967. Chemical Geology, 2:47-65.

Groves, D. I., Bierlein, F. P., Meinert, L. D., Hitzman, M. W. 2010. Iron Oxide Copper-Gold (Iocg) Deposits Through Earth History: Implications for Origin, Lithospheric Setting, And Distinction from Other Epigenetic Iron Oxide Deposits. Economic Geology, 105(3):641-654.

Grunsky, E. C. The Interpretation of Geochemical Survey Data. 2010. Geochemistry:

Exploration, Environment, Analysis, 10(1):27-74.

Grunsky, E. C., And Smee, B. W. The Differentiation Of Soil Types And Mineralization From Multi-Element Geochemistry Using Multivariate Methods And Digital Topography: Journal Of Geochemical Exploration, V. 67, P. 287–299. 1999.

Hitzman, M. W. Iron Oxide-Cu-Au Deposits: What, Where, When, And Why. 2000. In: Hydrothermal Iron Oxide Copper-Gold And Related Deposits: A Global Perspective, 1: 9-25.

Hitzman, M.W., Oreskes, N., And Einaudi, M.T. 1992. Geological Characteristics And Tectonic Setting Of Proterozoic Iron Oxide (Cu-U-Au-Lree) Deposits. 1992. Precambrian Research, 58:241–287.

Hollanda M. H. B. M. 2012. Geocronologia De Eventos Magmáticos E Mineralizações Associadas No Precambriano Da Faixa Seridó, Província Borborema. 2012. Phd Thesis, Universidade De São Paulo, São Paulo, Instituto De Geociências E Astronomia, 94p.

Hou, L., Peng, H., Ding, J., Zhang, J., Zhu, S., Wu, S., Wu, Y., Ouyang, H. 2016. Textures And in Situ Chemical and Isotopic Analyses Of Pyrite, Huijiabao Trend, Youjiang Basin, China: Implications For Paragenesis And Source Of Sulfur. Economic Geology. 111(2): 331–353.

Huhn, S. R. B. *Et al*. 2011. Caracterização Geológica Do Prospecto De Óxido De Ferro-Cobre-Ouro (Iocg), Aurora, Ceará, Brasil. Revista Brasileira De Geociências, 41(3):523-538.

Huhn, S. R. B. *Et al*. Geology of The Riacho Do Pontal Iron Oxide Copper-Gold (Iocg) Prospect, Bahia, Brazil: Hydrothermal Alteration Approached Via Hierarchical Cluster Analysis. 2014. Brazilian Journal of Geology, 44(2):309-324.

Hühn, S. R. B., Silva, A. M. Favorability Potential for Iocg Type Deposits in The Riacho Do Pontal Belt: New Insights for Identifying Prospects of Iocg-Type Deposits. 2018. In Ne Brazil. Brazilian Journal of Geology, 48(4).

Janoušek, V., Farrow, C. M., Erban, V. Interpretation of Whole-Rock Geochemical Data in Igneous Geochemistry: Introducing Geochemical Data Toolkit (Gcdkit). 2006. Journal of Petrology, 47:1255-1259.

Johnson, D.A. And Barton, M.D. Time-Space Development of An External Brine-Dominated, Igneous-Driven Hydrothermal System: Humboldt Mafic Complex, Western Nevada, Part I. In: Dilles, J.H., Barton, M.D., Johnson, D.A., Proffett, J.M. And Einaudi, M.T. 2000. Eds., Contrasting Styles of Intrusion-Associated Hydrothermal Systems: Guidebook Series, Vol. 32,

Society of Economic Geologists, 127-144 p.

Klein, E.L.; Moura, C.A.V. 2008. São Luís Craton and Gurupi Belt (Brazil): Possible Links with The West-African Craton and Surrounding Pan-African Belts. In: R.J. Pankhurst, R.A.J. Trouw, B.B. Brito Neves, M.J. De Wit (Eds) West Gondwana: Pre-Cenozoic Correlations Across the South Atlantic Region. Geologic Society London, Special Publications 294:137-151.

Large, R. R., Gemmell, J. B., Paulick, H., Huston, D. L. 2001. The Alteration Box Plot: A Simple Approach to Understanding the Relationship Between Alteration Mineralogy And Lithogeochemistry Associated to Volcanic-Hosted Massive Sulfide Deposits. Economic Geology, 96(5):957-971.

Large, R. R., Mcphie, J., Gemmell, J. B., Herrmann, W., Davidson, G. J., 2001. The Spectrum of Ore Deposit Types, Volcanic Environments, Alteration Halos, And Related Exploration Vectors in Submarine Volcanic Successions: Some Examples From Australia. Economic Geology, 96: 913- 938.

Large, R., Danyushevsky, L., Hollit, C., Maslennikov, V., Meffre, S., Gilbert, S., Bull, S., Scott, R., Emsbo, P., Thomas, H., Singh, B., Foster, J. 2009. Gold And Trace Element Zonation In Pyrite Using A Laser Imaging Technique: Implications For The Timing Of Gold In Orogenic And Carlin-Style Sediment-Hosted Deposits. Economic Geology. 104:635-668.

Large, R., Halpin, J., Danyushevsky, L., Maslennikov, V., Bull, S., Long, J., Gregory, D., Lounejeva, E., Lyons, T., Sack, P., Mcgoldrick, P., Calver, C., 2014. Trace Element Content Of Sedimentary Pyrite As A New Proxy For Deep-Time Ocean–Atmosphere Evolution. Earth And Planetary Science Letters. 389:209-220.

Loftus-Hills, G., Solomon, M. 1967. Cobalt, Nickel and Selenium In Sulfides As Indicators Of Ore Genesis. Mineralium Deposit*a* 2:228–242.

Maas, M. V. R. 2003. Integração De Dados De Geofísica Aérea E Geologia Aplicada A Exploração Mineral No Setor Sudoeste Do Cinturão Cuprífero Orós-Jaguaribe – Província Borborema. MS Dissertation, Instituto De Geociências, Universidade De Brasília, Brasília, 77 p.

Mabessone, J. M. 2002. História Geológica Da Província Borborema (Ne Brasil). Revista De Geologia Da Ufc, 15:119-129.

Machado, M. A. 2006. Caracterização Descritiva E Genética De Ocorrências Cupro-Hematíticas No Setor Sudoeste Do Sistema Orós-Jaguaribe Província Borborema..MS Dissertation, Instituto De Geociências, Universidade De Brasília, Brasília, 118 p.

Manuel Keith, Daniel J. Smith, Gawen R.T. Jenkin, David A. Holwell, Matthew D. Dye. 2018. A Review of Te and Se Systematics in Hydrothermal Pyrite from Precious Metal Deposits: Insights into Ore-Forming Processes. Ore Geology Reviews, 96:269-282.

Medeiros V.C. 2004. Evolução Geodinâmica E Condicionamento Estrutural Dos Terrenos Piancó-Alto Brígida E Alto Pajeú, Domínio Da Zona Transversal, Ne Do Brasil. Phd Thesis, Centro De Ciências Exatas E Da Terra, Universidade Federal Do Rio Grande Do Norte, Natal, 200 P.

Monteiro, L. V., Xavier, R. P., De Carvalho, E. R., Hitzman, M. W., Johnson, C. A., De Souza Filho, C. R., Torresi, I. 2008. Spatial And Temporal Zoning of Hydrothermal Alteration and Mineralization in The Sossego Iron Oxide-Copper-Gold Deposit, Carajás Mineral Province, Brazil: Paragenesis and Stable Isotope Constraints. Mineralium Deposita, 42:129-159.

Moreto C.P.N.; Monteiro L.V.S.; Xavier R.P.; Creaser R.A., Dufrane S.A., Tassinari C.C.G.; Sato K.; Kemp A.I.S., Amaral W.S. 2015. Neoarchean and Paleoproterozoic iron oxide-copper-gold events at the Sossego Deposit, Carajás Province, Brazil: Re-Os and U-Pb geochronological evidence. Economic Geology, 110:809-835.

Nascimento, M. A. L. Petrologia do magmatismo Tardi-Brasiliano no Maciço São José de Campestre (RN/PB), com ênfase no Plúton Alcalino Caxexa. 2000. Phd Thesis, Centro de Ciências Exatas e da Terra – Universidade Federal do Rio Grande do Norte, Natal. 129 f.

Nogueira Neto J.A. 2000. Evolução Geodinâmica das faixas granulíticas de Granja e Cariré, extremo noroeste da Província Borborema. PhD Thesis, Instituto de Geociências e Ciências Exatas, Universidade Estadual Paulista, 171 p.

Oliveira R., Medeiros W. 2018. Deep crustal framework of the Borborema Province, NE Brazil, derived from gravity and magnetic data. Precambrian Research, 315:45-65.

Oliveira, D. C.; Martins, G.; Branco, R. M. G. C.; *et al*. 2001. Um modelo alternativo para a formação da bacia do Jaibaras: implicações para a evolução final da cadeia brasiliana/pan-africana no noroeste da província Borborema. Revista de Geologia. Fortaleza, 14(1).

Oliveira, R. G. de. 2008. Arcabouço geofísico, isostasia e causas do magmatismo cenozóico da

Província Borborema e de sua margem continental (Nordeste do Brasil). 2008. Phd Thesis - Centro de Ciências Exatas e da Terra, Universidade Federal do Rio Grande do Norte, Natal, 415 p.

Oliveira, R., R.; Vilalva, F. C. J., Alves, A., Medeiros, V. C., DALAN, C. A. 2020. The Catolé do Rocha Batholith (RN-PB): A reduced A2-type granitic magmatism in the Rio Piranhas-Seridó Domain, Borborema Province, Northeastern of Brazil. Geologia USP Série científica. 20:166-190.

Parente, C. V. ; Arthaud, M. H. O. 2004a. Geologia e tipologia do minério da ocorrência de Cu-Fe associada à Sequência Metavulcano-Sedimentar Cachoeirinha, região de Aurora-CE. Revista de Geologia da UFC, 17(2):157-172.

Parente, C. V. ; Silva Filho, W. F. ; Almeida, A. R. 2004. Bacias do estágio de transição do domínio setentrional da Província Borborema. In: MANTESSO NETO V. *et al.* (Ed.). Geologia do Continente Sul-Americano: Evolução da obra de Fernando Flávio Marques de Almeida. Editora Beca, São Paulo, 11 p.

Parente, C. V. *et al.* 2011.Contexto geológico, tipológico e geoquímico isotópico das brechas hidrotermalizadas de ferro e cobre tipo IOCG associadas à bacia Eopaleozóica Jaibaras, da Província Borborema, Brasil. In : Contribuições da Metalogenia do Brasil. Frants, J.C., Marques, J.C. Hardy, J, 1:75-197.

Parente, C. V.; Arthaud, M. H. 1995. O Sistema Orós-Jaguaribe no Ceará, NE do Brasil. Revista Brasileira de Geociências, 25(4):297-306.

Pearce, T. H. 1968. A contribution to the theory of variation diagrams. Contributions to Mineralogy and Petrology, 19:142–157.

Pedrosa Junior, N. 2015. Interpretação e Modelagem de Dados Geofísicos no Estudo da Evolução Geotectônica do Rifte de Jaibaras – NE do Brasil. Phd Thesis, Instituto de Geociências, Universidade de Brasília, Brasília. 187 p.

Reich, M., Simon, A. C., Deditius, A., Barra, F., Chryssoulis, S., Lagas, G., Tardani, D., Knipping, J., Bilenker, L., Sánchez-Alfaro, P., Roberts, M. P., Munizaga, R. 2016. Trace Element Signature of Pyrite from The Los Colorados Iron Oxide-Apatite (Ioa) Deposit, Chile: A Missing Link Between Andean Ioa and Iron Oxide Copper-Gold Systems? Economic Geology. 111 (3): 743–761.

Santos Filho, F. F. B., Magini, C., Castelo Branco, R. M. G. 2015. Interpretação das Assinaturas Geofísicas Relacionadas a Estrutura da Bacia de Cococi e Mineralizações de Barita – SW do CE. Revista de Geologia da UFC, 28(2):79-100.

Santos, E. J. 1996. Ensaio preliminar sobre terrenos e tectônica acrescionária na Província Borborema. In: CONGRESSO BRASILEIRO DE GEOLOGIA, 39. Salvador. Anais. Salvador: SBG, 1996, 6:47-50.

Santos, T. J. S. *et al*. 2004. Structural and geochronological studies of the Médio Coreaú Domain, NE Brazil: Contraints on Brasiliano/Pan-African tectonic evolution in the NW part of the Borborema Province. Journal of the Virtual Explorer, 17:9-9.

Santos, T. J. S.; Garcia, M. G. M.; Amaral, W. S.; Caby, R.; Wernick, E.; Arthaud, M. H.; Dantas, E. L.; Santosh, M. 2009. Relics of eclogite facies assemblages in the Ceará Central Domain, NW Borborema Province, NE Brazil: Implications for the assembly of West Gondwana, Gondwana Research, 15:3–4.

Saraiva, C. E. R.; Rodrigues, T. F. R.; 2018. Mapeamento geológico e petrografia das ocorrências de cobre da Bacia de Carnaubinha, Pio IX - Piauí. Geology Graduation Monograph – Universidade Federal do Ceará, Fortaleza, 122 p.

Silva, João Gabriel Ferreira da Silva; Carneiro, Laryssa de Sousa. 2018. Mapeamento geológico e das alterações hidrotermais associadas às ocorrências de ferro na região de Pio IX – PI. Graduation Monograph – Universidade Federal do Ceará, Fortaleza, 148 p.

Stanley, C. R. Molar element ratio analysis of lithogeochemical data: a toolbox for use in mineral exploration and mining. Geochemistry: Exploration, Environment, Analysis. v. 20, p. 233–256. 2019.

Stanley, C. R., and Madeisky, H. E., 1994, Lithogeochemical exploration for hydrothermal ore deposits using Pearce element ratio analysis, in Short Course Notes 11: Waterloo, Geological Association of Canada, 193:212.

Tan, H., Shao, Y., Liu, O., Zhang, Y., Feng, Y., Zhang, Y., Shah, S. A. 2022. Textures, trace element geochemistry and in-situ sulfur isotopes of pyrite from the Xiaojiashan gold deposit, Jiangnan Orogen: Implications for ore genesis. Ore Geology Reviews, 144:104843.

Taylor, R. 2009. Ore Textures: recognition and interpretation. Springer, Berlin Heidelberg. 288 p.

Uvula, Eduardo Ernesto; Didoné, Maria Eduarda Zilio. 2019. Mapeamento Geológico E Petrografia Das Ocorrências De Cobre Na Bacia De São Bento, Extremo Leste Do Piauí-Pi. Graduation Monograph – Universidade Federal do Ceará, Fortaleza, 108 p.

Van der Wielen, S., Fabris, A., Halley, S., Keeling, J., Mauger, A., Gordon, G., Keeping, T., Giles, D., Hill, S. 2013. An exploration strategy for IOCG mineral systems under deep cover. MESA Journal. 71:18.

Van Schmus, W.R.; Kozuch, M.; Brito Neves, B.B. 2011 Precambrian history of the Zona Transversal of the Borborema Province, NE Brazil: Insights from Sm–Nd and U–Pb geochronology, Journal of South American Earth Sciences, 31:2–3.

Parente, C. U. V. *et al*. 2014.Carta geológica da folha Pio IX: SB. 24-YA-VI.

Veríssimo, C. U. V. et al. 2016. The Itataia phosphate-uranium deposit (Ceará, Brazil) new petrographic, geochemistry and isotope studies. Journal of South American Earth Sciences, 70:115–144.

Williams, P. J. *et al*. 2005. Iron oxide copper-gold deposits: Geology, space-time distribution, and possible modes of origin. Economic Geology, 371-405.

Xavier R.P., Wiedenbeck M., Trumbull R.B., Dreher, A.M., Monteiro, L.V., Rhede, D., Torresi, I. 2008. Tourmaline B-isotopes fingerprint marine evaporites as the source of high-salinity ore fluids in iron oxide copper-gold deposits, Carajás Mineral Province (Brazil). Geology, 36:743-746.

Xavier, R. P., Monteiro, L. V. S., Moreto, C. P. N., Pestilho, A. L. S., Melo, G. D., Silva, M. D., Silva, F. E. 2012. The iron oxide copper-gold systems of the Carajás mineral province, Brazil. Society of Economic Geologists, 16:433-453.

Zhou, D., Chang, T., Davis, J. C. 1983. Dual extraction of R-mode and Q-mode factor solutions. Journal of the International Association for Mathematical Geology, 15(5):581-606.

SUPPLEMENTARY DATA

Table S1. Summary of Petrographic features of hydrothermal alterations in OMB rocks

Hydrothermal Alteration Type	Zone	Style	Color	Mineral assemblage											
				Textural characteristics of minerals	Ab	Kfs	Qz	Ep	Chl	Cal	Hmt	Gth	Py	Cpy	Bn	Mlc
Albite	Distal	Structurally controlled, veins and veinlets; pervasive	Pink	Size variation (mm)	0.1-0.4	-	<0.1-0.8	-	-	-	-	-	-	-	-	-
				Shape	Subhedral to anhedral	-	Subhedral to anhedral	-	-	-	-	-	-	-	-	-
K-feldspar	Intermediate	Structurally controlled veins and veinlets; pervasive	Red	Size variation (mm)	0.1-0.3*	0.2-1.5	<0.1-0.3	-	-	0.1-0.6*	-	-	-	-	-	-
				Shape	Anhedral*	Subhedral to anhedral	Anhedral	-	-	Subhedral to anhedral*	-	-	-	-	-	-
Epidote	Intermediate	Structurally controlled veins; stockwork vein sets	Green	Size variation (mm)	-	-	0.1-1.0*	<0.1-0.2	-	0.1-0.4*	-	-	-	-	-	-
				Shape	-	-	Subhedral to anhedral*	Subhedral to anhedral	-	Subhedral to anhedral*	-	-	-	-	-	-
Chlorite	Intermediate	Structurally controlled veins and veinlets[1]; pervasive[2]	Green	Size variation (mm)	-	-	0.05-0.3*	<0.1*	0.1 – 0.6	0.06-0.6*	-	-	-	-	-	-
				Shape	-	-	Subhedral to anhedral*	Subhedral to anhedral*	Subhedral to anhedral	Subhedral to anhedral*	-	-	-	-	-	-
Silicification	Intermediate/ Proximal	Structurally controlled veins and veinlets[1]; pervasive[2]	Black, gray, white	Size variation (mm)	-	0.6-1.0*	<0.2-20	<0.1-0.6*	-	0.1-10*	-	-	<0.1-50*	<0.1-10*	1-10*	<0.1-1*0
				Shape	-	Euhedral to subhedral*	Anhedral to subhedral	Subhedral to anhedral*	-	Euhedral to anhedral*	-	-	Euhedral to anhedral*	Euhedral to subhedral*	Euhedral to subhedral*	Anhedral*

Silica-hematite	Proximal	Structurally controlled veins and veinlts	Black, brown	Size variation (mm)	-	-	<0.1 - 0.2	-	-	-	<0.1 - 0.4	<0.1 - 0.2	0.2	<0.1 – 0.5	-	<0.1 – 0.2
				Shape	-	-	Anhedral to subhedral	-	-	-	Anhedral	Anhedral	Euhedral to subhedral	Subhedral to anhedral	-	Subhedral to anhedral
Sulfide (copper enrichment)	Proximal	Structurally controlled veins and veinlets; pervasive	-	Size variation (mm)	-	-	-	-	-	-	-	-	<0.1-50	<0.1-20	-	<0.1-10
				Shape	-	-	-	-	-	-	-	-	Euhedral to anhedral	Euhedral to anhedral	-	Anhedral

*Mineral is not necessarily present in hydrothermal alteration assemblage, but it is common.

[1]characterizes the channeled silicification phase; [2]characterizes the pervasive silicification phase

Table S2. Petrographic features of the copper occurrences in the Orós Mobile Belt and basement.

Occurrence	**Hydrothermal Alteration (Mineral) Index**	**Textural characteristic**	**Qz**	**Ser**	**Hmt**	**Gth**	**Py**	**Cpy**	**Mlc**	**Mag**	**Ilm**	**Spl**	**Cpx**
Primavera	**Quartz-Hematite**	Grain-size variation (mm)	<0.1 - 0.2	-	<0.1 - 0.2	<0.1 - 0.2	0.2	<0.1	-	-	-	-	-
		Grain-shape	Anhedral to subhedral	-	Anhedral	Anhedral	Euhedral to subhedral	Subhedral to anhedral	-	-	-	-	-
	Magnetite	Grain-size variation (mm)	-	-	-	-	-	-	-	0.5 - 2	0.5 - 1	0.1 - 0.5	0.1 - 0.3
		Grain-shape	-	-	-	-	-	-	-	Euhedral to subhedral	Euhedral to subhedral	Subhedral to anhedral	Subhedral to anhedral
Jardim-Coroatá	**Quartz-hematite**	Grain-size variation (mm)	<0.1	0.1	<0.1- 0.2	<0.1- 1.0	-	-	-	-	-	-	-
		Grain-shape	Anhedral	Anhedral	Subhedral to anhedral	Anhedral	-	-	-	-	-	-	-

Cruz das Almas	**Sulfide and copper enrichment**	Grain-size variation (mm)	-	-	-	0.5 - 2	<0.1-50	<0.1-20	<0.1-10	-	-	-	-
		Grain-shape	-	-	-	Euhedral to subhedral	Euhedral to anhedral	Euhedral to anhedral	Anhedral	-	-	-	-
	Quartz enrichment	Grain-size variation (mm)	<0.2	-	-	-	-	<0.1 – 0.5	<0.1 – 0.2	-	-	-	-
		Grain-shape	Anhedral	-	-	-	-	Euhedral to subhedral	Subhedral to anhedral	-	-	-	-
Surubim	**Quartz enrichment**	Grain-size variation (mm)	0.1 - 0.2	-	-	-	-	-	-	-	-	-	-
		Grain-shape	Subhedral to anhedral	-	-	-	-	-	-	-	-	-	-
	Quartz-hematite	Grain-size variation (mm)	<0.2	-	<0.1 – 0.4	<0.1 – 0.2	-	-	-	-	-	-	-
		Grain-shape	Anhedral	-	Subhedral to anhedral	Anhedral	-	-	-	-	-	-	-

Table S3. Geochemistry results for the OMB and Carnaubinha basin ydrothermal alterations and copper occurrences.

Region		**Basement**															**Carnaubinha Basin**					
Lithotype		**Low alteration orthogneiss**		**Feldspar-alteration breccia**	**Epidote-chlorite alteration feldspar breccia**		**Silica-hematite alteration feldspar breccias**			**Silica-hematite breccias**						**Silica-sulphide breccia**	**K-Feldspar and Epidote-chlorite-alteration (veins) Conglomerate**	**Silicified conglomerate breccia**	**Chlorite-epidote-alteration conglomerate breccia**	**Silica-hematite volcanoclastic breccia**	**Silica-alteration volcanoclastic breccia**	**Silica-sulphide Volcanoclastic breccia**
Locality						**Jardim**	**Surubim**		**Coroatá**	**Coroatá**			**Jardim**	**Primavera**	**Jardim**	**Cruz das Almas**						
Sample		**PIO IX 711**	**P 885**	**PIO IX 444**	**PIO IX 449**	**J05A**	**SB05C**	**PIO IX 129 A**	**CROATA 2A**	**CROATA 3E**	**PIO IX 118 A**	**PIO IX 118 B**	**J12**	**C01A1**	**J01C**	**CDA01**	**THC24V**	**THC24A**	**C25A**	**C25C**	**THC25**	**THC26**
SiO2	%	76.00	74	73.8	73.7	58.05	72.3	73	59	61.49	84	84.3	48.07	82.46	90.11	86.79	74.73	83.53	75.68	68.59	74.64	78.64
TiO2	%	0.00	0	0.03	0.04	1.01	0.05	0.8	0.3	0.1	0.2	0.23	0.05	0.04	0.04	0.26	0.58	0.13	0.51	0.09	0.14	0.39
Al2O3	%	13.00	14	13.9	13.1	15.42	5.66	11	11	0.53	8.3	7.9	1.22	0.49	0.33	3.99	10.94	1.95	10.52	1.23	14.52	7.87
Fe2O3	%	1.00	1	1.07	2.4	7.94	18.48	5.2	22	37.14	3.1	2.89	49.57	14.26	5.62	3.9	3.88	1.27	3.32	27.59	2.04	4.52
MnO	%	0.00	0	0.01	0.02	0.06	0.01	0	0	<0.01	<0.01	<0.01	0.02	0.01	<0.01	0.01	0.06	0.07	0.05	0.01	0.02	0.01
MgO	%	0.00	0	0.04	0.02	0.08	0.06	0	0.1	<0.01	0	0.06	0.03	0.03	0.01	0.3	1.69	0.2	1.16	0.03	0.12	0.04
CaO	%	2.00	1	0.4	1.89	13	0.08	0.1	0.3	0.02	0.1	0.07	0.02	0.07	0.02	0.08	1.25	6.37	1.76	0.09	0.22	0.06
Na2O	%	3.00	3	2.36	3.27	1.35	1.59	1.7	5.6	0.03	0.1	0.03	0.01	<0.01	0.1	1.74	4.09	0.42	3.16	<0.01	6.32	2.39
K2O	%	5.00	6	7.43	4.79	0.15	1.94	7.3	0.6	<0.01	0.1	0.08	0.05	0.01	0.02	0.11	1.47	0.57	1.83	0.12	2.06	2.57
P2O5	%	0.00	0	0.03	0.02	0.25	0.02	0	0.1	<0.01	0.1	0.06	0.02	0.08	0.01	0.05	0.15	0.03	0.15	0.18	0.04	0.02
Cr2O3	%	<0.002	<0.002	<0.002	<0.002	0.01	0.01	<0.002	0	<0.002	<0.002	0.004	0.01	0.01	0.01	0.03	0.01	<0.01	0.02	0.01	<0.01	0.01
SO3	%	n.a.	n.a.	n.a.	n.a.	0.01	0.01	n.a.	n.a.	n.a.	n.a.	n.a.	0.07	0.46	0.19	0.02	0.01	0.41	0.01	0.1	0.01	8.7
SrO	%	n.a.	n.a.	n.a.	n.a.	0.41	0.01	n.a.	n.a.	n.a.	n.a.	n.a.	0.01	<0.01	<0.01	<0.01	0.01	0.01	0.04	<0.01	0.05	0.01
BaO	%	n.a.	n.a.	n.a.	n.a.	0.01	0.02	n.a.	n.a.	n.a.	n.a.	n.a.	0.01	0.02	0.01	0.01	0.07	0.03	0.11	0.01	0.12	0.1
TOTAL	%	100.00	99.00	100	99.9	99.37	100.75	100	100	99.94	100	99.96	99.91	100.1	98.9	100.9	100.65	100.5	99.4	99.43	101.1	109.25
LOI_wt	%	0	1	0.9	0.7	1.47	0.45	0.2	0.5	0.6	3.9	4.3	0.7	1.87	0.93	1.49	1.66	5.22	1.04	1.13	0.75	3.88

Al	%	n.a.	n.a.	n.a.	n.a.	1.64	0.26	n.a.	n.a.	n.a.	n.a.	n.a.	0.18	0.16	0.06	0.4	1.23	0.17	1.1	0.34	0.43	0.3
S	%	n.a.	n.a.	n.a.	n.a.	<0.01	<0.01	n.a.	n.a.	n.a.	n.a.	n.a.	0.02	0.18	0.08	<0.01	<0.01	0.17	<0.01	0.03	<0.01	3.46
Na	%	n.a.	n.a.	n.a.	n.a.	0.02	0.02	n.a.	n.a.	n.a.	n.a.	n.a.	<0.01	<0.01	<0.01	0.03	0.05	0.01	0.03	<0.01	0.07	0.05
Mg	%	n.a.	n.a.	n.a.	n.a.	0.03	0.04	n.a.	n.a.	n.a.	n.a.	n.a.	0.02	0.02	0.01	0.14	1.02	0.1	0.66	0.02	0.06	0.01
K	%	n.a.	n.a.	n.a.	n.a.	0.01	0.07	n.a.	n.a.	n.a.	n.a.	n.a.	0.03	0.01	0.01	0.01	0.04	0.04	0.06	0.02	0.05	0.14
Ca	%	n.a.	n.a.	n.a.	n.a.	2.46	0.04	n.a.	n.a.	n.a.	n.a.	n.a.	0.02	0.06	0.02	0.04	0.81	4.65	0.67	0.07	0.03	0.02
Li	ppm	n.a.	n.a.	n.a.	n.a.	0.4	0.3	n.a.	n.a.	n.a.	n.a.	n.a.	0.2	0.3	0.3	1.1	11.4	1.6	7.1	0.3	2.4	0.2
Be	ppm	1	<1	2	2	1.62	0.42	<1	2	<1	<1	<1	0.43	1.61	0.46	0.32	0.29	0.07	0.68	0.62	0.43	0.05
P	ppm	n.a.	n.a.	n.a.	n.a.	1020	70	n.a.	n.a.	n.a.	n.a.	n.a.	50	350	30	180	680	130	630	760	160	20
B	ppm	n.a.	n.a.	n.a.	n.a.	<10	<10	n.a.	n.a.	n.a.	n.a.	n.a.	<10	<10	<10	<10	<10	<10	<10	<10	<10	<10
Sc	ppm	<1	<1	<1	<1	3.1	2	2	3	3	4	4	3.2	0.6	0.4	0.9	4.1	1	3.1	0.9	0.8	0.5
Ti	%	n.a.	n.a.	n.a.	n.a.	0.189	0.015	n.a.	n.a.	n.a.	n.a.	n.a.	0.013	<0.005	0.006	0.006	0.196	0.005	0.164	<0.005	0.009	<0.005
V	ppm	<8	<8	12	22	17	93	20	139	75	20	26	100	69	15	16	36	5	31	13	9	2
Cr	ppm	n.a.	n.a.	n.a.	n.a.	21	9	n.a.	n.a.	n.a.	n.a.	n.a.	10	33	79	79	79	17	46	32	10	53
Mn	ppm	n.a.	n.a.	n.a.	n.a.	141	61	n.a.	n.a.	n.a.	n.a.	n.a.	120	88	39	53	485	526	339	93	106	26
Fe	%	n.a.	n.a.	n.a.	n.a.	1.64	9.68	n.a.	n.a.	n.a.	n.a.	n.a.	18.7	9.41	3.52	2.54	2.6	0.82	1.91	18.2	1.17	3.04
Co	ppm	1	2	1.3	0.7	0.4	3.4	0.4	5.9	1.8	1	1.1	3.3	7.9	3.4	7	8.8	1.3	6.2	13.4	2.1	38.9
Ni	ppm	2	3	1.1	1.8	4	1.6	1.1	2.5	1.4	1	1.6	1.3	13.4	3.3	12.7	24.2	4.6	22.1	10.2	4	9.9
Cu	ppm	4	4	3	2.5	15.3	56.7	2.8	2.2	2.4	3	16.2	14.5	**2400**	**>10000**	**>10000**	10.3	**2460**	47.2	1880	18.1	12
Zn	ppm	21	38	9	25	3	4	19	8	<1	43	54	19	9	2	6	70	9	39	18	34	2
Ga	ppm	12	16	20.7	19.2	11.5	1.9	8.5	11	2.3	10	10.5	1.96	1.89	0.31	1.87	6.77	0.78	6.02	1.2	1.73	1.06
Ge	ppm	n.a.	n.a.	n.a.	n.a.	0.95	0.08	n.a.	n.a.	n.a.	n.a.	n.a.	0.15	0.13	<0.05	<0.05	0.14	<0.05	0.15	0.22	<0.05	<0.05
As	ppm	<0.5	<0.5	<0.5	<0.5	0.7	0.5	<0.5	<0.5	0.7	<0.5	<0.5	1.8	16.1	0.6	3	1.6	0.7	1.5	6.6	1	0.6
Se	ppm	<0.5	<0.5	<0.5	<0.5	0.2	<0.2	<0.5	<0.5	<0.5	<0.5	<0.5	0.2	8.2	2.1	0.7	0.2	0.9	<0.2	36.3	<0.2	5
Rb	ppm	88	n.a.	321	218	1.5	7.5	214	21	0.6	8.2	4.9	6.5	1	0.3	0.5	1.8	2.2	3.6	0.8	3.1	2.7
Sr	ppm	n.a.	n.a.	91.1	398	849	10.7	120	128	14.1	74	38.8	12.2	8.4	10.2	6.8	16.1	42.5	107	12.3	10.7	6.7
Y	ppm	1	3	1.8	10.9	48.5	4.18	8.7	8.7	0.4	8	5.6	0.99	7.28	0.92	2.86	13.45	4.66	11.7	0.91	3.34	0.63
Zr	ppm	49	66	10.1	75.2	26.6	1.8	205	158	16.4	110	81.9	2.5	0.5	<0.5	0.9	7.8	1.3	10.9	3.2	6.3	2.6

Nb	ppm	1	1	2.6	4.1	1.18	4.23	9.9	6.4	4.4	4.9	5.4	0.53	0.07	0.2	<0.05	0.64	0.07	0.69	0.11	0.95	0.08
Mo	ppm	1	0	0.3	0.7	0.35	0.47	0.2	0.8	1.1	0.4	0.5	18.55	2.51	5.58	4.44	0.28	0.3	0.24	0.35	0.2	0.29
Ag	ppm	<0.1	<0.1	<0.1	<0.1	<0.01	<0.01	<0.1	<0.1	<0.1	<0.1	<0.1	0.06	0.83	2.62	0.68	0.01	0.38	0.02	0.84	0.06	0.12
Cd	ppm	<0.1	<0.1	<0.1	<0.1	0.01	<0.01	<0.1	<0.1	<0.1	<0.1	<0.1	0.01	0.01	<0.01	0.04	0.02	0.01	0.02	0.01	0.01	<0.01
In	ppm	n.a.	n.a.	n.a.	n.a.	0.062	0.005	n.a.	n.a.	n.a.	n.a.	n.a.	0.01	1.88	0.087	0.518	0.017	0.066	0.018	0.122	0.013	<0.005
Sn	ppm	<1	<1	1	1	3.3	3.9	6	3	1	2	<1	6.3	0.3	0.4	0.2	1.3	0.2	0.8	0.4	0.7	0.3
Sb	ppm	<0.1	<0.1	<0.1	<0.1	0.07	0.07	<0.1	<0.1	<0.1	<0.1	<0.1	0.12	0.11	0.06	0.07	0.1	0.1	0.07	0.1	0.28	0.07
Te	ppm	n.a.	n.a.	n.a.	n.a.	0.01	<0.01	n.a.	n.a.	n.a.	n.a.	n.a.	0.02	0.26	0.06	0.02	<0.01	0.01	0.01	1.6	0.02	0.09
Cs	ppm	1	0	1.6	1	0.13	0.05	2.2	0.1	<0.1	<0.1	0.1	0.09	0.05	<0.05	<0.05	0.06	0.07	0.1	<0.05	0.06	<0.05
Ba	ppm	n.a.	n.a.	123	293	20	120	n.a.	76	41	37	51	140	230	150	30	40	40	60	80	90	60
La	ppm	3	18	3.6	10.1	210	13.4	3.4	31	3.8	20	11.6	4.3	5.5	4	11.3	31.3	5.9	20.6	1.6	13.5	3.2
Ce	ppm	5	35	9.2	27.6	440	37.8	9.3	58	4.5	43	24.3	10.3	14.65	6.77	20.5	57.8	12.25	40	4.43	28.8	6.54
Pr	ppm	0	4	0.77	3.11	n.a.	n.a.	1.1	6.8	0.47	4.6	2.56	n.a.	n.a.	n.a.	n.a.	n.a.	n.a.	n.a.	n.a.	n.a.	n.a.
Nd	ppm	2	13	2.5	10.7	n.a.	n.a.	4.2	28	1.6	16	9.8	n.a.	n.a.	n.a.	n.a.	n.a.	n.a.	n.a.	n.a.	n.a.	n.a.
Sm	ppm	0	2	0.53	3.55	n.a.	n.a.	1.2	3.7	0.18	2.6	1.57	n.a.	n.a.	n.a.	n.a.	n.a.	n.a.	n.a.	n.a.	n.a.	n.a.
Eu	ppm	1	1	0.4	0.41	n.a.	n.a.	0.3	0.7	<0.02	0.4	0.33	n.a.	n.a.	n.a.	n.a.	n.a.	n.a.	n.a.	n.a.	n.a.	n.a.
Gd	ppm	0	1	0.34	2.96	n.a.	n.a.	1.1	2.3	<0.05	2	1.09	n.a.	n.a.	n.a.	n.a.	n.a.	n.a.	n.a.	n.a.	n.a.	n.a.
Tb	ppm	0	0	0.06	0.46	n.a.	n.a.	0.2	0.3	0.02	0.3	0.18	n.a.	n.a.	n.a.	n.a.	n.a.	n.a.	n.a.	n.a.	n.a.	n.a.
Dy	ppm	0	1	0.37	2.27	n.a.	n.a.	1.3	1.6	<0.05	1.5	1.15	n.a.	n.a.	n.a.	n.a.	n.a.	n.a.	n.a.	n.a.	n.a.	n.a.
Ho	ppm	0	0	0.06	0.39	n.a.	n.a.	0.3	0.3	<0.02	0.3	0.2	n.a.	n.a.	n.a.	n.a.	n.a.	n.a.	n.a.	n.a.	n.a.	n.a.
Er	ppm	0	0	0.17	1.06	n.a.	n.a.	0.9	0.8	0.04	0.8	0.69	n.a.	n.a.	n.a.	n.a.	n.a.	n.a.	n.a.	n.a.	n.a.	n.a.
Tm	ppm	0	0	0.02	0.15	n.a.	n.a.	0.2	0.1	<0.01	0.1	0.1	n.a.	n.a.	n.a.	n.a.	n.a.	n.a.	n.a.	n.a.	n.a.	n.a.
Yb	ppm	0	0	0.19	0.93	n.a.	n.a.	1.2	0.7	0.06	0.8	0.66	n.a.	n.a.	n.a.	n.a.	n.a.	n.a.	n.a.	n.a.	n.a.	n.a.
Lu	ppm	0	0	0.02	0.14	n.a.	n.a.	0.2	0.1	0.01	0.1	0.1	n.a.	n.a.	n.a.	n.a.	n.a.	n.a.	n.a.	n.a.	n.a.	n.a.
Hf	ppm	2	3	0.6	3.5	0.82	0.07	5.7	5.3	0.6	3	2.4	0.08	0.02	<0.02	0.04	0.41	0.05	0.46	0.12	0.27	0.07
Ta	ppm	0	<0.1	0.2	0.4	0.03	<0.01	0.9	0.4	<0.1	0.3	0.3	<0.01	<0.01	<0.01	<0.01	0.01	<0.01	<0.01	<0.01	<0.01	<0.01
W	ppm	<0.5	<0.5	<0.5	<0.5	0.1	19.7	1.2	4.8	77.5	<0.5	<0.5	76	0.8	5.16	<0.05	0.69	0.07	0.21	<0.05	0.43	<0.05
Re	ppm	n.a.	n.a.	n.a.	n.a.	<0.001	<0.001	n.a.	n.a.	n.a.	n.a.	n.a.	0.001	<0.001	0.001	0.001	<0.001	<0.001	<0.001	<0.001	<0.001	<0.001
Au	ppm	1	1	<0.5	<0.5	<0.02	<0.02	<0.5	<0.5	<0.5	<0.5	<0.5	<0.02	<0.02	<0.02	<0.02	<0.02	<0.02	<0.02	0.02	<0.02	<0.02

Hg	ppm	<0.01	<0.01	<0.01	<0.01	0.01	0.01	<0.01	<0.01	<0.01	<0.01	0.02	<0.01	0.04	<0.01	<0.01	<0.01	<0.01	<0.01	<0.01	<0.01
Tl	ppm	<0.1	<0.1	<0.1	<0.1	0.02	0.04	<0.1	<0.1	<0.1	<0.1	<0.1	0.06	<0.02	<0.02	<0.02	<0.02	0.02	0.02	<0.02	0.02	0.03
Pb	ppm	2	7	7.1	6.5	3.8	1.3	2.4	1.3	1.4	1.7	1	27.1	8.2	1.2	0.9	1.4	1.3	1.8	4.7	5.9	3.9
Bi	ppm	<0.1	<0.1	<0.1	<0.1	0.29	0.09	<0.1	<0.1	0.4	<0.1	<0.1	0.74	3.59	1.15	1.19	0.04	0.07	0.07	21.8	0.28	0.58
Th	ppm	1	8	10.1	85	36.4	3.6	5.1	18	1	11	11.4	3.2	0.4	0.2	1.2	4.6	1	5.7	2.2	6.1	1.3
U	ppm	0	1	1.8	21.8	3.56	1.34	3.8	3.3	0.6	1.5	2	2.93	1.81	6.13	4.85	0.53	0.07	0.76	0.7	0.52	0.09

Table S4. Results from hydrothermally altered samples principal component analysis

	Eigenvalues (λ)	Percent (λ%)	Cumulative % (Σλ%)
PC1	18.24	33.78	33.78
PC2	8.65	16.02	49.8
PC3	8.107	15.01	64.81
Eigenvectors	PC1	PC2	PC3
SiO2-CLR	0.2216	-0.02668	-0.09378
Fe2O3-CLR	0.1613	-0.09276	-0.2157
TiO2-CLR	0.03157	0.1799	-0.03083
Al2O3-CLR	-0.1011	-0.1199	0.01475
MnO-CLR	0.06095	0.05307	-0.1785
MgO-CLR	-0.03317	0.1715	0.06681
CaO-CLR	-0.1142	0.189	-0.05825
Na2O-CLR	-0.1244	-0.0466	0.1923
K2O-CLR	-0.06809	-0.19	0.2289
Li-CLR	-0.1237	0.1038	0.2027
Be-CLR	0.00745	0.07794	-0.2796
P-CLR	-0.1047	0.2525	-0.04527
B-CLR	0.05136	-0.1456	0.2683
Sc-CLR	-0.1888	-0.08335	-0.01846
Ti-CLR	-0.2093	0.03716	-0.0383
V-CLR	0.006043	-0.1086	-0.2228
Mn-CLR	-0.1251	0.07401	0.105
Fe-CLR	0.1483	-0.1632	-0.09844
Zn-CLR	-0.06693	0.02036	0.1116
Ga-CLR	-0.2048	0.0584	-0.02592
Ge-CLR	-0.1018	0.05193	-0.2325

As-CLR	0.1527	0.1433	-0.01845
Se-CLR	0.1846	0.07439	0.07756
Rb-CLR	-0.09912	-0.2594	0.08228
Sr-CLR	-0.1641	0.08431	-0.06496
Y-CLR	-0.1811	0.1413	-0.05348
Zr-CLR	-0.2004	-0.01458	0.05195
Nb-CLR	-0.148	-0.2073	-0.075
In-CLR	0.1296	0.2396	-0.06636
Sn-CLR	-0.1166	-0.2394	-0.1544
Sb-CLR	0.02262	-0.1448	0.1996
Te-CLR	0.187	0.03827	0.03518
Cs-CLR	-0.167	-0.1072	0.00337
Cu-CLR	0.1697	0.1358	0.04045
Cr-CLR	0.07111	0.1361	0.2027
Co-CLR	0.1132	-0.04881	0.2169
Ni-CLR	0.009171	0.2014	0.2319
Mo-CLR	0.1483	-0.08209	-0.09834
Ag-CLR	0.2059	0.06942	0.1039
Cd-CLR	-0.02731	0.1506	0.2001
Ba-CLR	0.1532	-0.2018	0.02465
La-CLR	-0.2002	0.05315	-0.03562
Ce-CLR	-0.2024	0.0392	-0.0597
Hf-CLR	-0.2066	0.005805	0.05912
Ta-CLR	-0.1256	0.01625	0.02782
W-CLR	0.0152	-0.24	-0.1557
Re-CLR	0.1057	-0.1313	0.153
Au-CLR	0.09402	-0.09947	0.2464
Hg-CLR	0.07939	-0.0242	-0.05143
Tl-CLR	-0.03495	-0.2912	0.08996

Pb-CLR	0.05968	-0.1763	-0.06625
Bi-CLR	0.196	0.03359	-0.03891
Th-CLR	-0.2045	-0.05372	-0.01226
U-CLR	0.06078	0.004835	-0.2119

Table S5. Micropobe analyses results in (%) for the pyrites from the western Borborema Province hydrothermal alterations.

sample	grain	position	No	Au	Se	As	Zn	Te	Sb	Ag	Fe	Bi	S	Cu	Ni	Sn	Co	Mn	Mo	Hg	Total
Basement silica-hematite breccia from Coroatá (BC01)	1	border	1	0	0	0.002	0.005	0.004	0	0	46.427	0	51.978	0	0.017	0	0.503	0.012	0	0.004	98.952
	1	interm.	2	0.032	0	0	0	0	0	0.004	47.173	0	51.789	0	0.032	0	0.01	0	0	0	99.04
	1	core	3	0	0.025	0.03	0	0	0	0.015	47.987	0	52.63	0	0.013	0	0.178	0	0	0	100.878
	1	interm.	4	0.024	0	0.015	0.002	0	0	0.002	47.14	0	52.542	0	0.015	0	0.739	0.009	0	0.016	100.504
	1	border	5	0	0.038	0	0.01	0.011	0	0	47.276	0	52.573	0	0.037	0	0.008	0	0	0.033	99.986
	2	border	6	0	0	0.004	0	0	0	0.015	47.391	0	52.772	0	0.008	0	0.289	0.001	0	0	100.48
	2	interm.	7	0	0.023	0.015	0	0	0	0	47.779	0	53.302	0.007	0.043	0.002	0.098	0	0	0.022	101.291
	2	core	8	0	0.008	0	0.005	0	0	0	46.117	0	50.42	0.003	0.021	0	0.592	0.008	0	0	97.174
	2	border	9	0	0	0.002	0	0	0	0.005	46.84	0	52.352	0	0.013	0.002	0	0.005	0	0.033	99.252
	2	border	10	0	0.003	0	0	0	0	0.008	47.361	0	52.674	0	0.022	0	0.039	0	0	0.011	100.118
	2	border	11	0.053	0	0.01	0.014	0	0	0	47.448	0	53.129	0.005	0	0	0.042	0	0	0	100.701
	2	interm.	12	0	0	0	0.004	0.001	0	0	46.835	0	52.795	0	0.007	0	0.023	0	0	0	99.665
	2	border	13	0	0.026	0.003	0	0	0	0.015	46.939	0	52.959	0	0	0	0.003	0	0	0.034	99.979
	3	border	14	0	0.034	0	0	0.004	0	0	47.602	0	53.225	0.001	0.016	0	0.139	0	0	0.013	101.034
	3	interm.	15	0	0	0	0	0.006	0	0	47.426	0	53.442	0	0.026	0	0.254	0.02	0	0	101.174
	3	interm.	16	0	0	0.002	0.011	0	0	0	47.472	0	53.098	0.003	0.016	0	0.016	0.008	0	0.001	100.627
	3	core	17	0	0.006	0	0.016	0	0	0.001	45.968	0	49.613	0	0.003	0	0.074	0.007	0	0.001	95.689
	3	core	18	0.044	0.01	0.009	0	0.012	0	0	47.21	0	53.637	0.014	0.001	0	0	0.003	0	0.035	100.975
	3	core	19	0.108	0	0.019	0.004	0	0	0.003	47.223	0	53.745	0	0.023	0	0.532	0	0	0	101.657
	3	core	20	0	0	0	0	0.021	0	0.013	47.313	0	53.256	0.003	0.01	0	0.108	0.007	0	0	100.731
	3	core	21	0	0.007	0.003	0	0	0	0	46.605	0	53.145	0	0.016	0	0.115	0.006	0	0.056	99.953
	3	interm.	22	0	0	0	0	0	0	0.011	47.182	0	53.611	0.009	0	0	0.578	0.012	0	0	101.403
	3	border	23	0	0.008	0	0	0	0	0	47.679	0	53.649	0	0.005	0	0.341	0	0	0	101.682

	3	border	24	0	0.013	0.019	0.001	0	0	0.006	46.9	0	53.708	0	0.025	0	0.499	0.012	0	0.027	101.21
	3	border	25	0.11	0	0.011	0	0	0	0.008	46.389	0	53.429	0	0.014	0	0.162	0.01	0	0.006	100.139
	4	interm.	26	0	0	0.017	0.023	0	0	0	47.008	0	53.724	0.003	0.017	0	0.692	0	0	0	101.484
	4	interm.	27	0	0.012	0	0	0	0	0.016	47.341	0	53.656	0	0.002	0	0.882	0	0	0.011	101.92
	4	interm.	28	0.023	0	0.026	0	0	0	0.009	46.097	0	53.315	0	0.008	0	1.027	0	0	0	100.505
	4	interm.	29	0	0.01	0	0.008	0	0	0.012	47.177	0	53.21	0.015	0.016	0	0.37	0.013	0	0.004	100.835
	4	core	30	0	0	0.031	0	0	0	0.003	47.217	0	53.93	0.01	0.016	0.006	1.171	0.001	0	0.019	102.404
	4	core	31	0	0	0.029	0.002	0.01	0	0	48.179	0	53.731	0.011	0.009	0	0.041	0.011	0	0	102.023
	4	border	32	0	0.019	0	0.006	0.01	0	0.015	46.555	0	53.492	0.004	0	0	0.548	0	0	0	100.649
	4	border	33	0	0	0.015	0	0	0	0.012	47.473	0	53.252	0	0.019	0	0.055	0	0	0.012	100.838
	4	border	34	0.027	0.015	0	0	0	0	0.016	48.062	0	53.615	0	0.031	0	0.046	0	0	0	101.812
	1	border	1	0.024	0.042	0.009	0.001	0.014	0	0.003	58.629	0.005	0.131	0.096	0.014	0	0.007	0	0	0	58.975
Carnaubinha silica-hematite breccia (C25C)	1	interm.	2	0	0.022	0	0	0.008	0	0	59.932	0.017	0.124	0.097	0	0	0.025	0	0.005	0	60.23
	1	core	3	0	0.027	0	0	0	0	0.014	60.881	0.024	0.107	0.133	0	0	0.027	0.014	0	0.013	61.24
	1	border	4	0.045	0.033	0	0	0	0	0	60.965	0	0.141	0.098	0.009	0	0.007	0.006	0	0.018	61.322
	1	interm.	5	0.047	0.036	0.003	0.015	0.009	0	0	59.138	0.007	0.109	0.134	0.006	0	0.003	0.012	0.009	0.054	59.582
	2	core	6	0	0	0.003	0	0	0	0	47.547	0	52.951	0.029	0.011	0	0.013	0.013	0	0.03	100.597
	2	border	7	0.046	0.02	0	0	0.02	0	0	46.931	0	52.697	0.144	0.008	0	0.082	0.003	0	0.028	99.979
	2	core	8	0	0.024	0	0	0	0	0.001	47.102	0	52.817	0.062	0	0	0.118	0	0	0.007	100.131
	2	border	9	0.001	0	0	0.01	0	0	0	47.063	0	53.405	0.053	0	0	0.332	0	0	0	100.864
	2	border	10	0	0.013	0	0	0.016	0	0.011	43.203	0	51.962	0.014	0.003	0	3.771	0	0	0	98.993
	2	core	11	0	0.033	0.037	0.03	0.003	0	0	46.489	0	53.936	0.028	0.025	0	0.034	0	0	0	100.615
	2	border	12	0	0.028	0	0	0.012	0	0	46.198	0	53.469	0.014	0.02	0	0.081	0.01	0	0.03	99.862
	2	border	13	0	0.006	0	0	0	0	0	44.715	0	52.465	0.056	0.011	0.004	2.469	0	0	0.007	99.733
	2	core	14	0	0.021	0.04	0	0.003	0	0.002	46.154	0	53.614	0.057	0	0.003	0.072	0	0	0.016	99.982

	2	border	15	0	0.047	0.021	0	0.007	0	0.006	46.219	0	53.656	0.086	0	0	0.026	0	0	0.013	100.081
	3	border	16	0.02	0	0.008	0.003	0	0	0.024	46.545	0	53.545	0.013	0.012	0.011	0.071	0.005	0	0.02	100.277
	3	core	17	0	0.001	0	0.025	0	0	0.005	46.879	0	52.47	0	0.003	0	0.006	0	0	0	99.389
	3	border	18	0	0	0	0	0	0	0.007	46.362	0	53.767	0.015	0	0	0.04	0	0	0.008	100.199
	3	border	19	0	0.017	0.01	0	0.009	0.002	0	46.847	0	53.638	0.011	0.003	0	0.025	0	0	0.047	100.609
	3	interm.	20	0	0	0.005	0	0	0	0	46.483	0	53.551	0.002	0	0	0.026	0.004	0	0.001	100.072
	3	core	21	0	0.044	0.004	0.005	0.006	0	0.003	46.507	0	52.344	0.004	0.021	0	0.007	0.014	0	0.048	99.007
	3	border	22	0.03	0.01	0	0.007	0.002	0	0	47.3	0	53.226	0.008	0.002	0	0.046	0.003	0	0	100.634
	3	border	23	0	0.009	0.028	0	0.004	0	0.01	46.355	0	53.417	0.038	0.001	0	0.039	0	0	0.023	99.924
	3	core	24	0	0.051	0.014	0	0	0	0	46.432	0	53.762	0.012	0.002	0	0.142	0	0	0	100.415
	4	border	25	0	0	0	0	0	0	0	46.526	0	53.282	0.06	0.01	0	0.059	0	0	0	99.937
	4	border	26	0	0.038	0	0	0.012	0	0	45.645	0	52.293	0.026	0	0	0.01	0.016	0	0	98.04
	4	interm.	27	0	0.007	0.047	0	0	0	0	46.153	0	53.391	0.012	0.035	0	0.143	0	0	0	99.788
	4	core	28	0	0.012	0.031	0	0	0	0	46.702	0	53.265	0.02	0.009	0	0	0.007	0	0.018	100.064
	4	interm.	29	0	0.024	0	0	0.005	0	0.017	46.419	0	53.486	0.02	0	0.001	0.125	0.002	0	0	100.099
	4	border	30	0	0.02	0.023	0.002	0.007	0	0.002	46.75	0	52.872	0.015	0	0	0.081	0.013	0	0.014	99.799
	4	border	31	0	0.055	0.017	0	0	0	0.002	61.2	0.012	0.185	0.179	0	0	0.009	0.02	0	0.023	61.702
	4	core	32	0	0.062	0	0.011	0	0	0	60.235	0.009	0.196	0.18	0	0	0.013	0.028	0.003	0.012	60.749
	4	core	33	0	0.055	0.035	0	0.001	0	0.009	60.587	0.003	0.221	0.096	0	0	0.013	0.003	0.009	0.012	61.044
	4	interm.	34	0.008	0.054	0	0	0	0	0	59.794	0	0.166	0.094	0.007	0	0.011	0.027	0	0	60.161
	4	border	35	0	0.078	0	0.016	0	0	0.011	61.435	0	0.205	0.103	0.017	0	0.021	0.032	0.001	0	61.919
São Bento basin (SB02)	1	border	1	0	0	0	0.002	0.001	0	0	47.784	0	54.127	0	0.046	0	0.022	0.002	0	0.012	101.996
	1	border	2	0	0	0	0	0	0	0	47.249	0	53.427	0.017	0.036	0	0	0	0	0	100.729
	1	interm.	3	0	0	0.006	0	0.006	0	0	47.587	0	53.677	0.001	0.016	0	0.002	0.004	0	0.042	101.341
	1	interm.	4	0.138	0.019	0	0	0.001	0	0.002	47.969	0	53.788	0.001	0	0	0	0.007	0	0	101.925

	1	interm.	5	0	0	0	0.028	0.003	0	0.012	47.803	0	54.126	0	0.011	0.002	0	0	0	101.985
	1	interm.	6	0	0.013	0.032	0	0.019	0	0	47.278	0	53.592	0.002	0	0	0.012	0.016	0	100.964
	1	interm.	7	0.001	0	0.032	0.011	0.016	0	0.015	47.335	0	53.46	0.014	0.003	0	0.032	0.013	0	100.932
	1	core	8	0	0.004	0.041	0.014	0.001	0	0.018	47.698	0	53.856	0.005	0.011	0	0.006	0	0	101.666
	1	core	9	0.03	0	0	0	0	0	0.005	48.096	0	53.325	0.023	0	0	0	0.001	0	101.48
	1	core	10	0	0	0	0.011	0	0	0	47.644	0	53.691	0	0.003	0	0.004	0	0	101.353
	1	core	11	0	0.011	0	0.018	0	0	0.024	47.167	0	53.302	0.013	0.012	0	0	0	0	100.586
	1	core	12	0	0	0.017	0	0	0	0	47.895	0	53.843	0.001	0	0	0.012	0.02	0	101.824
	2	border	13	0	0.023	0	0	0.002	0	0	47.722	0	54.036	0.004	0.011	0	0	0	0	101.831
	2	border	14	0	0.005	0	0.002	0.005	0	0.005	47.547	0	53.899	0	0	0	0.001	0.017	0	101.522
	2	border	15	0	0	0	0.008	0.006	0	0.007	46.435	0	53.599	0.011	0.008	0	0	0	0	100.103
	2	core	16	0.024	0	0.027	0.03	0	0	0.013	47.595	0	54.053	0.009	0.006	0	0	0	0	101.757
	2	interm.	17	0	0.03	0	0	0	0	0.003	47.643	0	53.756	0	0.018	0.002	0.025	0	0	101.499
	2	border	18	0	0.005	0	0.018	0	0	0	46.854	0	53.866	0.013	0	0.001	0	0.001	0	100.823
	2	border	19	0	0.046	0.003	0.002	0.009	0	0	47.12	0	53.871	0	0	0	0.011	0.004	0	101.095
	2	border	20	0	0.02	0.012	0	0	0	0.002	48.061	0	53.972	0	0.044	0.008	0.057	0	0	102.216
	2	border	21	0.053	0	0	0.023	0.006	0	0.001	47.881	0	53.909	0	0.009	0	0.032	0	0	101.914
Carnaubinha basin silica-sulphide breccia (THC26)								0	0	0	46.566	0	53.166	0	0.015	0	0.084	0.011	0	99.915
	1	interm.	2	0	0.021	0	0.027	0.01	0	0.003	46.737	0	52.499	0	0.01	0	0.026	0	0	0.01	99.343
	1	interm.	3	0.01	0	0	0	0.004	0	0	46.654	0	52.511	0	0.009	0	0.016	0.012	0	0.005	99.221
	1	border	4	0.029	0.041	0.011	0.001	0.003	0	0.009	46.933	0	52.314	0.005	0.046	0	0.463	0	0	0.013	99.868
	1	interm.	5	0	0	0	0.003	0	0	0.005	46.979	0	52.277	0	0	0.025	0.056	0.014	0	0.002	99.361
	1	core	6	0	0.032	0.056	0.008	0.02	0	0	46.309	0	53.408	0.006	0.029	0	0.02	0.016	0	0	99.904
	1	interm.	7	0	0	0.018	0.014	0	0	0	46.66	0	52.715	0	0.015	0	0.021	0	0	0.065	99.508
	1	interm.	8	0	0	0	0.008	0.005	0	0.001	46.674	0	53.084	0.002	0.025	0	0.028	0.001	0	0.002	99.83

1		core	9	0	0.02	0	0.004	0.002	0	0.011	46.453	0	53.213	0	0.118	0	0.112	0.018	0	0.034	99.985
1		interm.	10	0	0.001	0.04	0	0.019	0	0.004	46.691	0	53.325	0.011	0	0	0.003	0	0	0.01	100.104
2		border	11	0	0	0.006	0.006	0	0	0.018	46.789	0	53.061	0	0.008	0.006	0.085	0	0	0.039	100.018
2		core	12	0.057	0	0	0	0.015	0	0.014	47.476	0	52.936	0.014	0.051	0.003	0.02	0	0	0.047	100.633
2		interm.	13	0	0.027	0.001	0.002	0	0	0	47.839	0	52.844	0.002	0.015	0	0.008	0.001	0	0	100.739
2		border	14	0	0.021	0	0	0.015	0	0.001	47.426	0	52.788	0.015	0.059	0	0.043	0	0	0	100.368
2		core	15	0	0	0.024	0	0.006	0	0	47.048	0	51.938	0	0.013	0	0.011	0.002	0	0.04	99.082
2		interm.	16	0	0	0.019	0	0.008	0	0	48.048	0	53.201	0.007	0.028	0	0.061	0.009	0	0	101.381
3		border	17	0	0	0	0.002	0	0	0.017	47.993	0	53.372	0	0.006	0	0.013	0.013	0	0.032	101.448
3		interm.	18	0	0	0.014	0	0	0	0	44.742	0	52.873	0.006	0.014	0	2.619	0.01	0	0.006	100.284
3		border	19	0	0	0	0	0.019	0	0.006	47.211	0	53.574	0.002	0	0	0	0.009	0	0.031	100.852
3		interm.	20	0.06	0	0	0	0.004	0	0	47.772	0	53.325	0	0	0	0.004	0.001	0	0.04	101.206
3		core	21	0.02	0.008	0.004	0	0	0	0.005	47.472	0	53.457	0.005	0.001	0	0.002	0.004	0	0	100.978
3		core	22	0.008	0	0	0	0.004	0	0	46.73	0	53.466	0.009	0.032	0	0.015	0.005	0	0	100.269
3		interm.	23	0	0.011	0.031	0	0.005	0	0	47.323	0	53.61	0	0.003	0	0.022	0.022	0	0.053	101.08
3		interm.	24	0	0	0.012	0	0	0	0.002	47.799	0	53.683	0	0	0	0.012	0	0	0.022	101.53
3		border	25	0	0.018	0	0	0	0	0	47.138	0	52.921	0	0.009	0	0.174	0.006	0	0	100.266
4		border	26	0	0	0	0	0.004	0	0	46.657	0	53.454	0.001	0.011	0.001	0	0.001	0	0.002	100.131
4		interm.	27	0	0.029	0.002	0.003	0	0	0	47.495	0	52.897	0	0.045	0	0.09	0	0	0.007	100.568
4		core	28	0	0.021	0	0	0.005	0	0.009	47.909	0	53.409	0	0.014	0	0.038	0	0	0.009	101.414
4		core	29	0	0	0.044	0.013	0.01	0	0.011	46.754	0	53.206	0	0.022	0	0.145	0.007	0	0.012	100.224
4		interm.	30	0	0	0.06	0	0	0	0	46.714	0.003	53.668	0.005	0.002	0	0.011	0	0	0	100.463
4		Border	31	0.002	0	0	0.017	0	0	0	47.256	0	53.191	0.017	0.134	0	0.094	0.005	0	0	100.716
4	core		32	0	0.013	0.006	0.01	0	0	0	47.04	0	53.463	0.004	0.04	0	0.154	0	0	0.029	100.759

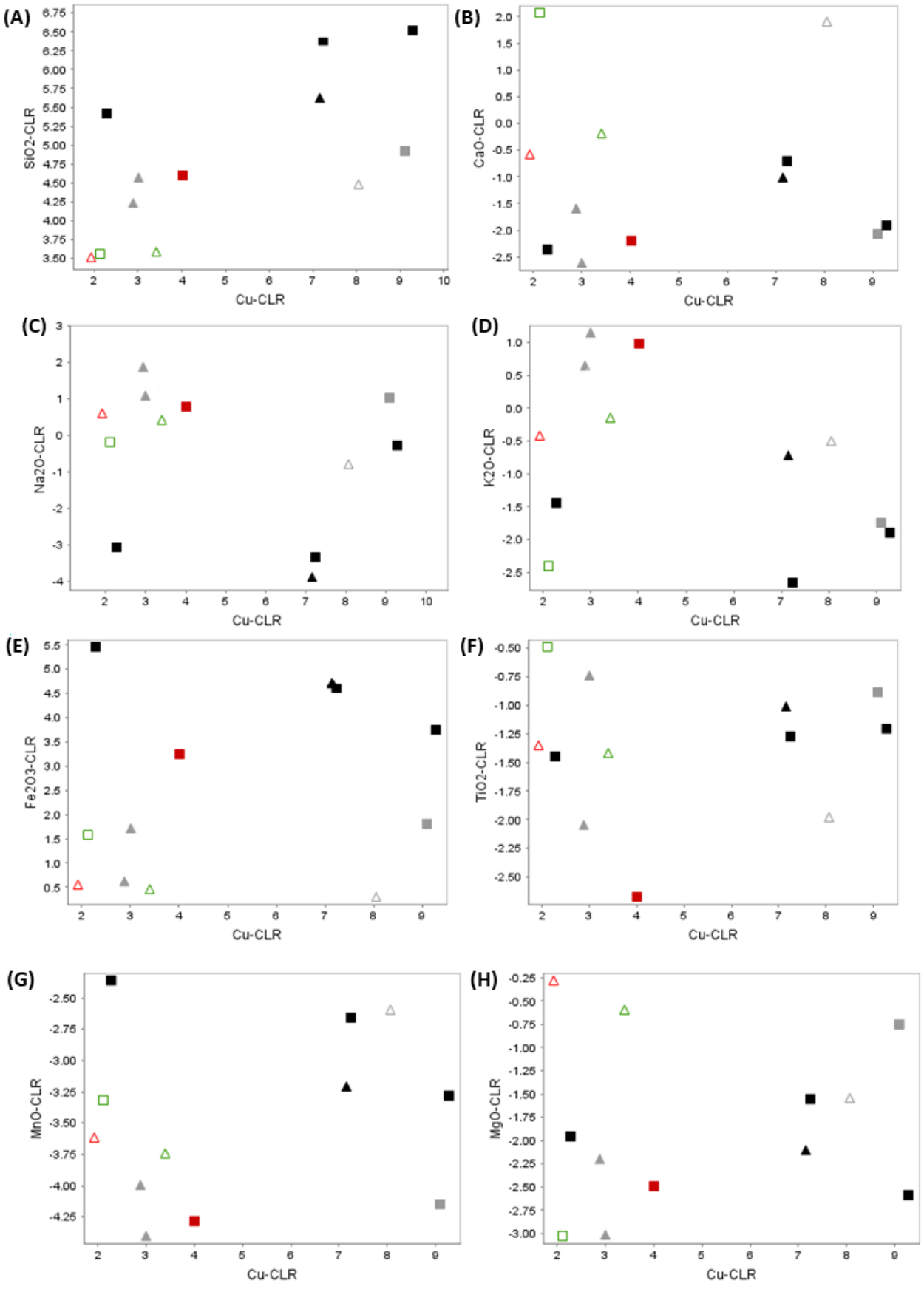
(A)
SiO2-CLR
Cu-CLR
(B)
CaO-CLR
Cu-CLR
(C)
Na2O-CLR
Cu-CLR
(D)
K2O-CLR
Cu-CLR
(E)
Fe2O3-CLR
Cu-CLR
(F)
TiO2-CLR
Cu-CLR
(G)
MnO-CLR
Cu-CLR
(H)
MgO-CLR
Cu-CLR

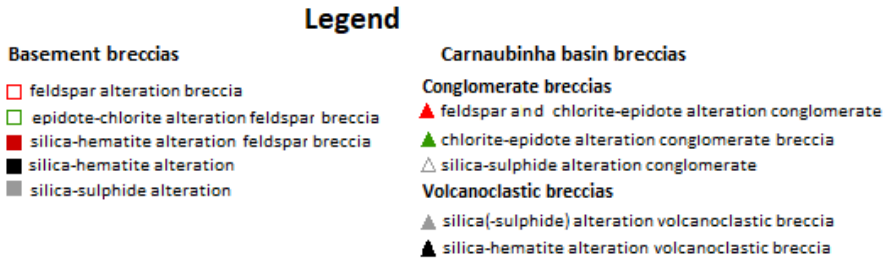

Figure S1. Biplots showing centered log ratios of Cu vs. major elements.

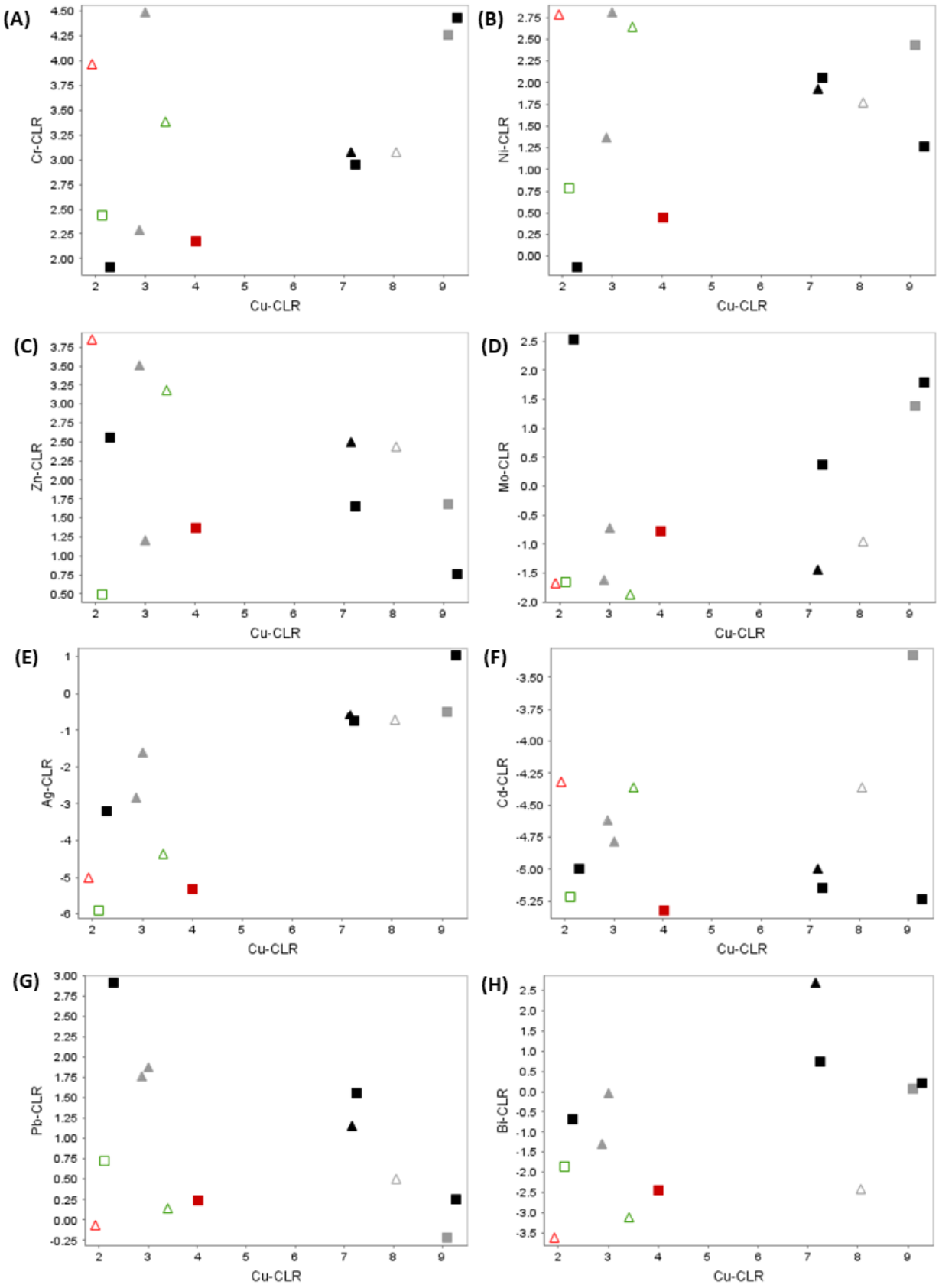
(A)
Cr-CLR
Cu-CLR
(B)
Ni-CLR
Cu-CLR
(C)
Zn-CLR
Cu-CLR
(D)
Mo-CLR
Cu-CLR
(E)
Ag-CLR
Cu-CLR
(F)
Cd-CLR
Cu-CLR
(G)
Pb-CLR
Cu-CLR
(H)
Bi-CLR
Cu-CLR

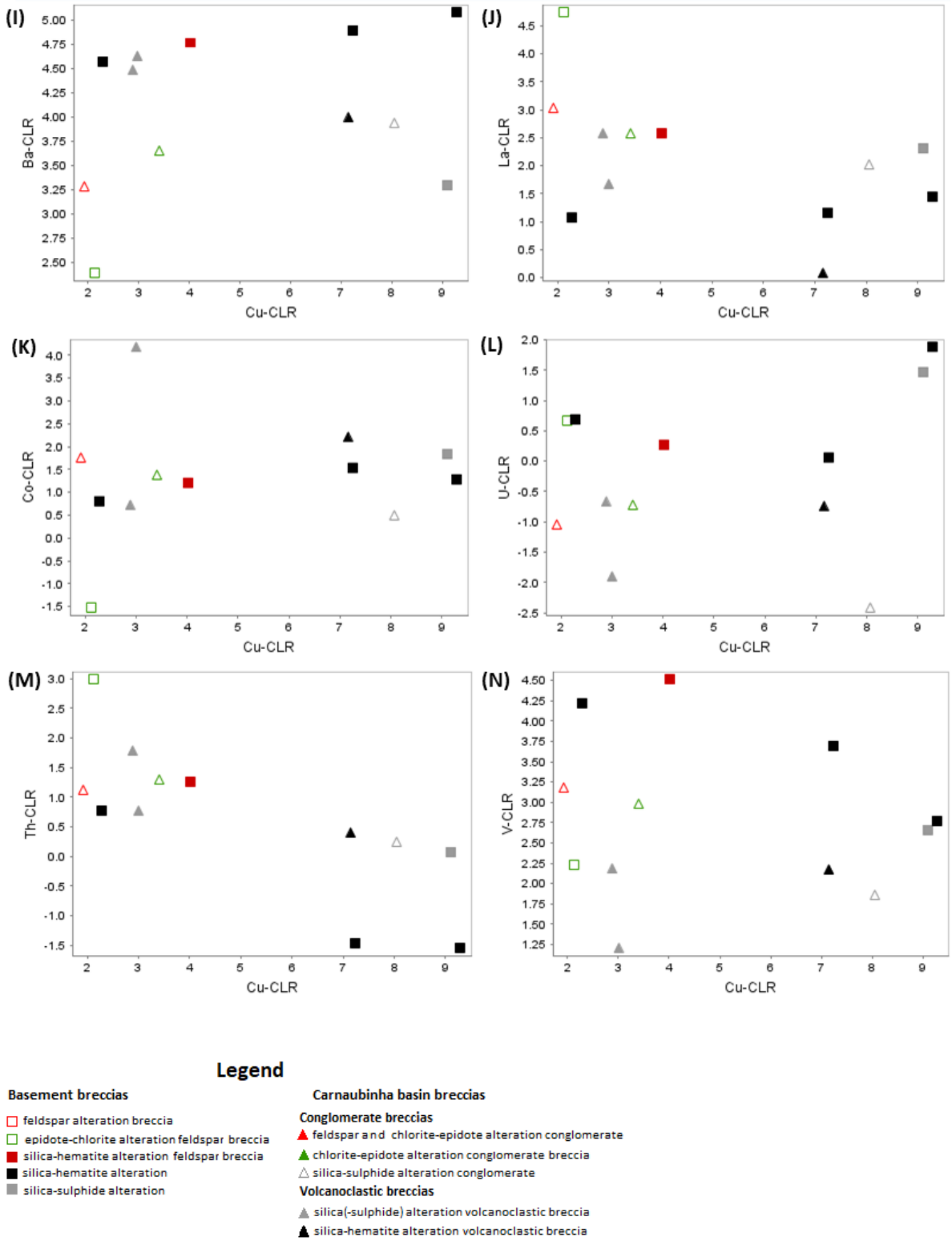

Figure S2. Biplots showing centered log ratios of Cu vs. minor elements.

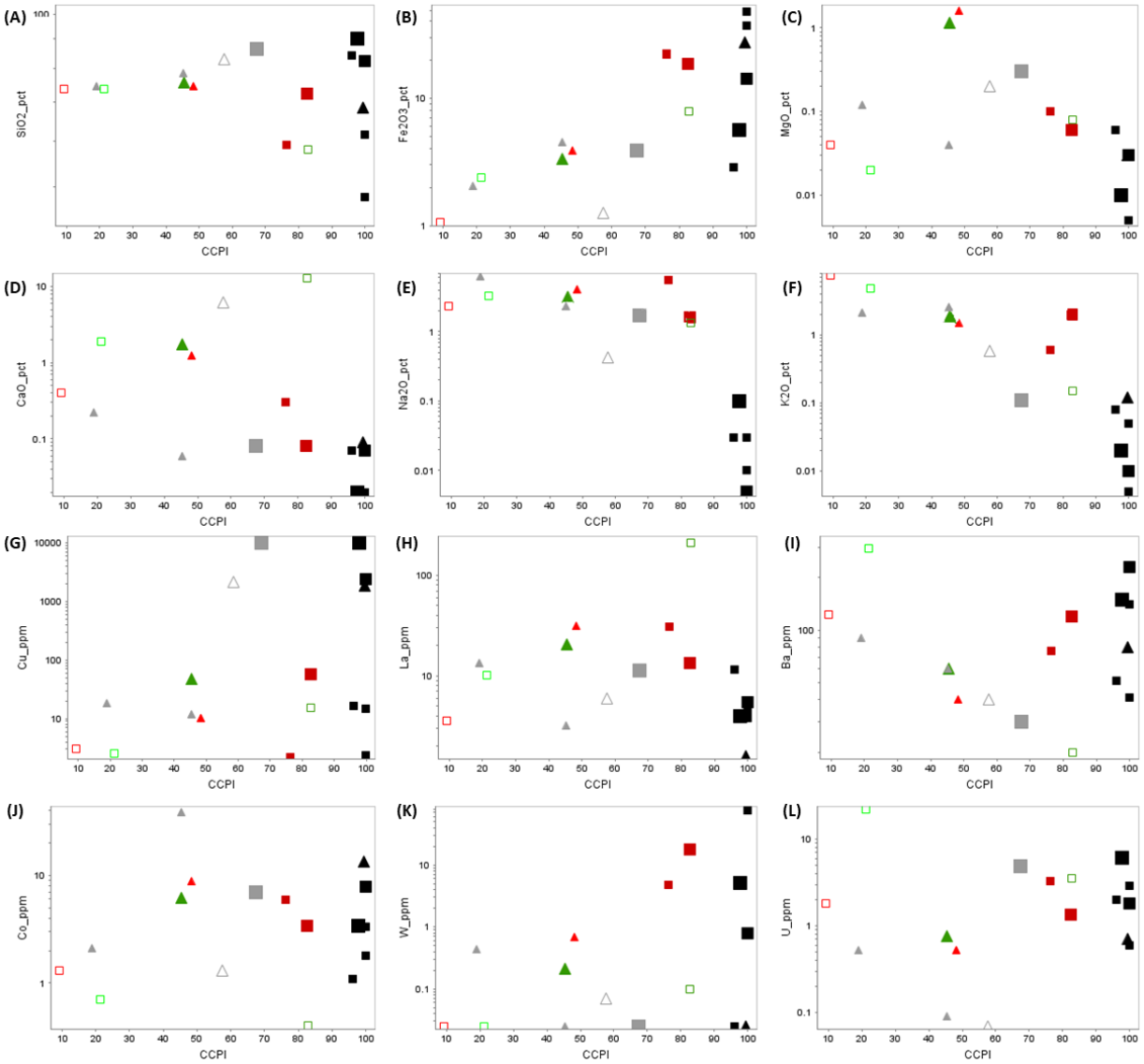

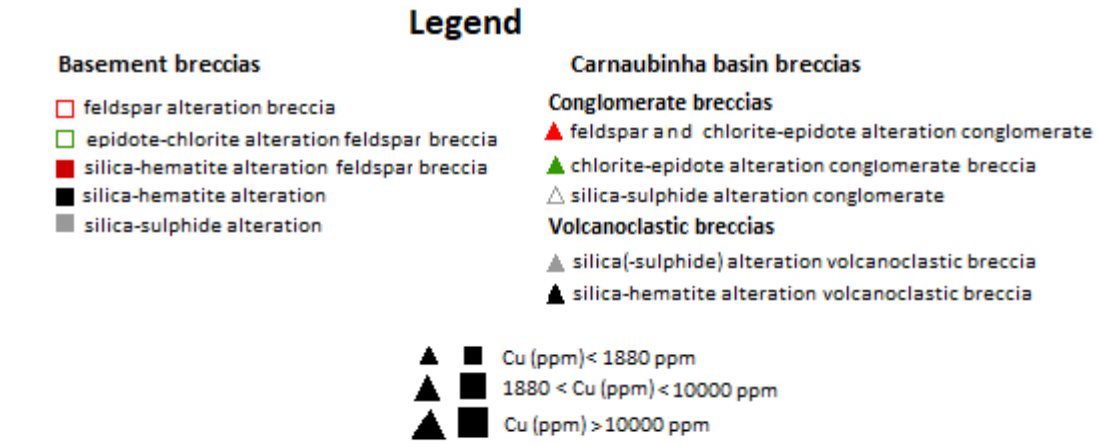

Figure S3. Biplots of alteration index CCPI (chlorite carbonate pyrite) (source) versus major and trace elements.

7. Pyrite mineral chemistry

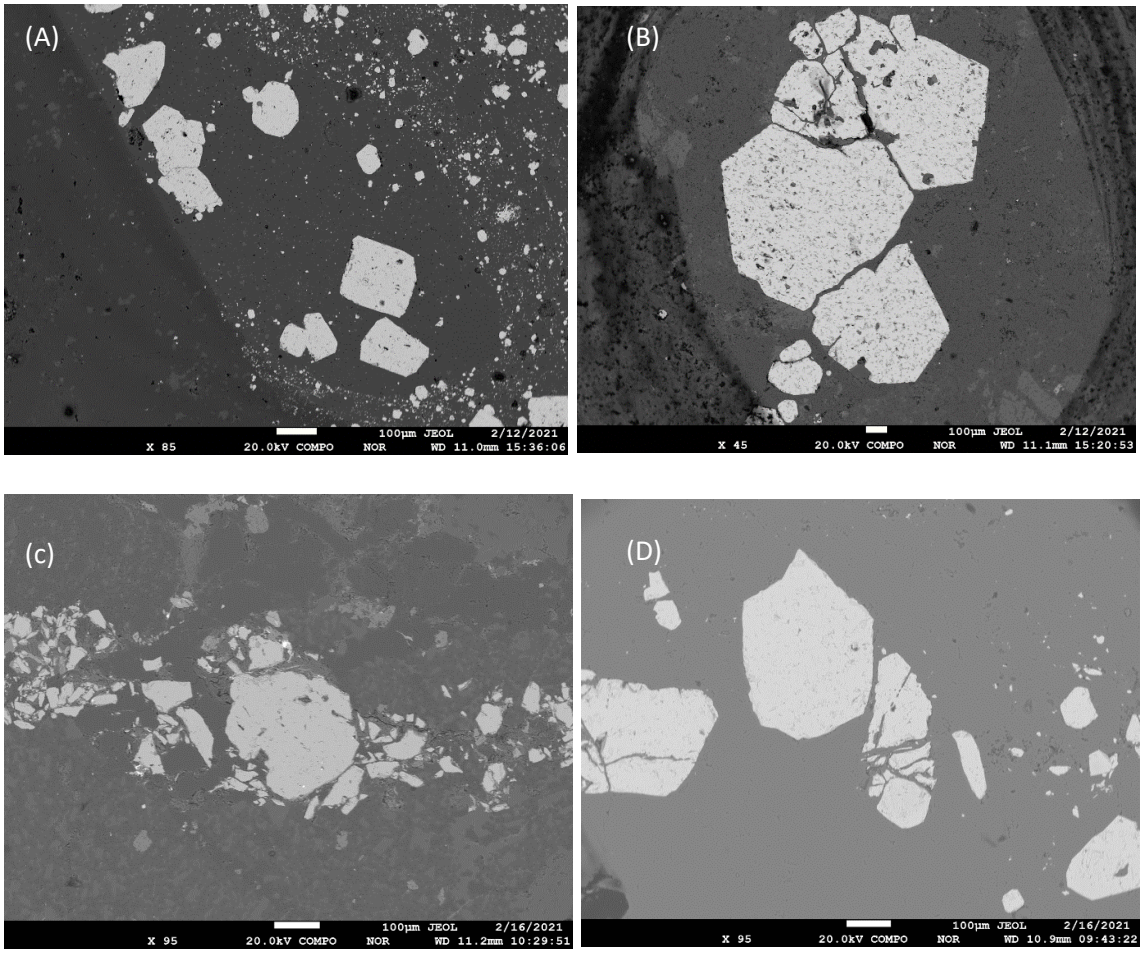

Figure S4. Carnaubinha basin pyrites. (A) Silica-hematite breccia pyrites, the larger crystals are inside a volcanic clast, while fine grained pyrite is associated with the silica-hematite matrix. (B) Silica-sulphide breccia pyrite inserted in the silica matrix. (C) São Bento conglomerate pyrites exhibiting brittle-ductil deformation features. (D) Coroata basement silica-hematite breccia pyrite associated with the hydrothermal alteration.